The sheath of an RF plasma : measurements and simulations of the ion energy distribution

The sheath of an RF plasma: measurements and simulations of the ion energy distribution

R.J.M.M. Snijkers

The sheath of an RF plasma: measurements and simulations of the ion energy distribution

PROEFSCHRIFT

ter verkrijging van de graad van doctor aan de
Technische Universiteit Eindhoven, op gezag van
de Rector Magnificus, prof. dr. J.H. van Lint,
voor een commissie aangewezen door het College
van Dekanen in het openbaar te verdedigen op
dinsdag 12 oktober 1993 om 16.00 uur

door

Robertus Johannes Maria Mathilde Snijkers

Geboren te Schaesberg

Dit proefschrift is goedgekeurd
door de promotoren

prof. dr. F.J. de Hoog
en
prof. dr. F.W. Sluijter

co-promotor
dr. ir. G.M.W. Kroesen

aan Vera, Lonne en Bente

Contents

1 General introduction

1.1 Applications of RF plasmas

Radio frequency (RF) plasmas are used in the microelectronics industry for etch and deposition processes in the manufacturing of integrated circuits (IC). During the etching a mask pattern is reproduced in the surface layer of the semiconductor device by removing the surface material which is not covered by the mask. This etching process is only one of several processes during the manufacturing of IC's, but a very crucial one: it determines the limits where in IC's can be produced with sufficient accuracy. Knowledge about RF plasmas is necessary in order to control the etch process so the production of IC's can be optimized from an economical point of view. The investigations presented in this thesis contribute to the understanding of the RF plasma.

IC's are very important for our economy and have a big impact on our society. They are the basis of computer technology, all automatization processes and they are widely used in all kinds of equipment. Since the first IC was developed in the early sixties, a constant demand for better, faster and more advanced devices exists. In order to fulfil this demand, devices have to become smaller, and new production techniques had to be developed.

In the past chemically reactive liquids were used to create a device pattern in semiconductor material (wet etching). The pattern is formed with the help of a mask which is put on the surface of the toplayer through lithographic techniques. The surface material which is not covered by the mask reacts chemically with species of a liquid. A good choice of the liquid provides the proper selectivity which means that only the semiconductor material of the toplayer is etched and not the mask nor the underlayer. The chemically active species have no preferential etching direction, so the etching takes place isotropically and undercutting of the mask cannot be prevented (see figure 1.1). If the ratio

1
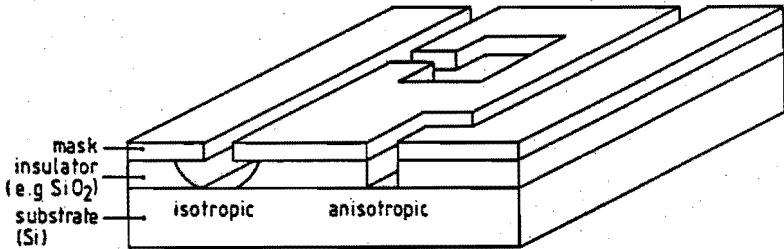
Figure 1.1: Schematic representation of isotropic and anisotropic etch profiles in a toplayer.

of depth to width of the etched pattern is smaller than 1, these wet etching techniques satisfy very well and devices with structures of at least 2-3 μm can be produced with good reproducibility. But when aspect ratios larger than 1 are required, anisotropic etch techniques are necessary. Therefore in the seventies dry etching techniques were developed by which line resolutions up to 0.5 μm can be reached.

RF plasma etching is one of these dry etching techniques. In the plasma chemically active radicals and ions are produced, which both contribute to the etch process. Four different etch mechanisms can be distinguished depending on the etch gas, the device material, and the plasma conditions [Man89]. In the case of sputtering, the surface is bombarded with highly energetic ions and surface atoms are ejected outwards purely by physical processes. This sputter etching requires very high ion energies (> 1000 eV) although these high energies also can cause surface damage through which the device may become useless. This mechanism provides also low etch rates and a low selectivity.

The chemically reactive radicals can etch the surface as a result of a chemical reaction of the radicals and surface atoms. Spontaneous etching appears when the newly formed molecules are volatile so they can desorb from the surface. There are no plasma restrictions to chemical etching and the selectivity is very good although the etch rate is rather low. The largest disadvantage of this mechanism is the isotropic etch result (see figure 1.1).

The chemical etching can be enhanced by energetic positive ions with energies up to hundreds of eV. These ions enhance the rates of the surface reactions. As a consequence of a synergetic effect the etch rate can increase by one order as shown in figure 1.2 and this is much more than the added effects of sputtering and chemical etching. At plasma conditions which provide an ion
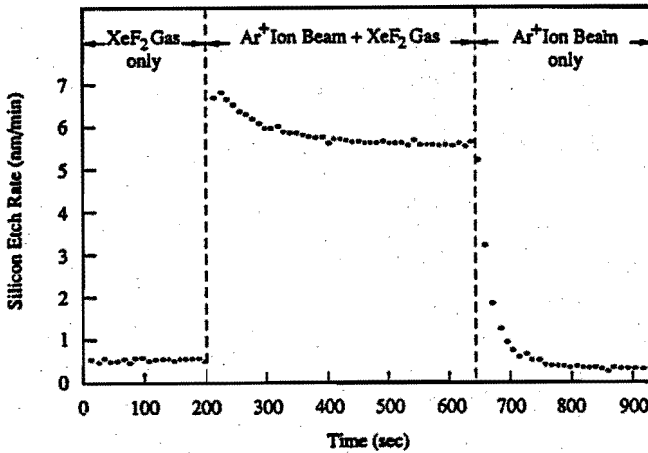
Figure 1.2: Experiment showing the synergetic effect of ion-enhanced etch reactions. The etch rate of the combination of ions and chemical active species cannot be explained by the addition of the separate etch effects [Cob79].

angular distribution mainly directed to the surface, anisotropic etch profiles can be achieved (see figure 1.1), even with large depth-to-width-ratios.

This etch mechanism is also applicable in the case where the product molecules formed by the reactive radicals and surface atoms are not volatile. A very thin passivation layer may then be built which covers the device layer and stops the etching process. Ion bombardment breaks the inhibitor layer so chemical etching can take place again [Oeh87]. Because of the directed ion flux the inhibitor layer on the sidewall of an etch profile is not broken and subsequently this etch mechanism is anisotropic.

Ions directed perpendicalur to the surface, are essential for anisotropical etch results. The angular distribution depends on the plasma conditions just like the ion energy distribution. The etch rate is strongly correlated to the ion energy. At small ion energies the etch rate is low and unfavourable from an economical point of view. The etch rate rises rapidly with increasing energy although at very high ion energies surface damage can be caused which is fatal for microdevices. Controlling the ion energies is very important and essential for good results.

In most cases halogen-containing feed gases, like F_2, Cl_2, CF_4, CHF_3, SF_6, CF_2Cl_2, CF_3Br, are used for etching processes. The atomic halogen radicals

formed in the plasma are chemical very reactive with semiconductor materials like Si, SiO_2, Ga, $GaAs$ or Ge. As a consequence of the used gases and the formed etching products a lot of different species are present in the plasma and, subsequently, the complexity is very large. This can even be enlarged when gases like O_2 or H_2 are added to increase the selectivity [Man89]. In the case of halogen containing gases besides the positive ions, negative ions are formed in the plasma [Hav91]. Although these ions do not take part in the etching mechanism, they influence the plasma.

When investigating and modelling RF plasmas it is impossible to take into account all species, but to get realistic results as many as possible species and certainly the most important ones have to be investigated. When investigating and modelling RF plasma etch systems, it takes a large effort to develop a fully consistent description of the plasma as well as of the surface mechanism. Up to now studies have been carried out concentrating only on partial problems. If any progress is to be made however, the results of these partial studies will act as basis for more consistent descriptions. The investigation described in this thesis is concerned with one of the important aspects of reactive ion etching (RIE): the dynamics in the sheath between plasma and substrate.

1.2 RF plasmas

Several plasma etch reactors are designed based on the mechanisms described in section 1.1 [Man89]. The best etch results (anisotropy, high etch rates, uniform etching over the wafer) are reached in a single wafer etcher. The plasma is generated between two electrodes normally situated in a parallel geometry and is capacitively (AC) coupled to the power source as shown in figure 1.3. The plasma is created by the oscillating electric field between the electrodes. During ignition electrons gain energy from the oscillating field and produce excited atoms and molecules by excitation processes, as well as ions and electrons by ionization of neutrals. Charged particles are lost by recombination or by diffusion to the electrodes and to the reactor wall. Because of the higher mobility of the electrons compared to the ions, the electron loss at the electrodes and wall is larger than the ion loss. Subsequently, the electrodes will be charged negatively with respect to the plasma. In front of both electrodes an electric field is formed between the plasma and the electrode, in which the electrons are repelled and the ions are accelerated towards the electrode. These positive space charge regions are called the sheaths. Most of the applied voltage appears
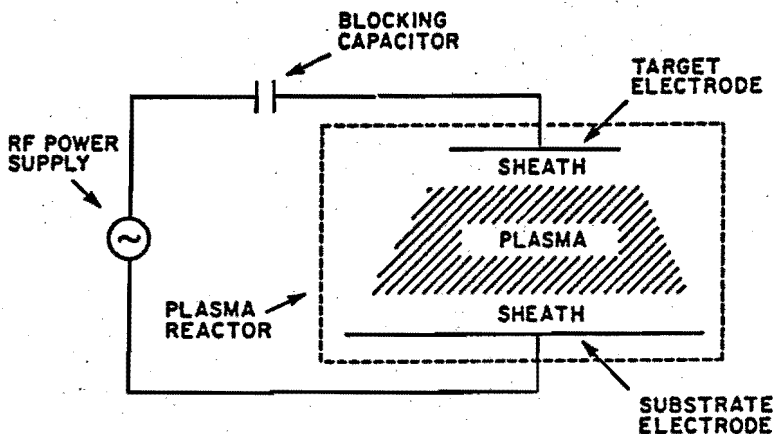
Figure 1.3: Schematical view of AC coupled RF plasma

across these regions. Due to the RF voltage over the electrodes, the sheath voltage is RF modulated too. Ions accelerated in the sheath are influenced by the oscillating voltage and the ion energy distribution (IED) of the ions hitting the electrode is an image of the sheath behaviour.

The RF plasmas used for plasma etching operate at low pressure, typically in the range of 1 - 500 mTorr. The plasma glow is quasi-neutral and the electric field in the glow is smaller than 10 V/cm. The ion and electron density in the glow are typically 10^{16} m^{-3} so the plasma can be classified as weakly ionized. The electron temperature is about 1 - 4 eV while the ion temperature is about room temperature (0.03 eV).

The frequency used in industrial etch reactors is 13.56 MHz which frequency is allowed by international authorities. Because of the interest of the industry a lot of research and modelling has been done both for 13.56 MHz plasmas as on RF plasmas in the range of 50 - 500 kHz. In 1982 a research project was started at the Department of Applied Physics of the Eindhoven University of Technology to study capacitively coupled RF plasmas used in single wafer etch reactors. Experimental results on the electron and negative ion density, measured with microwave techniques, particle densities in the glow measured with Fourier transform spectroscopy and IED's measured at the grounded electrode are presented in the Ph.D. theses of T.H.J. Bisschops [Bis87] and M. Haverlag [Hav91]. In the thesis of P.M. Vallinga [Val88] theoretical results based on fluid models of the glow region and the sheath are presented.

1.3 Scope of this thesis

This thesis is on the ion dynamics and the sheath behaviour in an RF plasma. For that purpose models are presented which describe the electric field in the RF sheath by which the ions are accelerated. The IED of the ions when they hit the electrode can be derived from these models. The IED of the ions at the electrodes also have been determined experimentally in a 13.56 MHz plasma in Ar, N_2 and CF_4.

The electric field in the sheath is described by Poisson's law where the space charge mainly exist of positive ions. The ions also are accelerated in this field. Consequently the sheath is a complicated system which has to be treated self-consistently. In the case of a DC sheath where the sheath voltage is fixed, the sheath is quite well understood although an analytic self-consistent description of the whole sheath region is hard to find when taking into account both the positive ions and the negative charged particles. In the case of an RF plasma where the sheath voltage is time modulated the sheath behaviour becomes much more complex. A lot of research has already been done on RF plasma sheaths but a time depending selfconsistent solution has not been found up till now and the sheath behaviour has not completely been understood. In this thesis some models are presented which contribute to the understanding of the sheath behaviour.

A set-up has been built to measure mass-resolved the IED at the grounded and the driven electrode. In the collisionless sheath, the IED is saddle structured in between a maximum and minimum enery. The sheath behaviour can be characterized by the splitting and the average enery of this saddle structure. The influence of collisions in the sheath is demonstrated by Monte Carlo simulations. By comparison of the measured and the calculated IED's, the RF sheath models can be verified. Mass-resolved measurements also offer the possibility to study the chemistry in the sheath of more complicated gases like CF_4.

In chapter 2 some general properties on RF plasmas and the sheaths are discussed. We have concentrated on AC coupled RF plasma configurations which are used in industrial processes. Also an overview of investigations on the sheath in RF plasmas both theoretical and experimental which are published in literature, is presented.

In chapter 3 the models to describe the electric feld RF plasma sheath are discussed. It is proved that these models are quasi self-consistent. The

IED which has been derived from the high frequency models show typically RF saddle structures in the case the sheath is (nearly) collisionless. In the case collisions in the sheath become important, the IED is changed. We distinguish elastic scattering and charge exchange collisions, where the charge exchange collisions generate typical features in the IED.

The etch reactor which is used to generate the 13.56 MHz plasma and the mass and energy spectrometer to determine mass-resolved the IED are described in chapter 4. Every part of the spectrometer is discussed in detail.

In chapter 5 the results of the experiments are presented and discussed and some conclusions about the sheath behaviour as function of the sheath voltage and the pressure are drawn. Some results also are compared with simulations based on the models described in chapter 3.

References

[Bis87]   T.H.J. Bisschops, *Investigations on an RF plasma related to plasma etching*. Ph.D. thesis, Eindhoven University of Technology, the Netherlands, 1987.

[Cob79]   J.W. Coburn and H.F. Winters, *J. Appl. Phys.* **50**, 3189 (1979).

[Hav91]   M. Haverlag, *Plasma chemistry of fluorocarbon RF discharges used for dry etching*. Ph.D. thesis, Eindhoven University of Technology, the Netherlands, 1991.

[Man89]   D.M. Manos and D.L. Flamm, *Plasma etching, an introduction*. (Academic Press, London, 1989).

[Oeh87]   G.S. Oehrlein and Y.H. Lee, *J. Vac. Sci. Techn.* **A5**, 1585 (1987).

[Val88]   P.M. Vallinga, *Modelling of RF plasmas in a parallel plate etch reactor*. Ph.D. thesis, Eindhoven University of Technology the Netherlands, 1988.

2 RF plasmas

2.1 Introduction

In this chapter some general information on RF plasmas is given which is essential for the understanding of the sheath and the voltage drop across the sheath. This voltage drop in combination with the sheath thickness, the RF frequency and the collisional behaviour of the ions determines the ion energy distribution.

RF plasmas are complex because of the non-linear electrical behaviour and because the plasma conditions depend on a number of parameters like the pressure, the input power, the gas mixture, the electrode configuration and the frequency. The plasma glow is charged positively with respect to the electrodes as a result of the mass and energy difference between the ions and the electrons. The sheath between the plasma glow and the electrode is formed by positive ions and the thickness is of the order of a few times the Debye length [Cha80]. RF plasmas used in industry are usually AC coupled by a blocking capacitor between the RF generator and the driven electrode. This means that the net current (integrated over 1 RF period) through the electrical circuit including the plasma is zero and this is of large influence on the averaged voltage drops across the sheaths. If the electrode areas differ an autobias voltage is generated. With some simple analog circuit models this autobias can be calculated as function of the ratio of the electrode areas.

In section 2.2, some properties of RF plasmas will be discussed, which are important to understand RF plasmas and the sheath behaviour. The frequency is an important parameter and has a large impact on the electrical characterization of the sheath. We can split the frequency range in different parts where the excitation frequency ω has to be compared to the ion plasma frequency $\omega_{p,i}$ and the electron plasma frequency $\omega_{p,e}$. In section 2.3 some sheath models which have been presented in the literature, are discussed.

2.2 RF plasma properties

2.2.1 The autobias voltage

Due to the ion and electron flux, a floating electrode in contact with a plasma will be biased negatively compared to the plasma and a sheath is formed between the electrode and the plasma. The sheath potential will increase till the ion and electron current will be balanced. This is called the floating potential.

In the case this sheath potential is RF modulated, the electron current is strongly modulated too. Due to the non-linear I-V character, the time averaged electron current increases and exceeds the total ion current. To get a new balanced current situation a DC offset is needed and subsequently the averaged sheath potential is higher than the floating value [Cha80].

When we consider an AC coupled RF plasma, the net current through the whole circuit and also through both sheaths must be zero. This condition is of influence on the plasma potential and the DC bias generated at the driven electrode which is connected by a blocking capacitor to the RF generator (see figure 1.3). In the case of a symmetric AC coupled RF plasma (symmetric means that the electrode areas are the same) no bias will be generated and the plasma potential ($V_p(t)$) adjusts itself such that the total net current through both sheaths is zero. In the case of an asymmetric AC coupled RF plasma a DC bias is needed to balance the net current through both sheaths. This is called the autobias voltage ($V_{autobias}$). When the AC coupled driven electrode is smaller than the grounded electrode, the autobias will be negative. Subsequently the averaged potential across the sheath in front of this electrode is increased. Normally this is the situation used in industry. Due to the higher sheath voltages, the ion energy is increased and the etch results are improved. In the case of a DC coupled RF plasma, without a blocking capacitor, the voltage of the driven electrode is defined by the RF generator and a net current may go through the system. The plasma potential and the net current adjust itself to the imposed external conditions.

The investigations described in this thesis concentrate on asymmetric AC coupled RF plasmas, similar to industrial systems.

2.2.2 The RF frequency

The plasma potential is always higher than the instantaneous electrode potential and due to the driven RF potential the sheath potential is RF modulated too (see figure 2.1). The excitation RF frequency ($\omega/2\pi$) has a large influence
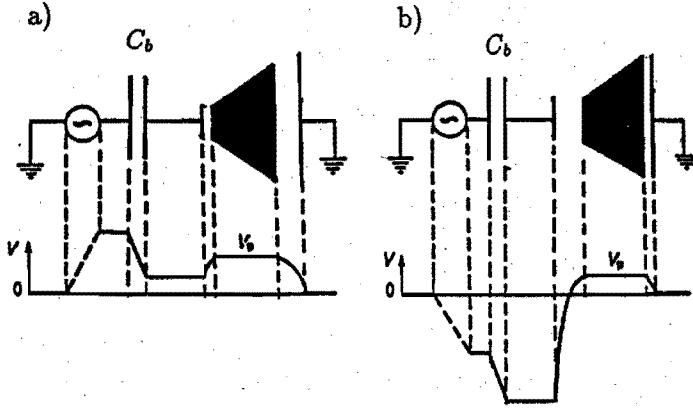
Figure 2.1: Schematical representation of the voltages in an AC coupled asymmetric RF plasma. a) maximum RF voltage condition, b) minimum RF voltage condition. V_p is the plasma potential.

on the sheath behaviour and the modulation of the sheath potential.

Good parameters to characterize the influence of the frequency is the ion ($\omega_{p,i}$) and the electron plasma frequency ($\omega_{p,e}$), given by:

$$\omega_{p,i}^2 = \frac{N_{i,0}q_i^2}{\varepsilon_0 m_i} \tag{2.1}$$

$$\omega_{p,e}^2 = \frac{N_{e,0}q_e^2}{\varepsilon_0 m_e} \tag{2.2}$$

where $N_{i,0}$ and $N_{e,0}$ are the ion and electron densities, q_i and q_e the ion and electron charges, m_i and m_e the ion and electron masses, respectively, and ε_0 the permittivity of free space. Under normal plasma condition $\omega_{p,i}/2\pi$ and $\omega_{p,e}/2\pi$ are of the order of 3 MHz and 0.9 GHz, respectively, (e.g., an argon plasma with ion and electron densities of $10^{16}\ m^{-3}$).

In the low frequency region where the RF field frequency is smaller than the ion plasma frequency ($\omega \ll \omega_{p,i} \ll \omega_{p,e}$) both the ions and the electrons follow the field oscillations in the sheath instantaneously. The low frequency RF plasma can be seen as a quasi DC discharge at every instant [Cha80, Glä89]. The transfer time of the ions to cross the sheath is shorter than 1 RF period and the energy of the ions will be between a minimum and a maximum energy determined by a minimum and a maximum sheath voltage as illustrated in figure 2.2.
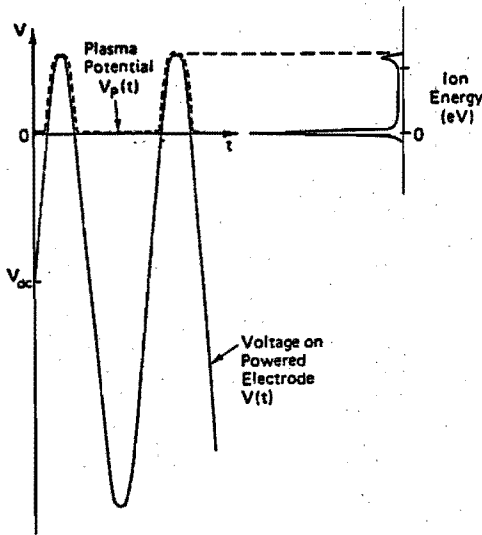
Figure 2.2: The relation-
ship between ion energies
and minimum and maxi-
mum sheath voltage in a
low frequency RF plama.
The sheath voltage in
this case is the difference
of the plasma potential
$V_p(t)$ and the grounded
electrode [Köh85b].

In the high frequency region the RF field frequency is larger than the ion plasma frequency but smaller than the electron plasma frequency ($\omega_{p,i} < \omega \ll \omega_{p,e}$). The ions cannot follow the field oscillations and their dynamic behaviour is determined by the time averaged field in the sheath. The transfer time to pass the sheath is several or more RF periods. The energy of the ions is determined by the averaged sheath potential. This is of course in the situation in which ions do not lose energy by collisions in the sheath. The ion current is rather constant in time. The electrons are able to react instantaneously to the field oscillations. Most of the RF period the sheath voltage is large so the electron current is negligible. The constant ion current is compensated by a short electron pulse at the moment the plasma potential equals the electrode potential.

In the 13.56 MHz plasma the ions can hardly follow the field oscillations but some RF modulation is observed in the ion dynamics with typical conse-quences for the ion energy distribution (IED). The energy of the ions when they do not collide in the sheath is in between a minimum and a maximum energy, with local maxima of the IED at this minimum and maximum energy as shown in figure 2.3. This distribution is called saddle structured. In chapter 3 and 5 this is discussed in more detail and illustrated by simulations and measure-ments, respectively, of the IED.
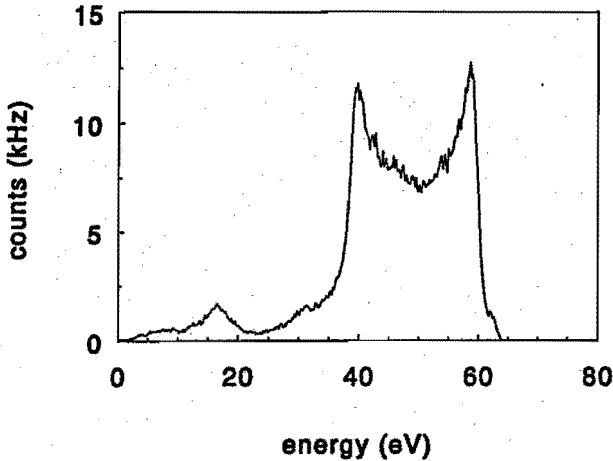
Figure 2.3: Measurment of the IED of ArH^+ in a 13.56 MHz plasma at 40 mTorr, showing a typically saddle structured IED. The features at energies lower than 39 eV are caused by collisions.

2.2.3 Sheath characterization

Based on the frequency classification, we can characterize the sheath behaviour in electrical terms. We can represent the RF plasma glow and sheath as shown in figure 2.4 [Köh85a].

The glow is quasi-neutral and is represented by a resistor R_g. The sheath can be treated as a capacitor (C_{s1}, C_{s2}), a resistor (R_{s1}, R_{s2}) and a diode, all coupled parallel. The diodes are present because the plasma potential is always positive with respect to the electrodes. It is known that the sheath behaviour is capacitive in the high frequency range [Gou64]. In analog circuit models of high frequency RF plasmas it is assumed that the resistors in the equivalent circuit are negligible (R_{s1}, $R_{s2} \to \infty$, $R_g = 0$) and the sheath is purely capacitive [Koe70]. These models are also known as capacitive sheath models (CSM) and are applied by Coburn *et al.* [Cob72] and Köhler *et al.* [Köh85a,b]. In these models the voltage drop across the sheaths ($V_{s1}(t)$, $V_{s2}(t)$), the plasma potential and the autobias are described as function of the ratio of the electrode areas. They give a good insight in the capacitive sheath behaviour. Because of the purely capacitive sheath approximation, the RF modulation of the sheath potentials and the plasma potential is sinusoidal. In figure 2.5 the
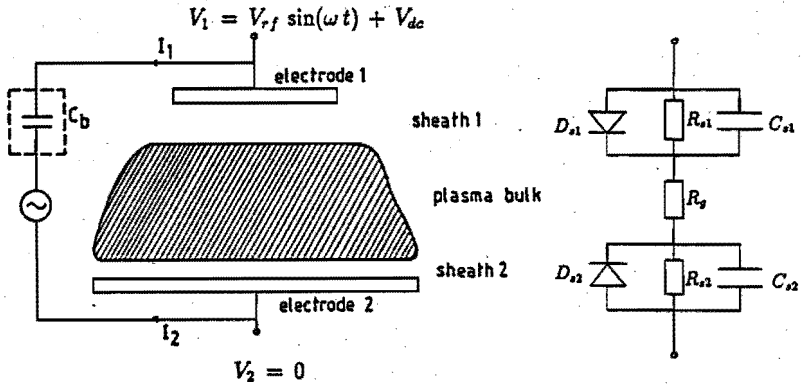
Figure 2.4: Equivalent electrical circuit of an RF plasma generated between two parallel electrodes. The impedance of the glow is represented by a resistor R_g, the sheaths by the capacitors C_{s1} and C_{s2} parallel to the resistors R_{s1} and R_{s2}. The diodes are present because the plasma glow has positive potentials with respect to the electrodes. The AC coupling of the RF generator to the electrodes has been indicated by the external blocking capacitor C_b. The amplitude of the RF voltage is V_{rf} and where V_{dc} represents the autobias voltage.

capacitive sheath behaviour is illustrated on the basis of three different electrode geometries. This has been done for an AC and a DC coupled RF plasma. The model containes no information about the dynamical sheath behaviour, the sheath kinetics, the sheath thickness and the electric field in the sheath. The CSM is elucidated in appendix A.

The CSM is used in this thesis to support the choice for a different electrode geometry, which makes it possible to measure the ion energies at the driven, smaller electrode. In etch reactors the etching takes place at this electrode, because here the averaged voltage drop is higher than that across the larger, grounded electrode. For practical reasons however, which are discussed in chapter 4, it is only possible to determine the mass resolved IED's at the grounded electrode. When the larger, previously grounded electrode can be driven, at the smaller grounded one higher sheath potentials develop. In the CSM shows that the higher potentials are the same, irrespective of the fact whether the electrode is driven or grounded (see appendix A).

The capacitive sheath nature has also as a consequence the fact that the conduction current is negligible with respect to the displacement current [Val88,
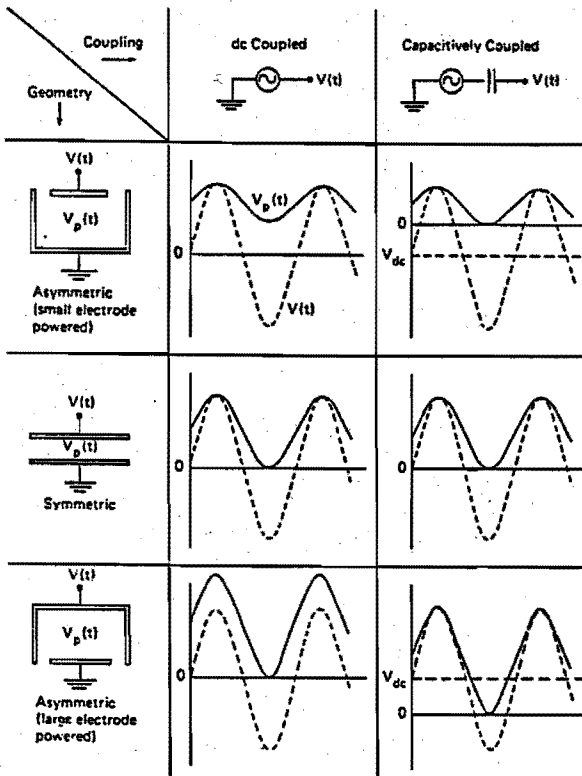
Figure 2.5: Illustration of the sheath potentials, assuming purely capacitive sheath behaviour and expressed as the difference between the plasma potential $V_p(t)$ (solid curves) and ground, and the plasma potential and the excitation electrode voltage (dashed curves), for three different electrode geometries and for an AC and DC coupled RF plasma [Köh85b].

Köh85b]. The displacement current is due to the movement of the space charge in the interelectrode space, which is a consequence of the modulation of the discharge potential.

In the low frequency region the displacement current is small compared to the conduction current. In this case the sheath voltage behaviour can be represented by neglecting the sheath capacitors in the equivalent circuit $(C_{s1}, C_{s2} \rightarrow 0)$. The sheath behaviour is resistive [Zar83] and the modulation of the RF sheath potential is non-sinusoidal (see appendix A) [Met86, Val88].

In the 13.56 MHz plasma, $\omega_{p,i}$ is only a little bit smaller than ω. The sheath behaviour is mainly capacitive although at higher input powers some influence of the resistive behaviour is noticed as will be shown in chapter 5. At higher input powers the ion density is increased. Consequently the conduction current,

although still quite small, has a certain influence on the sheath behaviour. As a further consequence, the modulation of the sheath potential is not entirely sinusoidal any more. The average voltage drop decreases a little bit, which is reflected in the IED. This will be shown in chapter 5.

The capacitive sheath model assumes that the sheath capacities are constant in time and are related to the electrode areas. Recently, Raizer and Schneider developed a high frequency model based on time dependent sheath capacities due to the time dependent sheath movements and sheath voltages [Rai92]. They assumed that the total charge in the two sheaths is constant in time. Based on the assumption that the ion density is the same everywhere in the sheath, the addition of the sheath thickness of both sheaths is constant. The model also shows that the modulation of the sheath potential and the plasma potential is only sinusoidal if the electrode areas are the same. In other cases an autobias voltage is generated and the modulation of the potentials is not sinusoidal. Particularly this is noticed at the plasma potential and the voltage drop across the sheath in front of the largest electrode as shown in figure 2.6b. The modulation of the voltage drop across the sheath in front of the smallest, AC coupled, electrode (the difference of the plasma potential and the excitation voltage) is mainly determined by the higher excitation voltage and hardly deviates from sinusoidal behaviour.

2.3 RF plasma sheath investigations

Because of the interest of the industry, a lot of research has been done on capacitively coupled RF plasmas. Plasma-wall interaction is an important issue, which is linked directly to the production techniques and industrial results. Industrial applications require control of the ion and radical flux towards the electrode or substrate and the energy and angular distribution of the ions.

The RF plasma glow region can be seen as the place where the plasma particles are produced. The sheath regions, separating the glow from the electrodes, have a dominant role in the transport of the charged particles.

When constructing models of RF sheaths it is possible to separate the sheath from the glow once the electron temperature or rather the electron energy distribution and the electron and ion densities of the glow region are known.

In contrast with the field in the glow, the electric field in the sheath is much higher. Here the positive ions are accelerated towards the electrode and
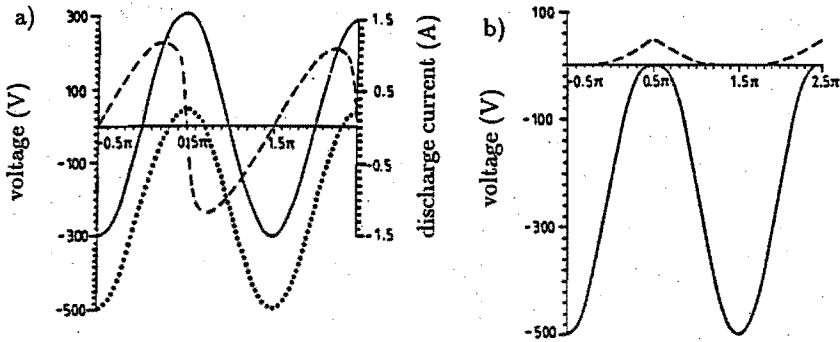
Figure 2.6: The time dependent behaviour of the voltage of the small, driven electrode and the sheath voltages in an AC coupled RF plasma. a) The full curve represents the generator voltage, the dotted curve the potential of the small electrode and the dashed curve represents the discharge current. b) The full and dashed curve represents the voltage drop near the small and large electrode respectively [Rai92].

the negative particles (ions, electrons) are repelled.

Analytically it is hard to calculate exactly the self-consistent electric field in the sheath, even in the case of a sheath in a DC discharge or a low frequency RF plasma which can be considered a sequence of DC discharges in time. Several authors published about the sheath formation in a DC discharge and the coupling between the plasma glow and the sheath [Ton29, Boh49, Sel63, Rie81, Poi86b, Bie88, Sch88, Bis89, Val89b].

High frequency sheath modelling is much more complicated, due to the time modulation of the space charge and because of the fact that the positive ions hardly can follow the field oscillations. The self-consistent time dependent approach can not be solved analytically. Several types of models are developed, all with their own approach and assumptions. Also a lot of models are developed to explain the sheath behaviour connected to a specific RF plasma reactor, electrode geometry or discharge configuration, and concentrate on the 13.56 MHz plasma. One can distinguish analog circuit models, analytic models, fluid models and kinetic or particle models, or a combination of these (hybrid models).

Analog circuit models are the least sophisticated models, describing the plasma glow and the sheath in electrical terms. They are developed mostly to predict the time averaged plasma and sheath potentials or to predict the

autobias voltage [Koe70, Kel79, Hor83, Köh85a, Köh85b, Rai92].

Analytic models based on the Poisson and Boltzmann equations will fully describe the plasma and the sheath. They not only include the transport equations for the charged particles but also the rate equations for the chemistry of the different species in the plasma. However, these general formulations are unfeasible to derive analytical expressions for e.g. the electric field or the ion velocity profile. Assumptions have to be made to get analytical results or numerical methods have to be used. The plasma glow and the sheath are often treated separately. Goedheer and Meijer [Goe91] calculated numerically the time dependent electric field in the sheath using the Boltzmann equation for the ions in combination with Poisson's law. They assumed a Maxwellian electron velocity distribution.

Many other authors who developed high frequency sheath models and dealt with the ion dynamics in the sheath, used Poisson's law in combination with expressions derived from the general Boltzmann equation like the Maxwell-Boltzmann electron density equilibrium,, the Hertz-Langmuir formula for the electron fluxes to the electrodes [Rie89] or the Child-Langmuir law for the space charge limited ion motion in the case of a collisionless sheath [Bie89, Far92a]. In the high pressure region where the sheath is collision dominated, mobility limited models are developed based on the ion mobility [Gra86, Ric87, Lie88, Lie89a]. All these approximate models are called fluid models and are often developed to calculate the local instantaneous electric field in the sheath or the electron and ion fluxes and densities. The solutions are not self-consistent, due to the approximations in the models. To calculate the electric field an assumption with respect to the ion density or the ion flux is made. For some models, the sheath conditions are not realistic although they contribute to the understanding of the sheath behaviour. Pointu [Poi87a] ,e.g., considered a constant sheath thickness while Farouki *et al.* [Far92b] considered a constant electric field and a time varying sheath thickness.

An expression for the IED has been derived by Benoit-Cattin and Bernard [Ben68]. They considered a constant sheath thickness and an RF modulated sheath voltage. The energy of an ion depends on the times the ion enters the sheath and hits the electrode. This model is not very realistic. The thickness of the space charge region is considered constant whereas in reality the thickness of this region is varying in time due to the time dependent voltage modulation across the sheath. Because an ion needs several RF periods to cross the sheath, the ion acceleration is strongly modulated. Also the model does not include the collisional effects on the IED in the sheath.

To model the acceleration and the collisional effects, Monte Carlo or Par-

ticle In Cell (PIC) simulations are required. Models based on these techniques are called particle or kinetic models. To determine an IED using a Monte Carlo simulation, the ion trajectories of many ions are calculated. The main difference between the simulations published in the literature is the assumption on the time and space dependent field in the sheath. Farouki *et al.* [Far92b] calculated ion trajectories using a homogeneous electric field in the sheath. Although the calculated IED lies in between a maximum and a minimum energy, the saddle structure differs strongly from measured distributions. Field *et al.* [Fie91] and May *et al.* [May92] used Monte Carlo simulations to investigate the effects of momentum transfer and resonant charge transfer on the IED of ions hitting the electrode. They used an electric field derived from the collisionless Child-Langmuir potential. Kushner [Kus85] and Liu *et al.* [Liu90] studied the IED and angular distribution of the ions striking the electrode, using a Monte Carlo model for the ion trajectories. Kushner used a parametrized model for the time dependent electric field within the sheath, while Liu *et al.* used a spatially uniform RF electric field. Manenschijn [Man91a] and Wild and Koidl [Wil91] prescribed the ion density in the sheath and derived an expression for the electric field. This field is used to calculate the IED showing collisional features, using a Monte Carlo method.

PIC simulation is an efficient computational technique to solve problems dealing with a large number of particles forming a self-consistent system under externally imposed forces. Birdsall *et al.* [Bir85, Pro90], Vender and Boswell [Ven90] and van Breda *et al.* [Bre92] applied the PIC method to simulate the high frequency RF plasma. Although these calculations are self-consistent the results strongly depend on the kinetic phenomena which are included.

The high frequency RF sheath has also been investigated experimentally, with most of the experiments concentrating on the 13.56 MHz capacitively coupled RF plasma. The ion dynamics in the sheath can be studied by emission and laser induced fluorescence (LIF) measurements [Got84, Mei91, Hai92]. Although the emission rate in the sheath is quite low due to the small electron density in the sheath, the sheath movements have been localized. LIF measurements have been carried out to determine the time dependent electric field in the sheath and to study the ion dynamics in the transition region between the glow and the sheath. Flux measurements have been performed to determine absolute fluxes of positive ions hitting the electrode in a SF_6 and O_2 RF plasma [Man89]. Temporal ion and electron current modulations have been measured by Wild and Koidl [Wil91].

Non-mass-resolved IED's are determined by several investigators using retarding grid energy analyzers. In 1972 Coburn and Kay presented the first

mass-resolved IED measured at the large, grounded electrode of a 13.56 MHz plasma [Cob72]. Köhler _et al._ extended these investigations and determined the averaged plasma potential from the IED in an argon plasma [Köh85a, Köh85b]. Thompson _et al._ [Tho86] and Ingram _et al._ [Ing88] used a retarding grid analyzer to measure the IED (non-mass-resolved) at the grounded electrode. Green _et al._ [Gre88] measured the energy and the current of Ar^+ and ArH^+ impinging on the grounded electrode. Kuypers [Kuy89], Manenschijn [Man91b] and Wild and Koidl [Wil91] determined the non-mass-resolved IED at the powered electrode. Both Kuypers and Manenschijn used an electrostatic energy analyzer built directly behind the powered electrode. Because the analyzer is instantaneously coupled to the voltage of the powered electrode, the output coupling of the detector signal has to be done by complex electrical circuits or opto-coupling systems. Wild and Koidl used an electrode geometry with a large driven electrode similar to the method used in this thesis. All the results are non-mass-resolved which restrict the experiments to simple atomic systems and to low pressure IED determination to exclude collisional features. Otherwise the IED's are very complex and features from one specific ionic species are difficult to recognize.

Recently commercially available energy analyzing systems coupled to a mass-spectrometer are developed by VG, Hayden and Balzers. The first measurements using these systems are already published. Janes _et al._ [Jan92] used a system to determine the mass-resolved IED and angular distribution at the driven electrode in an O_2 RF plasma in an open electrode geometry. Recent publications also show that the interpretation of the IED requires knowledge about the technical aspects of the diagnostic. Olthoff _et al._ [Olt92] measured several species in an argon RF plasma and interpreted the IED's of the Ar^+ and Ar^{2+} as within the same energy range while in reality the doubly charged ions gain double as much energy in the sheath as the singly charged ions.

This thesis presents mass-resolved IED's at both the largest and smallest electrode. The plasma is completely confined in the electrode geometry. The ratio of the electrode area is such that the voltage across the sheath in front of the largest electrode is considerably modulated. This in contrast to an open electrode geometry where the plasma potential is nearly time independent and equals the floating potential. Measurements of the IED's at the smallest, i.e. the grounded electrode are similar to the IED's at the powered electrode in an etch reactor. IED's determined in CF_4, N_2 and Ar plasmas are presented. From the IED's, ion- molecule reactions which occur in the CF_4 sheath, can be studied.

Appendix A: Analog circuit models

A.1 The capacitive sheath model

In the capacitive sheath model we assume the sheath to be purely capacitive and the plasma glow to be equipotential (R_{s1}, $R_{s2} \to \infty$, $R_g = 0$). The RF plasma can be represented as shown in figure A.1.
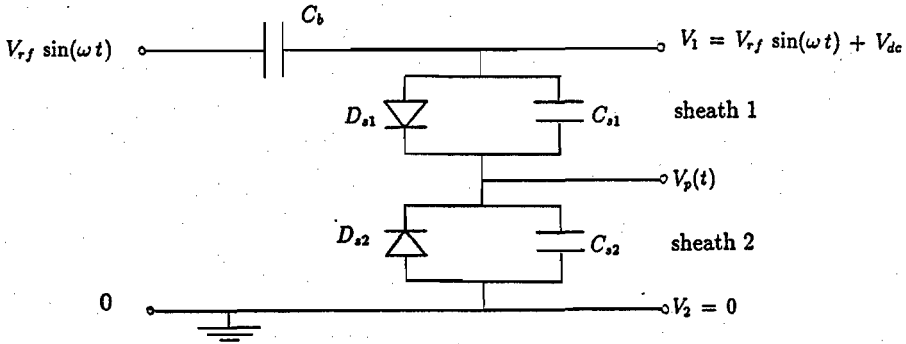
Figure A.1: Equivalent circuit of the capacitive sheath model. C_{s1} and C_{s2} are capacities representing the sheath. D_{s1} and D_{s2} are diodes providing that the plasma potential $V_p(t)$ is alwys positive with repect to the electrodes.

The voltage of the driven electrode is given by

$$V_1 = V_{dc} + V_{rf} sin(\omega t), \tag{A.1}$$

where V_{rf} is the amplitude of the excitation voltage and V_{dc} the autobias voltage. Because of the pure capacitive sheath behaviour, the plasma potential $V_p(t)$ can be expressed as

$$V_p(t) = \overline{V}_p + \Delta V_p sin(\omega t), \tag{A.2}$$

where $\overline{V}_p$ is the time averaged plasma potential and ΔV_p the amplitude of the modulation of the plasma potential. ΔV_p is determined by the capacitive voltage

division of V_{rf} and is given by

$$\Delta V_p = \frac{C_{s1}}{C_{s1} + C_{s2}} V_{rf}, \tag{A.3}$$

where C_{s1} and C_{s2} are the capacities representing the sheath in front of the driven and the grounded electrode, respectively. The instantaneous plasma potential is always higher than the electrode potentials. This means that

$$V_{p,max} = \overline{V}_p + \Delta V_p \geq V_{dc} + V_{rf}, \tag{A.4}$$

$$V_{p,min} = \overline{V}_p - \Delta V_p \geq 0 \tag{A.5}$$

In the AC coupled circuit, once every period the plasma potential equals as well the driven electrode potential as the grounded one to balance the net current through the sheath. This means that (A.4) and (A.5) becomes equalities. $\overline{V}_p$ can be expressed in terms of V_{rf} and V_{dc}

$$\overline{V}_p = \frac{1}{2} (V_{dc} + V_{rf}). \tag{A.6}$$

The relation between V_{dc} and V_{rf} can be calculated from (A.3), (A.5) and (A.6) and expressed with the help of the sheath capacities

$$V_{dc} = \frac{C_{s1} - C_{s2}}{C_{s1} + C_{s2}} V_{rf}. \tag{A.7}$$

$\overline{V}_p$ also can be expressed in terms V_{dc} and hence in terms of V_{rf}

$$\overline{V}_p = \frac{C_{s1}}{C_{s1} - C_{s2}} V_{dc} = \frac{C_{s1}}{C_{s1} + C_{s2}} V_{rf}. \tag{A.8}$$

The time dependent voltage across the sheaths $V_{s1}(t)$ and $V_{s2}(t)$ can be described by

$$V_{s1}(t) = \frac{C_{s2}}{C_{s1} + C_{s2}} V_{rf} - \frac{C_{s2}}{C_{s1} + C_{s2}} V_{rf} sin(\omega t), \tag{A.9}$$

$$V_{s2}(t) = \frac{C_{s1}}{C_{s1} + C_{s2}} V_{rf} + \frac{C_{s1}}{C_{s1} + C_{s2}} V_{rf} sin(\omega t). \tag{A.10}$$

From equation (A.7) it is clear that the autobias voltage is negative if $C_{s2} > C_{s1}$. This is the case if the driven electrode is smaller than the grounded one. In reality C_{s1} and C_{s2} are determined by the average sheath thickness and the electrode areas. The plasma will be identical when the ratio of the areas is the same, whether the grounded or the driven one is the largest. The largest

voltage across the sheath will occur across the sheath in front of the smallest electrode. Also the voltage modulation will be the same. This means that the sheath in front of the smallest electrode always will be the same whether it is the driven or the grounded electrode if both the ratio of the electrode areas and the electrode gap are held constant. The only difference between a small or a large driven electrode is the autobias voltage. In the case of a large, AC coupled driven electrode the autobias is positive, while in the case of a small driven electrode it is negative, but the absolute values are the same. From equation (A.9) and (A.10) it is clear that the sheath modulation is sinusoidal in the pure capacitive sheath approximation.

Although the time averaged sheath capacities C_{s1} and C_{s2} will be determined primarily by the relative area of the electrodes, they are also influenced significantly by the magnitude of the voltage drops across both sheaths [Köh85a, Koe70]. A lot of investigations have already been done on the relation between the autobias and the excitation voltage [God76, God80, Köh85b, Poi86a, Poi87b, Lie88, Rie89, Vall89, Lie89b, Mei91] ,but there is still a small, unexplained difference between the experiments and the models used. The capacitive sheath model must be seen as a good approximation of the high frequency RF plasma.

A.2 The resistive sheath model

The resistive sheath model can be applied in the low frequency range, where the displacement current is much smaller than the ion conduction current. The sheath capacities in the equivalent circuit (figure 2.4) are negligible (C_{s1}, $C_{s2} \rightarrow 0$) and the plasma glow is assumed to be equipotential ($R_g = 0$). The sheath can be considered as purely resistive. The plasma potential instantaneously follows the electrode potential, although the plasma potential is always higher than the electrode potentials. The plasma potential can be described by [Köh85b]

$$V_p(t) = V_{rf}sin(\omega t) + V_{dc} + V_f \quad \text{if} \quad V_{rf}sin(\omega t) + V_{dc} > 0, \quad (A.11)$$

$$V_p(t) = V_f \quad\quad\quad\quad\quad\quad\quad \text{if} \quad V_{rf}sin(\omega t) + V_{dc} \leq 0, \quad (A.12)$$

where V_f, the floating potential, is given by [Cha80] as

$$V_f = \frac{kT_e}{2e} \, ln\left(\frac{m_i}{2.3m_e}\right). \quad (A.13)$$
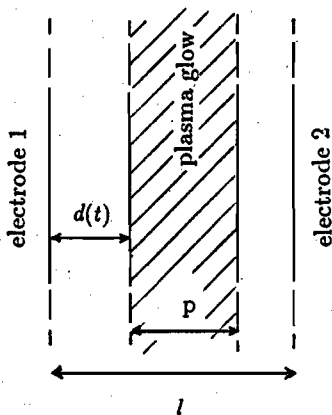
Figure A.2: The plasma glow between two infinite long electrodes. The electrode gap is l, the glow width p, and d(t) the time dependent thickness of the sheath in front of electrode 1.

with k the Boltzmann constant, T_e the electron temperature, e the elementary charge, m_i and m_e the ion and electron masses, respectively. The time dependency of $V_p(t)$ is depicted in figure 2.2.

The modulation of the sheath voltage is far from sinusoidal. This is also shown by [Val88, Poi86b, Met86]. As a consequence of the resistive sheath behaviour the averaged sheath voltage drop is lower than in the case of the capacitive sheath.

The applicability of the capacitive or resistive sheath model is determined mainly by the ratio of the displacement to conduction current. The conduction current J_c equals the averaged ion current which enters the sheath. This can be determined from the ion density at the presheath sheath transition $N_{i,0}$ and the Bohm velocity u_{Bohm} at which the ions enter the sheath [Boh49]

$$J_c = e\,N_{i,0}\,u_{Bohm}, \qquad\qquad (A.14)$$

where e is the elementary charge.

The displacement current can be derived from the change of the electric flux to the electrode due to the change of the position of the electrons imposed by the RF modulation. The ion density may be considered constant and homogeneous distributed so the ions cause no change of the net electromagnetic flux to the electrode.

We consider a plasma between two infinite long electrodes. The gap between the electrodes is l, and the glow width is p. This is schematically shown in figure A.2. The electrons are confined to the glow which oscillates between the electrodes. The time dependent thickness of the sheath in front of electrode 1 is $d(t)$. The flux $\varphi(x)$ from electrode 1 to the electrons in the glow which are at

a position x from electrode 1, is

$$\varphi(x) = e N_e \left(1 - \frac{x}{l}\right), \tag{A.15}$$

where N_e is the electron density in the glow. The factor $\left(1 - \frac{x}{l}\right)$ can be derived from fundamental electromagnetic theory. The total flux from electrode 1 to the electrons in the glow is given by

$$\varphi(t) = \int_{d(t)}^{p+d(t)} e N_e \left(1 - \frac{x}{l}\right) dx, \tag{A.16}$$

$$= e N_e \left[p - \frac{p^2}{2l} - \frac{pd(t)}{l}\right]. \tag{A.17}$$

The displacement current $J_d(t)$ is given by the variation of the flux in time

$$J_d(t) = \frac{d\varphi(t)}{dt} = -e N_e \frac{p}{l} \frac{d}{dt}(d(t)). \tag{A.18}$$

When we assume a sinusoidal sheath thickness variation

$$d(t) = \frac{d_{max}}{2} \left(1 + \sin(\omega t)\right), \tag{A.19}$$

where d_{max} is the maximum sheath thickness. The displacement current then becomes

$$J_d(t) = -e N_e \omega \frac{d_{max}}{2} \frac{p}{l} \cos(\omega t). \tag{A.20}$$

For d_{max} one finds

$$d_{max} = l - p \tag{A.21}$$

Equation (A.20) now becomes

$$J_d(t) = -e N_e \omega \frac{d_{max}}{2} \left(1 - \frac{d_{max}}{l}\right) \cos(\omega t). \tag{A.22}$$

For real situation d_{max}/l may be estimated at 0.3. The effective, time averaged displacement current

$$J_d \simeq -e N_e \omega d_{max}. \tag{A.23}$$

N_e and $N_{i,0}$ are equal due to the quasi neutrality of the plasma glow. The ratio between J_d and J_c now becomes

$$\frac{J_d}{J_c} = \frac{d_{max} \omega}{u_{Bohm}}. \tag{A.24}$$

Equation (A.24) can be interpreted as the number of RF periods which an ion with the Bohm velocity needs to cross the sheath. When an ion needs more

than 1 period the sheath is capacitive. The sheath thickness is in the order of 1 to 10 mm and the Bohm velocity is about 10^3 (for argon ions) to 10^4 m/s (for hydrogen ions). In a 13.56 MHz plasma the sheath is capacitive, although for the light ion plasmas like hydrogen the criterion is just fulfilled. The sheath in a 100 kHz plasma is resistive.

References

[Ben68]   P. Benoit-Cattin and L. Bernard, *J. Appl. Phys.* **39**, 5723 (1968).

[Bie88]   S. Biehler, G. Ecker and K.-U. Riemann, *Phys. Fluids* **31**, 1999 (1988).

[Bie89]   S. Biehler, *Appl. Phys. Lett.* **54**, 317 (1989).

[Bir85]   C.K. Birdsall and A.B. Langdon, *Plasma Physics via Computational Simulation*, (McGraw-Hill, New York, 1985).

[Bis89]   R.C. Bissel, P.C. Johnson and P.C. Stangeby, *Phys. Fluids*, **B1**, 1133 (1989).

[Boh49]   D. Bohm, *The Characteristics of Electrical Discharges in Magnetic Fields*, (McGraw-Hill, New York, 1949).

[Bre92]   J. van Breda, internal report, Eindhoven University of Technology, the Netherlands, VDF/NG 92-02, 1992.

[Cha80]   B. Chapman, *Glow discharge processes.* (Wiley, New York, 1980).

[Cob72]   J.W. Coburn and E. Kay, *J. Appl. Phys.* **43**, 4965 (1972).

[Far92a] R.T. Farouki and M. Dalvie, *J. Appl. Phys.* **68**, 6106 (9192).

[Far92b] R.T. Farouki, S. Hamaguchi and M. Dalvie, *Phys. Rev. A*, *45*, 5913 (1992).

[Fie91]   D. Field, D.F. Klemperer, P.W. May and Y.P. Song, *J. Appl. Phys.* **70**, 82 (1991).

[Glä89]   A.O. Glänzer, internal report, Eindhoven University of Technology, the Netherlands, VDF/NT 89-18, 1989.

[God76]   V.A. Godyak, *Sov. J. Plasma Phys.* **2**, 78 (1976).

[God80]   V.A. Godyak and Z.Kh. Ganna, *Sov. J. Plasma Phys.* **6**, 372 (1980).

[Goe91]   W.J. Goedheer and P.M. Meijer, *IEEE Trans. Plasma Sci.* **19**, 245 (1991).

[Got84]   R.A. Gottscho, R.H. Burton, D.L. Flamm, V.M. Donnely and G.P Davies, *J. Appl. Phys*, **55**, 2707 (1984).

[Gou64]   R.W. Gould, *Phys. Lett.* **11**, 236 (1964).

[Gra86]   D.B. Graves and K.F. Jensen, *IEEE Trans. Plasma Sci.* **14**, 78 (9186).

[Gre88]   W.M. Green, M.A. Hartney, W.G. Oldham and D.W. Hess, *J. Appl. Phys.* **63**, 1367 (1988).

[Hai92]   M. Hain, R.J.M.M. Snijkers, G.M.W. Kroesen and F.J. de Hoog, submitted to *Appl. Phys. Lett*, (1992).

[Hav91]   M. Haverlag, *Plasma chemistry of fluorocarbon RF discharges used for dry etching.* Ph.D. thesis, Eindhoven University of Technology, the Netherlands, 1991.

[Hor83]   C.M. Horwitz, *J. Vac. Sci. Technol.* A **1**, 60 (1983).

[Ing88]   S.G. Ingram and N.St.J. Braithwaite,

           J. Phys. D: Appl. Phys. **21**, 1496 (1988).

[Jan92]   J. Janes and C. Huth, *J. Vac. Sci. Techn.* A **10**, 3086 (1992).

[Kel79]   J.H. Keller and W.B. Pennebaker, *IBM J. Res. Develop.* **23**, 3 (1979).

[Koe70]   H.R. Koenig and L.I. Maissel, *IBM J. Res. Dev.* **14**, 168 (1970).

[Köh85a]   K. Köhler, J.W. Coburn, D.E. Horne, E. Kay and J.H. Keller,
           J. Appl. Phys. **57**, 59 (1985).

[Köh85b]   K.Köhler, D.E. Horne and J.W. Coburn, *J. Appl. Phys.* **58**, 3350 (1985).

[Kus85]   M.J. Kushner, *J. Appl. Phys.* **58**, 4024 (1985).

[Kuy89]   A.D. Kuypers, *High flux reactive-ion etching in a magnetic multipole reactor.* Ph.D. thesis, Utrecht, the Netherlands, 1989.

[Lie88]   M.A. Liebermann, *IEEE Trans. Plasma Sci.* **16**, 638 (1988).

[Lie89a]   M.A. Liebermann, *IEEE Trans. Plasma Sci.* **17**, 338 (1989).

[Lie89b]   M.A. Liebermann, *J. Appl. Phys.* **65**, 4186 (1989).

[Liu90]   J. Liu, G.L. Huppert and H.H. Sawin, *J. Appl. Phys.* **68**, 3916 (1990).

[Man89]   A. Manenschijn, G.C.A.M. Janssen, E. van der Drift and S. Radelaar,
           Proc. IXth ISPC, edited by R. d'Agostino (Pugnochiuso, Italy, 1989).

[Man91a]   A. Manenschijn and W.J. Goedheer, *J. Appl. Phys.* **69**, 2923 (1991).

[Man91b]   A. Manenschijn, *Ion bombardment and ion-assisted etching in RF discharges.* Ph.D. thesis, Delft University of Technology,
           the Netherlands, 1991.

[May92]   P.W. May, D. Field and D.F. Klemperer, *J. Appl. Phys.* **71**, 3721 (1992).

[Mei91]   P.M. Meijer, *The electron dynamics of RF discharges.*
           Ph.D. thesis, Utrecht, the Netherlands, 1991.

[Met86]   A. Metze, D.W. Ernie and H.J. Oskam, *J. Appl. Phys.* **60**, 3081 (1986).

[Olt92]   J.K. Olthoff, R.J. van Brunt and S.B. Radovanov,
           J. Appl. Phys. **72**, 4566 (1992).

[Poi86a]   A.M. Pointu, *Appl. Phys. Lett.* **48**, 762 (1986).

[Poi86b]   A.M. Pointu, *J. Appl. Phys.* **60**, 4113 (1986).

[Poi87a]   A.M. Pointu, *Appl. Phys. Lett.* **50**, 316 (1987).

[Poi87b]   A.M. Pointu, *Appl. Phys. Lett.* **50**, 1047 (1987).

[Pro90]   R.J. Procassini, C.K. Birdsall and E.C. Morse,
           Phys. Fluids, **B2**, 3191 (1990).

[Rai92]   Yu.P. Raizer and M.N. Schneider,
           Plasma Sources Sci. Techn. **1**, 102 (1992).

[Ric87]   A.D. Richards, B.E. Thompson and H.H. Sawin,
           Appl. Phys. Lett. **50**, 492 (1987).

[Rie81]   K.-U. Riemann, *Phys. Fluids*, **24**, 2163 (1981).

[Rie89]   K.-U. Riemann, *J. Appl. Phys.* **65**, 999 (1989).

[Roo91]   A.J. van Roosmalen, J.A.G. Baggerman and S.J.H. Brader,
          Dry etching for VLSI, (Plenum, New York, 1991).

[Sam93]   M.J.M. van Sambeek, internal report, Eindhoven University of
          Technology, the Netherlands, VDF/NG 93-05, 1993.

[Sel63]   S.A. Self, *Phys. Fluids*, **6**, 1762 (1963).

[Sch88]   J.T. Scheuer and G.A. Emmert, *Phys. Fluids*, **31**, 1748 (1988).

[Tho86]   B.E. Thompson, K.D. Allen, A.D. Richards and H.H. Sawin,
          J. Appl. Phys. **59**, 1890 (1986).

[Ton29]   L. Tonks and I Langmuir, *Phys. Rev.* **34**, 876 (1929).

[Val88]   P.M. Vallinga, *Modelling of RF plasmas in a parallel plate etch reactor*,
          Ph.D. thesis, Eindhoven University of Technology, the Netherlands, 1988.

[Val89a] P.M. Vallinga, P.M. Meijer and F.J. de Hoog,
          J. Phys. D. **22**, 1650 (1989).

[Val89b] P.M. Vallinga and F.J. de Hoog, *J. Phys. D.* **22**, 925 (1989).

[Ven90]   D. Vender and R.W. Boswell, *IEEE Trans. Plasma Phys.* **18**, 725 (1990).

[Wil91]   C. Wild and P. Koidl, *J. Appl. Phys.* **69**, 2909 (1991).

[Win84a] R. Winkler, H. Deutsch, J. Wilhelm and Ch. Wilke,
          Beitr. Plasmaphys. **24**, 285 (1984).

[Win84b] R. Winkler, H. Deutsch, J. Wilhelm and Ch. Wilke,
          Beitr. Plasmaphys. **24**, 303 (1984).

[Zar83]   C.B. Zarowin, *J. Electrochem. Soc.* **130**, 1144 (1983).

3 The RF sheath

3.1 Introduction

The ion energy distributions (IED's) which are experimentally determined in the high frequency sheath, show saddle structures typical for RF discharges, and at higher pressures also collisional features. Simplified models which deal with a constant thickness of the space charge region or a time varying linear electric field in the sheath, are not very realistic and there is a lack of agreement between the measured and the theoretically derived IED's.

In this chapter, more realistic solutions for the electric field in the sheath, both in the low and high frequency region are developed. The sheath is considered to be collisionless which means that the energy is conserved. The electric field is determined by the space charge in the sheath and obeys Poisson's law. The sheath thickness is implicitly determined by the sheath models and depends on the boundary conditions like the ion density in the glow and the imposed sheath voltage.

In the low frequency case, which is described in section 3.2, the ions and electrons react instantaneously to the oscillations of the electric field with respect to the RF frequency. Therefore the sheath in the low frequency region may be treated as a DC sheath. The electric field in the ionic sheath where the electrons can be neglected, can be determined self-consistently. It is shown that the influence of the electrons which are assumed to obey the Maxwell-Boltzmann relation, is restricted to a small region at the beginning of the sheath. The IED in the low frequency region is determined by the time modulation of the sheath voltage, due to the relatively short transit time of the ions to cross the sheath with respect to the RF period.

The high frequency region is discussed in section 3.3. In this case the ions can not follow the field oscillations in the sheath, due to their inertia. Their

31

density may be assumed constant in time. The electron mobility is high and they react instantaneously to the sheath voltage modulation. Two models are developed to describe the time dependent electric field in the high frequency sheath. They deal with the collisionless sheath and are quasi-self-consistent. The first model (A) is based on the self-consistent solution for the DC sheath; it is adapted to the high frequency case. This model is explained in subsection 3.3.2. The second model (B) is elucidated in appendix B and is based on results of Particle-in-Cell (PIC) simulations. This model leads to a simpler expression for the electric field, although the model is less sophisticated.

The time dependent electric fields are applied to simulate the IED (subsection 3.3.3). These are compared with experimentally determined IED's in chapter 5. Collisional features have been investigated by Monte Carlo simulations. Here we distinguish charge exchange collisions and elastic momentum transfer. The effects of these collisions on the IED are quite different as will be shown in subsection 3.3.4.

In electro-negative gases, negative ions are produced. Due to the positive plasma potential and the voltage decrease in the sheath, they are repelled from the sheath and because of their low temperature the negative ion density in the sheath may be neglected. However, the negative ions influence the Bohm velocity at which the positive ions have to enter the sheath. Consequently this affects the ion density in the sheath and thus also the electric field and the sheath thickness. This holds in both the DC and the high frequency sheath.

3.2 The sheath in the low frequecy region

In the low frequency region ($\omega \ll \omega_{p,i}$), the electrons and the ions reacts instantaneously to the time modulation of the sheath voltage and the sheath structure is similar to the DC sheath.

The first, simplified analytic sheath model for DC discharges was published in 1929 by Tonks and Langmuir [Ton29]. They considered collisionless ion transport through the sheath and solved the Poisson equation by Taylor expansion. A problem which arose was the coupling between the quasineutral glow and the sheath region. Bohm solved this problem in 1949 by introducing the Bohm criterion [Boh49]. This criterion assumes a monoenergetic ion beam which enters the space charge region with at least the Bohm velocity u_{Bohm} given by
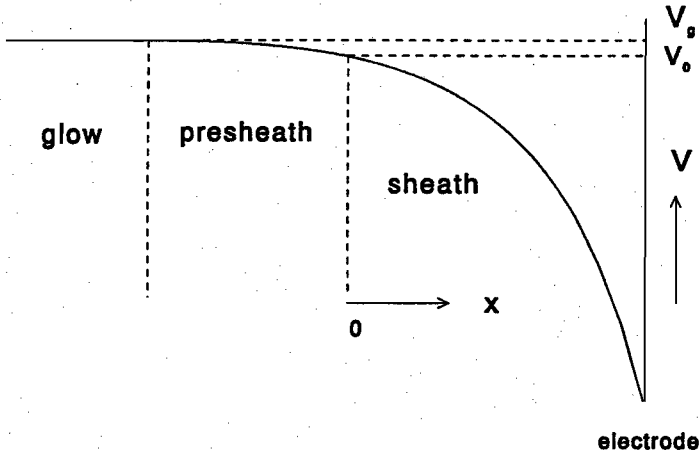
$$u_{Bohm} = \sqrt{\frac{kT_e}{m_i}}, \tag{3.1}$$

Figure 3.1: A schematic view of the sheath and presheath formation in a plasma. The potential at the sheath edge is V_0. V_g is the potential of the plasma glow.

where k is the Boltzmann constant, T_e the electron temperature and m_i the ion mass. When the velocity is less, a negative space charge will arise which conflicts with the monotoneous voltage drop in the sheath. The ions acquire the Bohm velocity in the quasineutral presheath region between the glow and the sheath [Boh49, Rie91] (see figure 3.1). Harrison and Thompson [Har59], Caruso and Cavaliere [Car62] and Riemann [Rie81, 89] generalized the Bohm criterion by taking into account e.g. the ion energy distribution, but the criterion did not change in essence. A review about the Bohm criterion is written by Riemann in 1991 [Rie91]. In the treatment of the sheath given in this section, we assume the Bohm criterion to be fulfilled. The Bohm energy is small with respect to the energy of the ions which they gain in the sheath and has not a large influence on the sheath structure. The sheath models only consider the region between the presheath and the electrode. At the sheath-presheath edge the ion and electron densities are lower with respect to the glow due to the small presheath voltage drop. The densities at the edge ($N_{i,0}$ and $N_{e,0}$) are given by [Boh49]

$$N_{i;e,0} = 0.607 \, N_{i;e,glow}. \tag{3.2}$$

When we consider a collisionless sheath and take into account only positive ions and electrons, the exact solution of the self-consistent sheath with a certain

voltage across the sheath and ion density at the sheath edge, can be calculated numerically . The electric field ($\mathcal{E}(x)$) in the sheath satisfies Poisson's equation in which the space charge density (ρ) is determined by the ion (N_i) and electron (N_e) densities in the sheath

$$\frac{d^2V(x)}{dx^2} = -\frac{d\mathcal{E}(x)}{dx} = -\frac{e}{\varepsilon_0}(N_i(x) - N_e(x)), \tag{3.3}$$

e is the elementary charge and x is the position in the sheath with x equals to zero at the position at the sheath edge. The ion density is assumed to consist of singly charged ions. The electrons are assumed to have a Maxwellian distribution so the electron density may be described by the Boltzmann relation

$$N_e(x) = N_{e,0}\exp\left(\frac{-e(V_0 - V(x))}{kT_e}\right), \tag{3.4}$$

where $V(x)$ is the potential distribution in the sheath, V_0 the potential at the sheath edge. The electron density in the sheath is small and we assume that the production of ions in the sheath is negligible. The ions are accelerated in the sheath and the flux is conserved

$$N_i(x)\,u_i(x) = N_{i,0}\,u_{i,0}, \tag{3.5}$$

where $u_i(x)$ the ion velocity in the sheath. The ion density at the sheath edge $N_{i,0}$ equals $N_{e,0}$ due to the quasineutrality in the glow and the presheath. $u_{i,0}$ is the ion Bohm velocity. The ions are accelerated in the space charge field and the ion motion satisfies

$$\frac{e}{m_i}\,\mathcal{E}(x) = u_i(x)\frac{du_i(x)}{dx}. \tag{3.6}$$

Combination of equations (3.3) to (3.6) with the fact that the energy is conserved in the collisionless sheath leads to an integro-differential expression for the ion velocity

$$\frac{dv_i}{dx} = \frac{\omega_{p,i}\sqrt{2}}{v_i u_{i,0}}\sqrt{\frac{u_{i,0}^2}{2\omega_{p,i}^2}\left(\left[v_i\frac{dv_i}{dx}\right]_{x=0}\right)^2 + (v_i - 1) - \frac{1}{2W_0}[1 - \exp(W_0(1 - v_i^2))]}, \tag{3.7}$$

where v_i is the normalized velocity

$$v_i = \frac{u_i}{u_{i,0}}, \tag{3.8}$$

$\omega_{p,i}$ the ion plasma frequency given by equation (2.1) and

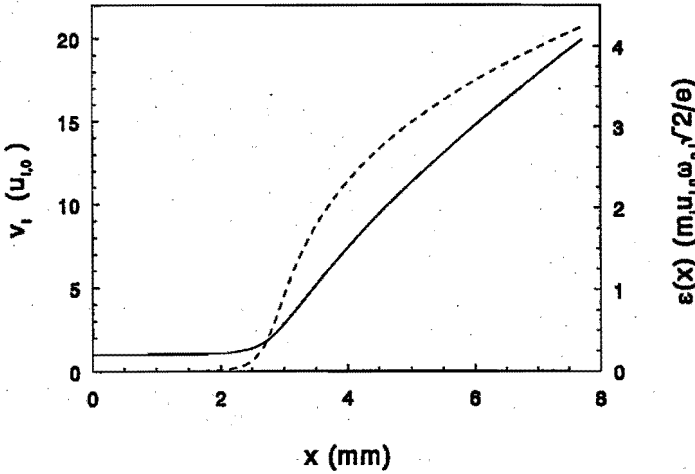$$W_0 = \frac{m_i u_{i,0}^2}{2kT_e}. \tag{3.9}$$

Figure 3.2: The numerically, exact solution of the velocity profile (solid line) and the electric field (dashed line) in a collisionless DC sheath in argon. The ion density in the glow is 10^{16} m^{-3}. The profile corresponds to a sheath voltage of 400 V at an electron temperature of 2 eV.

W_0 equals 0.5 when the ions fulfil the Bohm criterion strictly. The first term in (3.7) represents the electric field at the sheath edge and can be assumed zero, due to the quasi-neutrality of the presheath. Equation (3.7) can be solved numerically with a Runge Kutta method. The sheath thickness d_{sh} depends on the imposed voltage across the sheath which determines the velocity at the electrode.

The result for the sheath in an argon plasma with an ion density of 10^{16} m^{-3} at the sheath edge, a sheath potential of 400 V and an electron temperature of 2 eV is shown in figure 3.2 ($\omega_{p,i}$ is 20.8 MHz and $u_{i,0}$ is 2.20 10^3 m/s). Because of the increase of the ion velocity, the ion density decreases towards the electrode. The electron density decreases even more rapidly, due to the generated space charge field. The density profiles are shown in figure 3.3 where they are represented in normalized units

$$n_{i,e} = \frac{N_{i,e}}{N_{i;e,0}}. \tag{3.10}$$

As shown in figure 3.3, the influence of the electrons is limited to the beginning of the sheath and the largest part of the sheath is dominated by the ions. The

sheath thickness develops so that the integrated space charge fulfils the imposed voltage conditions. Although the sheath region stretches mathematically from 0 to 7.74 mm, the space charge becomes significant only from about 2.5 mm. Therefore it is proper to define the sheath as the space charge region. This is to be more specific in figure 3.3, the region beyond 2.5 mm.
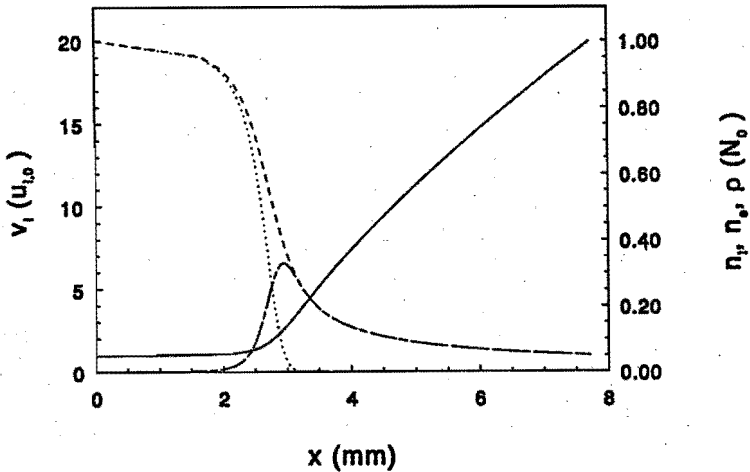

Figure 3.3: The numerically, exact solution of the ion density (dashed line), the electron density (dotted line) and the space charge (dash dotted line) in an argon DC sheath. The solid line is the velocity profile. The conditions are the same as in figure 3.2.

To describe the sheath analytically, it is possible to use the following arguments. The electron density in the sheath decreases rapidly (see figure 3.3). Due to this we may consider an electron free sheath where the electron density is approximated by a step function at the sheath edge. Then an analytic self-consistent expression for the velocity profile in the sheath can be derived. The space charge is caused by the ions and equation (3.7) becomes

$$\frac{dv_i}{dx} = \frac{\omega_{p,i}\sqrt{2}}{v_i u_{i,0}} \sqrt{\frac{u_{i,0}^2}{2\omega_{p,i}^2} \left(\left[v_i \frac{dv_i}{dx} \right]_{x=0} \right)^2 + (v_i - 1)}, \qquad (3.11)$$

This equation can be solved analytically. First we write equation (3.11) in normalized units. For that purpose we define the dimensionless position y in

the sheath as

$$y = \frac{x}{d_{sh}},$$
(3.12)

where d_{sh} is the sheath thickness. d_{sh} depends on the sheath voltage, the space charge in the sheath and the Bohm velocity. It will be determined absolutely from the calculated dimensionless profiles in the sheath. Until then d_{sh} will be treated as a general sheath parameter. Because the space charge region is sharply defined due to the step behavior of the electron density at the sheath edge, d_{sh} can be determined without ambiguity. Equation (3.11) now becomes

$$\frac{dv_i}{dy} = \frac{\Lambda\sqrt{2}}{v_i} \sqrt{\frac{1}{2\Lambda^2} \left(\left[v_i \frac{dv_i}{dy} \right]_{y=0} \right)^2 + (v_i - 1)},$$
(3.13)

where

$$\Lambda^2 = \omega_{p,i}^2 \frac{d_{sh}^2}{u_{i,0}^2} = \frac{q_i^2 N_0 d_{sh}^2}{\varepsilon_0 m_i u_{i,0}^2}.$$
(3.14)

The various values of Λ represent the different sheath conditions. Assuming again that $\left(\left[v_i \frac{dv_i}{dy} \right]_{y=0} \right)$ is zero at the sheath edge and integrating (3.13) with v_i is 1 at the sheath edge gives

$$\frac{2}{3} (v_i + 2) \sqrt{v_i - 1} = \Lambda y \sqrt{2}.$$
(3.15)

The velocity profile satisfies

$$v_i + 1 =$$
$$\left[1 + \tfrac{9}{4}\Lambda^2 y^2 + \Lambda y \sqrt{\tfrac{9}{2} + \tfrac{81}{16}\Lambda^2 y^2} \right]^{1/3} + \left[1 + \tfrac{9}{4}\Lambda^2 y^2 - \Lambda y \sqrt{\tfrac{9}{2} + \tfrac{81}{16}\Lambda^2 y^2} \right]^{1/3}.$$
(3.16)

The electric field in the sheath can be derived from equations (3.6) and (3.13). With

$$\eta = \frac{eV}{m_i u_{i,0}^2},$$
(3.17)

the electric field in dimensionless units $\Psi(y)$ is given by

$$\Psi(y) = \Lambda\sqrt{2} \sqrt{v_i(y) - 1}.$$
(3.18)

The dimensionless ion density in the sheath is determined by

$$n_i(y) = \frac{1}{v_i(y)},$$
(3.19)

where $v_i(y)$ satisfies equation (3.16).

The sheath thickness in the self-consistent ionic sheath can be derived from equation (3.14) and (3.15). Because the sheath is assumed to be collisionless, the ion energy is conserved which leads to an expression for the sheath thickness given by

$$d_{sh} = \sqrt{\frac{2\varepsilon_0 m_i u_{i,0}^2}{9e^2 N_0}} \left(2 + \sqrt{\frac{2eV_{sh}}{m_i u_{i,0}^2} + 1} \right) \sqrt{-1 + \sqrt{\frac{2eV_{sh}}{m_i u_{i,0}^2} + 1}}, \qquad (3.20)$$

where V_{sh} is the sheath voltage. At high sheath voltages this expression can be approximated by

$$d_{sh} = \sqrt{\frac{2\varepsilon_0 m_i u_{i,0}^2}{9e^2 N_0}} \left(\frac{2eV_{sh}}{m_i u_0^2} \right)^{3/4}, \qquad (3.21)$$

in which one can discern the Child-Langmuir relation for the space charge limited ion current sheath condition.

In figure 3.4 and 3.5 the velocity profile, the electric field and the ion density are shown according to the self-consistent ionic sheath solution for the same plasma conditions as in figure 3.2. This has been done in non-dimensionless units; so it is easier to compare the results with the exact, numerically calculated sheath solution as shown in figure 3.2 and 3.3

Comparison between the exact, numerical sheath solution and the self-consistent analytical solution shows only a difference near the sheath edge. The transition region from the glow to the sheath is larger in the exact solution, due to the smaller space charge near the sheath edge. This also means that the total sheath thickness in the exact solution is a little bit larger although this difference has not a large influence on the sheath formation. Because the difference between the two approximations is restricted to the transition region where the ion energy is low, the self-consistent ionic sheath solution describes the sheath very well.

The transit time of the ions through the sheath in the low frequency case is small with repect to the RF period. Due to this, the ion energy is determined by the instantaneous voltage drop across the sheath $V_{sh}(t)$. The IED is determined by the sheath voltage modulation, which is dicussed in chapter 2. The instantaneous sheath thickness $d_{sh}(t)$ is determined by $V_{sh}(t)$ and given by

$$d_{sh}(t) = \sqrt{\frac{2\varepsilon_0 m_i u_{i,0}^2}{9e^2 N_0}} \left(2 + \sqrt{\frac{2eV_{sh}(t)}{m_i u_{i,0}^2} + 1} \right) \sqrt{-1 + \sqrt{\frac{2eV_{sh}(t)}{m_i u_{i,0}^2} + 1}}, \qquad (3.22)$$

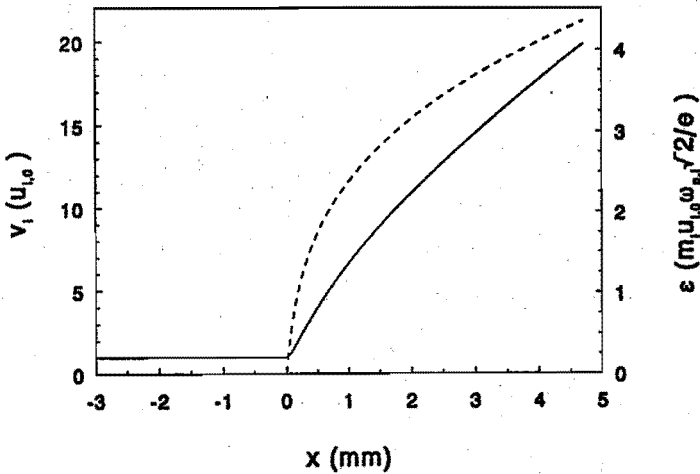The net total current through the plasma and also through the sheaths in

Figure 3.4: The velocity profile (solid line) and the electric field (dashed line) as calculated in the self-consistent ionic sheath solution. The plasma conditions are the same as in figure 3.2.

an AC coupled plasma is zero, as discussed in chapter 2. In the low frequency case the sheath voltage equals the floating potential for a part of the RF period, while the other moments of the RF period the sheath voltage is higher [Köh85] (see appendix A.2). This holds for both the sheath in front of the grounded and of the driven electrode. When the sheath voltage is higher than the floating potential, the ion current exceeds the electron current. The total ion current is compensated by an electron pulse at the moment the sheath voltage has decreased again. The instantaneous sheath voltage is minimized ($V_{sh} \approx 0$) for a short moment ($\approx 10 - 20$ ns). This is schematically shown in figure 3.6, where arrow A and B mark the moment the electron pulse compensates the ion current to the grounded and the driven electrode respectively.

Electro-negative gases

In the case of electro-negative gases, negative ions are produced in the plasma. Due to their low temperature and large masses they are confined in the plasma glow. Because of the quasineutrality of the glow positive ions are hold by the negative ones [Yon90]. The negative ion density (N_-) in the sheath can be
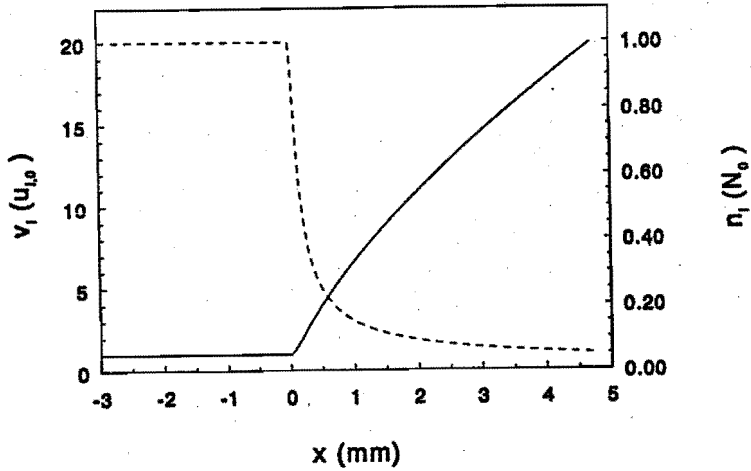
Figure 3.5: The velocity profile (solid line) and ion density (dashed line) as calculated in the self-consistent ionic sheath solution. The plasma conditions are the same as in figure 3.2.

described by the Boltzmann relation [Bra88]

$$N_-(x) = N_{-,0} \exp\left(\frac{-e(V_0 - V(x))}{kT_-}\right), \tag{3.23}$$

where T_- is the negative ion temperature and $N_{-,0}$ the negative ion density at the sheath-presheath edge. A small voltage drop at the sheath edge leads to a rapid decrease in the negative ion density. Due to the higher temperature and lower mass, the electrons can penetrate further in the space charge region than the negative ions. The resulting formation of a positive space charge region influences the velocity of the positive ions in such a way that they may enter the space charge region. This modified Bohm criterion is expressed by [Bra88]

$$u_{Bohm} = \sqrt{\frac{(N_{-,0} + N_{e,0})kT_-T_e}{m_i(N_{-,0}T_e + N_{e,0}T_-)}}. \tag{3.24}$$

The corresponding presheath potential across which the ions have to be accelerated may be given in normalized form by

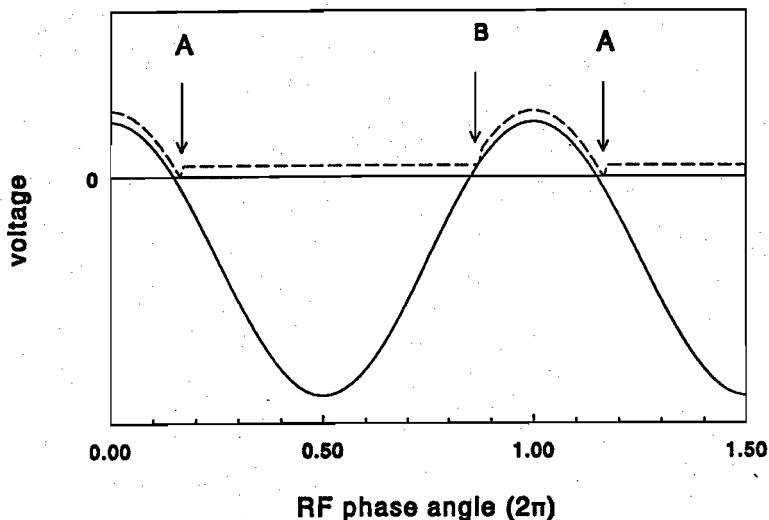$$\eta_0 = \frac{(1 + \alpha_0)}{2(1 + \gamma\alpha_0)}, \tag{3.25}$$

Figure 3.6: The time dependent voltage of the driven electrode (solid line) and the plasma potential (dashed line) in an AC coupled, low frequency plasma. The arrows mark the moment the electron pulse compensates the ion current to the grounded (A) and driven electrode (B).

where α_0 is the ratio of the negative-ion-to-electron-density at the sheath edge and γ the ratio of the electron-to-negative-ion-temperature. This relation is shown in figure 3.7. From this figure it follows that for real discharges in CF_4, where α_0 may be of the order 5 and γ may be 35, the Bohm velocity can easily be reduced to a value of one order of magnitude lower. This influences the value of Λ; however, the influence through negative ions in the sheath itself can be neglected.

In figure 3.8 the density profiles in the sheath of a CF_4 plasma are shown. Only CF_3^+ and F^- ions and the electrons are taken into account. The CF_3^+ density is assumed to be 10^{16} m^{-3} and the ratio of the negative-ion-to-electron-density is 5, The electron temperature, kT_e, is 2 eV, the ratio of the electron-to-negative-ion-temperature is 33. The sheath thickness in this case is 10.3 mm. The influence of the negative ions is restricted to the glow and the area very near the sheath edge. The space charge region is mainly dominated by the positive ions just as in the situation without the negative ions. The space charge region in the electro-negative gases can be treated by taking into account only the positive ions, as discussed earlier in this section.
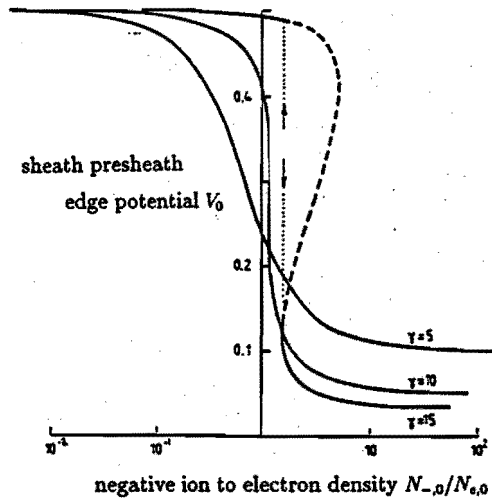
Figure 3.7: The normalized sheath edge potential against the ratio of the negative ion to the electron density at the sheath edge, for three values of γ, the ratio of the electron to negative ion temperature. At high γ values a jump in sheath edge potential has to be made [Bra88].

3.3 The sheath in the high frequency region

3.3.1 Sheath dynamics

Two high frequency models are developed to describe the time dependent electric field in the sheath. One model (A) is described in this section and is based on the self-consistent ionic sheath solution as derived in the DC sheath and adapted to the high frequency region. The other model (B) is based on the emperical result of PIC simulations. In accordance with the emperical results the assumption is made that the ion velocity increases in the sheath proportional to the position. This model is elucidated in appendix B and leads to simpler expressions, although model A is more sophisticated. Both models will prove to be close to self-consistency. The sheath dynamics in both models is the same and will be treated in this section. First, the sheath in plasmas with only positive ions will be discussed and later on the influence of negative ions
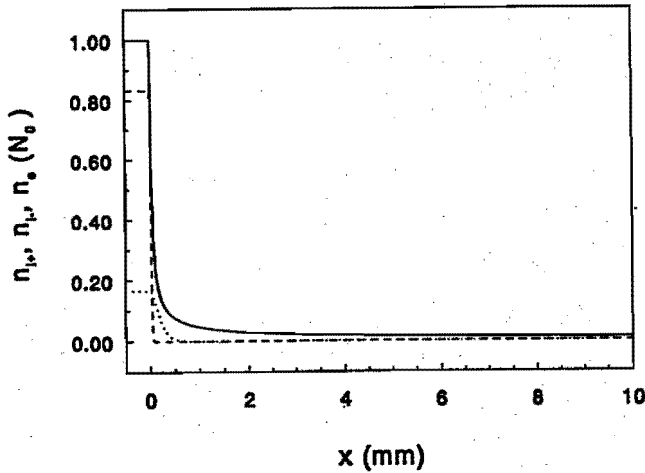
Figure 3.8: The density profiles of CF_3^+ (solid line), F^- ions (dashed line) and the electrons (dotted line) in the sheath of a CF_4 plasma. The CF_3^+ density at the sheath edge is 10^{16} m^{-3}, and the ratio between the F^- density to the electron density at this position is 5. $T_- = 0.06$ eV and $T_e = 2$ eV. The sheath thickness is 10.3 mm.

will be elucidated.

In the high frequency region ($\omega_{p,i} \ll \omega \ll \omega_{p,e}$) the positive ions hardly can follow the field oscillations in the sheath. They feel an average voltage drop towards the electrode. Consequently, the ion density may be assumed constant in time and decreasing towards the electrode. This in contrast to the low frequency region where the ion density adjusts itself to the sheath voltage. The electrons react instantaneously to the field oscillations due to their high mobility. The instantaneous voltage drop across the sheath is related to the integrated space charge in the sheath. In this analysis the electrons move into the sheath region to compensate the positive space charge. The position of the electron front is determined by the instantaneous sheath voltage so that the space charge region which remains, is in accordance with to the sheath voltage. The electron density is assumed to equal the local ion density or to be zero according to

$$N_e(x,t) = N_i(x) \qquad \text{for} \quad 0 \leq x \leq x_s(t), \qquad (3.26)$$
$$N_e(x,t) = 0 \qquad \text{for} \quad x_s(t) < x < d_{sh,max}. \qquad (3.27)$$

where $x_s(t)$ is the position of the electron front and $d_{sh,max}$ the maximum sheath thickness. x equals to 0 is the position of the sheath-presheath edge. Since the electron density cut-off is comparable with the assumptions in section 3.2, $x_s(t)$ acts as the real front where the space charge starts and ambiguities with respect to the sheath thickness do not occur. The ion and electron density profiles at a certain time are schematically shown in figure 3.9.
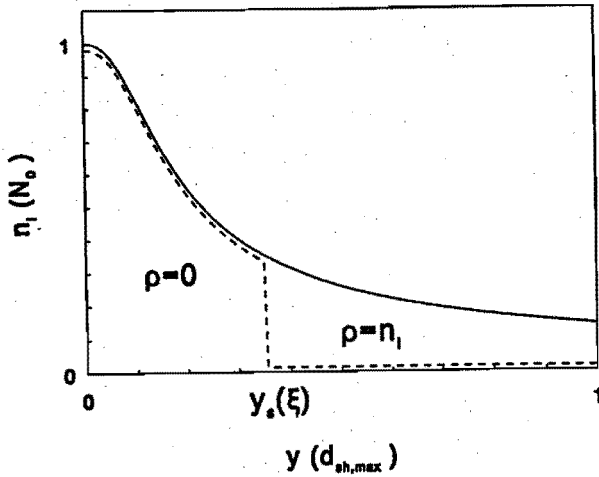

Figure 3.9: The ion and electron density in the high frequency sheath. The ion density (solid line) is constant in time whether the electron density (dashed line) behaves step-like. The electron front oscillates due to the sheath voltage modulation.

3.3.2 The high frequency sheath model

Due to the ion inertia, the ion density in the high frequency sheath may be assumed nearly constant in time. To describe the ion density profile in the collisionless sheath, we consider the self-consistent ionic sheath solution in the DC sheath as given by equation (3.19) with the average ion velocity at the electrode $\overline{u}_{i,electrode}$ determined by the time average sheath voltage $\overline{V}_{sh}$, given by

$$\overline{u}_{i,electrode} = \sqrt{\frac{2e\overline{V}_{sh}}{m_i} + u_{i,0}^2}. \tag{3.28}$$

In the case of a purely sinusoidal sheath voltage modulation

$$\overline{V}_{sh} = \frac{1}{2}(V_{sh,max} + V_{sh,min}),$$ (3.29)

where $V_{sh,max}$ and $V_{sh,min}$ are the maximum and the minimum sheath voltages, respectively. We introduce the parameter b as the dimensionless average ion velocity at the electrode $(\overline{u}_{i,electrode})$

$$b = \frac{\overline{u}_{i,electrode}}{u_{i,0}}.$$ (3.30)

Riemann proved that the Bohm criterion derived for the DC sheath is also valid in the RF situation [Rie92], so $u_{i,0}$ in the RF situation also equals the Bohm velocity as defined in equation (3.1).

The dimensionless parameter Λ^2 which scales with the ion density, is determined from equation (3.15) for the boundary condition at the electrode in the RF situation and is defined by

$$\Lambda = \frac{\sqrt{2}}{3}(b+2)\sqrt{b-1}.$$ (3.31)

The dimensionless ion density profile is now given by

$$n_i(y) =$$
$$\left[\left[1 + \tfrac{1}{2}B^2y^2 + \sqrt{B^2y^2 + \tfrac{1}{4}B^4y^4}\,\right]^{1/3} + \left[1 + \tfrac{1}{2}B^2y^2 - \sqrt{B^2y^2 + \tfrac{1}{4}B^4y^4}\,\right]^{1/3} - 1\right]^{-1},$$ (3.32)

with

$$B = (b+2)\sqrt{b-1}.$$ (3.33)

Equation (3.32) can be reduced to

$$n_i(y) = \left[P^{1/3}(y) + P^{-1/3}(y) - 1\right]^{-1},$$ (3.34)

with

$$P(y) = p + \sqrt{p^2 - 1},$$ (3.35)

and

$$p = 1 + \frac{1}{2}B^2y^2,$$ (3.36)

The ion density profile is shown in figure 3.10 in dimensionless units for the sheath in a high frequency plasma. The density at the sheath edge is $6\ 10^{15}$ m^{-3},
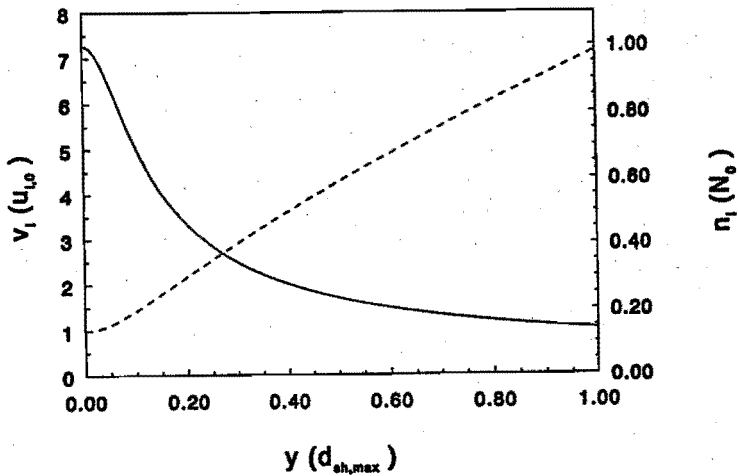
Figure 3.10: The ion density profile (solid line) and the average ion velocity
(dashed line) in a high frequency sheath in an argon plasma. $N_0=6\ 10^{15}\ m^{-3}$,
$V_{sh,max}=100\ V$, $V_{sh,min}=0\ V$ and $u_{i,0}=2.20\ 10^3\ m/s$ (with $T_e=2\ eV$); b in
this case is 7.14 and $d_{sh,max}=2.1\ mm$.

$V_{sh,max}$ is 100 V and $V_{sh,min}$ is 0 V, while the voltage modulation is purely sinu-
soidal. b in this case equals 7.14. In this figure also the average dimensionless
ion velocity profile is shown.

We consider the situation that the electron front is at a certain position
$x_s(t)$ in the sheath: $0 \leq x_s(t) \leq d_{sh,max}$. In dimensionless terms, the position of
the electron front is given by $0 \leq y_s(t) \leq 1$.

The electric field at a position x in the sheath is determined by the space
charge. Poisson's law leads to

$$\mathcal{E}(x, x_s(t)) = \int_0^x \frac{e}{\varepsilon_0} \left(N_i(x') - N_e(x') \right) dx' + \mathcal{E}_c(t), \qquad (3.37)$$

where $\mathcal{E}_c(t)$ is the integration constant. With equation (3.26) and (3.27) this
leads to

$$\mathcal{E}(x, x_s(t)) = \int_{x_s(t)}^x \frac{e}{\varepsilon_0} N_i(x') dx' + \mathcal{E}_c(t) \qquad \text{for} \quad x_s(t) \leq x \leq d_{sh,max}, \quad (3.38)$$

$$= \mathcal{E}_c(t) \qquad \qquad \text{for} \quad 0 \leq x < x_s(t). \quad (3.39)$$

The electric field in the glow and presheath is very small and negligible with

respect to the field in the sheath. Because of the continuity of the field, $\mathcal{E}_c(t)$ equals zero.

The potential at a position x in the sheath is also determined by Poisson's law and given by the integrated field

$$V(x, x_s(t)) = -\int_0^x \mathcal{E}(x', x_s(t)) \, dx' + V_c(t), \tag{3.40}$$

which leads to

$$V(x, x_s(t)) = -\int_{x_s(t)}^x \mathcal{E}(x', x_s(t)) \, dx' + V_c(t) \quad \text{for} \quad x_s(t) \le x \le d_{sh,max}, \tag{3.41}$$

$$= V_c(t) \quad\quad\quad\quad\quad \text{for} \quad 0 \le x < x_s(t). \tag{3.42}$$

$V_c(t)$ is the integration constant and equals the time dependent plasma potential $V_p(t)$. The potential across the sheath is given by

$$V_{sh}(t) = V_p(t) - V(d_{sh,max}, x_s(t)) = \int_{x_s(t)}^{d_{sh,max}} \mathcal{E}(x, x_s(t)) \, dx. \tag{3.43}$$

In dimensionless terms equations (3.38), (3.39), (3.41), (3.42) and (3.43) become respectively

$$\Psi(y, y_s(\xi)) = \Lambda^2 \int_{y_s(\xi)}^y n_i(y') \, dy' \quad\quad \text{for} \quad y_s(\xi) \le y \le 1, \tag{3.44}$$

$$= 0 \quad\quad\quad\quad\quad\quad \text{for} \quad 0 \le y < y_s(\xi). \tag{3.45}$$

$$\eta(y, y_s(\xi)) = -\int_{y_s(\xi)}^y \Psi(y', y_s(\xi)) \, dy' + \eta_p(\xi) \quad \text{for} \quad y_s(\xi) \le y \le 1, \tag{3.46}$$

$$= \eta_p(\xi); \quad\quad\quad\quad\quad\quad \text{for} \quad 0 \le y < y_s(\xi). \tag{3.47}$$

$$\eta_{sh}(\xi) = \int_{y_s(\xi)}^1 \Psi(y, y_s(\xi)) \, dy. \tag{3.48}$$

with

$$\Lambda^2 = \frac{e^2 N_0 d_{sh,max}^2}{\varepsilon_0 m_i u_{i,0}^2} = \frac{2}{9} B^2, \tag{3.49}$$

and ξ the dimensionless time given by

$$\xi = \omega t \tag{3.50}$$

The dimensionless electric field in the space charge region is determined by solving equation (3.44) with $n_i(y)$ given by equation (3.34)

$$\Psi(y, y_s(\xi)) = \frac{2}{3} B \left[P^{1/6}(y) - P^{-1/6}(y) - P^{1/6}(y_s(\xi)) + P^{-1/6}(y_s(\xi)) \right]$$

$$\text{for} \quad y_s(\xi) \le y \le 1, \qquad (3.51)$$

$$= 0 \qquad \text{for} \quad 0 \le y < y_s(\xi). \qquad (3.52)$$

The time dependent electric field is shown in figure 3.11 for 6 positions of the electron front in the sheath of a high frequency plasma. The sheath conditions are the same as in figure 3.10.
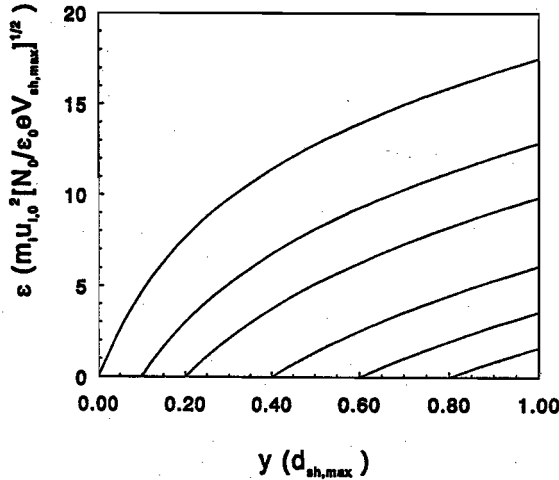

Figure 3.11: *The time dependent electric field in a high frequency plasma. The field is drawn for 6 different positions of the electron front: $y_s(\xi)=0$, 0.1, 0.2, 0.4, 0.6 and 0.8. The sheath conditions are the same as in figure 3.9.*

From the time dependent expression for the electric field, the potential in the sheath can be derived according to equations (3.46) and (3.47). The potential is given by

$$\eta(y, y_s(\xi)) = \eta_p(\xi) - \frac{1}{2} \left[P^{2/3}(y) + P^{-2/3}(y) - 2P^{1/3}(y) - 2P^{-1/3}(y) - \right.$$

$$- P^{2/3}(y_s(\xi)) - P^{-2/3}(y_s(\xi)) + 2P^{1/3}(y_s(\xi)) +$$

$$\left. + 2P^{-1/3}(y_s(\xi)) \right] +$$

$$+ \frac{2}{3} B \left(y - y_s(\xi) \right) \left[P^{1/6}(y_s(\xi)) - P^{-1/6}(y_s(\xi)) \right]$$

$$\text{for} \quad y_s(\xi) \leq y \leq 1, \qquad (3.53)$$

$$= \eta_p(\xi) \qquad \text{for} \quad 0 \leq y < y_s(\xi). \qquad (3.54)$$

The voltage across the sheath $\eta_{sh}(\xi)$ is determined by

$$\eta_{sh}(\xi) = \eta_p(\xi) - \eta(1, y_s(\xi)). \qquad (3.55)$$

where $\eta(1, y_s(\xi))$ is the potential at the electrode with y equals to 1. When $\eta_{sh}(\xi)$ is known for instance because it is imposed on the plasma, then the position of the electron front is determined by equations (3.53) and (3.55). In a purely capacitive sheath $\eta_{sh}(\xi)$ is sinusoidal and can be expressed as

$$\eta_{sh}(\xi) = \eta_{sh,min} + \frac{1}{2} \left(\eta_{sh,max} - \eta_{sh,min} \right) \left(1 + \cos(\xi) \right). \qquad (3.56)$$

The movement of the electron front in a capacitive sheath is shown in figure 3.12 for the same sheath conditions as given in figure 3.10.
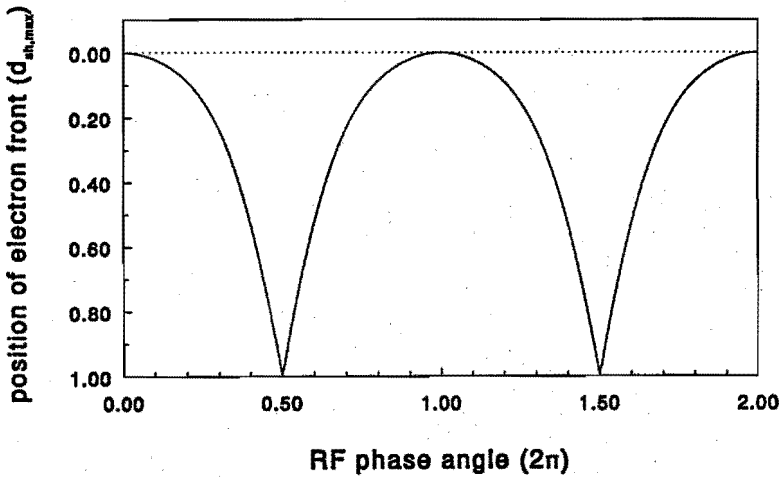

Figure 3.12: The movement of the electron front in according to the high frequency sheath model as described in subsection 3.3.2, due to a sinusoidal sheath voltage modulation, during two RF periods. The sheath conditions are the same as in figure 3.9.

Although the voltage modulation is sinusoidal, the movement of the electron front is not. This is due to the ion density profile in the sheath. Near the sheath edge ($x = 0$), the density is higher than near the electrode. Consequently, near the presheath a smaller change of the position is needed for a certain voltage change than near the electrode.

The maximum sheath thickness is determined by the maximum sheath voltage. In this situation the electron front is at position $y_s(\xi) = 0$. The maximum sheath voltage is described by

$$
\begin{aligned}
\eta_{sh,max} = \ & \frac{1}{2} \left[P^{2/3}(1) + P^{-2/3}(1) - 2P^{1/3}(1) - 2P^{-1/3}(1) - \right. \\
& \left. - P^{2/3}(0) - P^{-2/3}(0) + 2P^{1/3}(0) + 2P^{-1/3}(0) \right] + \\
& + \frac{2}{3} B \left[P^{1/6}(0) - P^{-1/6}(0) \right].
\end{aligned} \tag{3.57}
$$

Since $P(1)$ is given by equation (3.35) and (3.36), and $P(0)$ is 1, equation (3.57) becomes

$$
\eta_{sh,max} = \frac{1}{2} \left[P^{2/3}(1) + P^{-2/3}(1) - 2P^{1/3}(1) - 2P^{-1/3}(1) + 2 \right]. \tag{3.58}
$$

For $\eta_{sh,max}$ also

$$
\eta_{sh,max} = \frac{eV_{sh,max}}{m_i u_{i,0}^2} = \frac{2}{9} B^2 \frac{\varepsilon_0 V_{sh,max}}{eN_0 d_{sh,max}^2}. \tag{3.59}
$$

Equalization of equations (3.58) and (3.59) leads to

$$
d_{sh,max}^2 = \frac{4\varepsilon_0 B^2 V_{sh,max}}{9N_0 e} \left[P^{2/3}(1) + P^{-2/3}(1) - 2P^{1/3}(1) - 2P^{-1/3}(1) + 2 \right]^{-1}. \tag{3.60}
$$

The maximum sheath thickness for the parameter set used in figure 3.10 is 2.1 mm.

The model is close to self-consistency. This can be proved by calculating numerically the time averaged potential at every position in the sheath. Due to the conserved energy of the ions in the collisionless sheath, the velocity profile corresponding to this time averaged potential can be derived, and subsequently, also the density profile. The comparison between the velocity and density profiles according to the model and the profiles derived from the time averaged potential is shown in figure 3.13. The profiles in the figure have been derived for the same sheath conditions as in figure 3.10. The profile in both approximations is quite similar. Due to this the model may be classified as close to self-consistency.
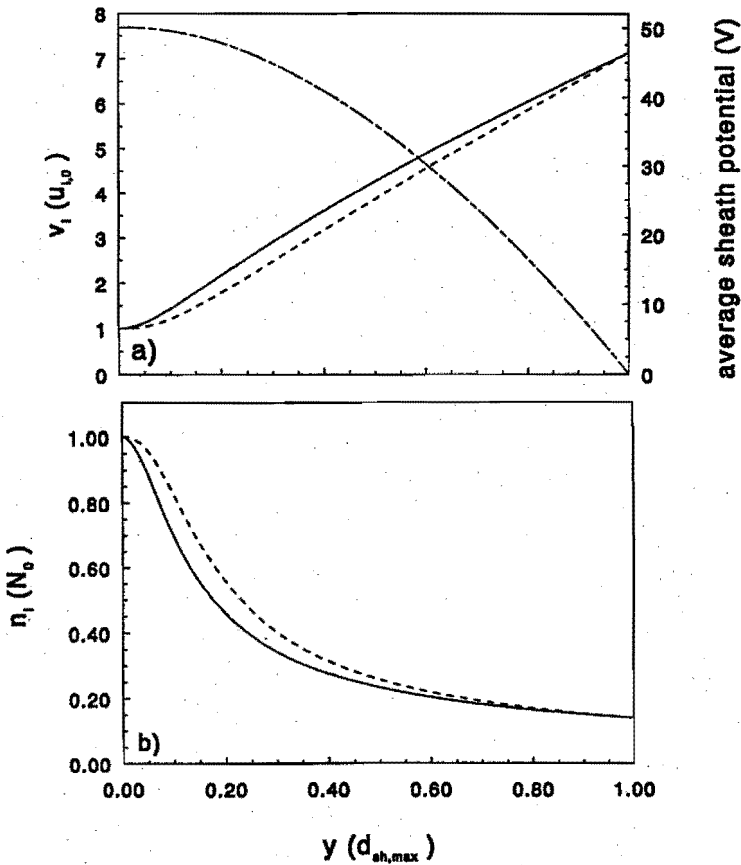
Figure 3.13: The average potential in the sheath (a, dash dotted line) diverted from the sheath model. The average velocity profile according to the model (a, solid line) and derived from the average potential (a, dashed line). The density profiles are shown in figure b. The solid line represents the profile according to the model and the dashed line the profile derived from the average potential.

In appendix B sheath model B is presented. This is based on the empirical assumption that

$$\frac{du_i(x)}{dx} = constant. \tag{3.61}$$

This assumption is based on the results of PIC calculations and leads to much

simpler expressions for the density, average velocity, electric field and the potential in the sheath than those of model A. The second model can also be proved to be close to self-consistency. When we compare both models one can conclude that the profiles of the assumed ion density and velocity in both models are even rather similar, although the derivatives of the average velocity and the density at the sheath edge in model B are not continuous to the glow conditions.

In the case of electro-negative gases, the negative ions are confined in the glow. Due to the time averaged electric field in the high frequency sheath, these ions are repelled from the sheath region ($y > 0$). This is confirmed by calculations in the literature [Yon90]. The negative ion density near the sheath edge is determined by the time averaged potential in the sheath and obey the Boltzmann relation. Due to the small negative ion temperature the density drops rapidly in the sheath. Consequently, only the positive ions and electrons are involved in the sheath behavior as far as the voltage modulation is concerned. Although the electron density in the glow is lower than that of the positive ions due to the quasi neutrality in the glow, the electrons compensate the positive space charge in the high frequency sheath where the electron density in the sheath can be higher than in the glow. The position of the electron front is determined by the instantaneous sheath voltage. The density profiles of the electrons, the positive and the negative ions in the beginning of the sheath at a certain RF phase angle are shown in figure 3.14. Thus the sheath dynamics in an electro-negative gas are assumed to be the same as in a plasma that consists of electrons and positive ions only. The difference is that the Bohm velocity is lower in the electro-negative gas which leads to different sheath conditions. This is expressed by a different value of Λ when the ion density at the sheath edge and the sheath voltage are assumed to be the same.

3.3.3 The sheath voltage modulation

The high frequency sheath may be assumed capacitive as shown in appendix A. Consequently, the sheath voltage may be considered sinusoidal due to the imposed RF voltage across the electrodes.

The sheath voltage is minimized once every period, where the minimum sheath voltage is of influence on the total electron current. The plasma potential adjusts itself so that $V_{sh,min}$ balances the ion and the electron current over one RF period to satisfy the zero net total current condition in the AC coupled plasma and the sheaths. The ion current is determined by the ion density at
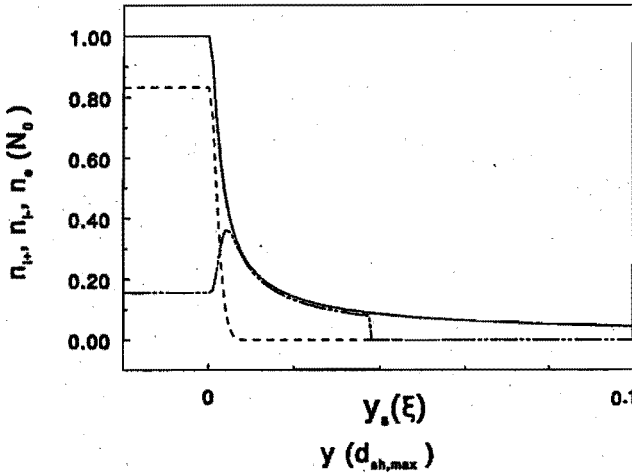
Figure 3.14: The density of the positive ions (solid line), negative ions (dashed line) and the electrons (dotted line) in the sheath at a certain phase angle of the driven RF voltage. Only the first 10 % of the sheath is depicted to show the influence of the negative ions.

the sheath edge $(y = 0)$ and the Bohm velocity

$$J_i = eN_0\sqrt{\frac{kT_e}{m_i}}. \tag{3.62}$$

The electron current at a certain phase angle depends on the instantaneous sheath voltage and the electron density at the space charge edge, which equals the ion density at the edge, and is given by [Cha80]

$$J_e(t) = eN_e(x_s(t))\left(\frac{kT_e}{2\pi m_e}\right)^{1/2}\exp\left(\frac{-e\left(V_p(t) - V_{electrode}(t)\right)}{kT_e}\right). \tag{3.63}$$

From the high frequency model, the total electron current can be determined numerically as function of average sheath voltage $\overline{V}_{sh}$ and the modulation λ_{sh} of the voltage. The sheath voltage is given by

$$V_{sh}(t) = \overline{V}_{sh}\left(1 + \lambda_{sh}\sin(\omega t)\right), \tag{3.64}$$

where $V_{sh,min}$ equals $\overline{V}_{sh}(1 - \lambda_{sh})$. The quantities λ_{sh} and $V_{sh,min}$ have been calculated as function of $\overline{V}_{sh}$ under the condition that the total electron current
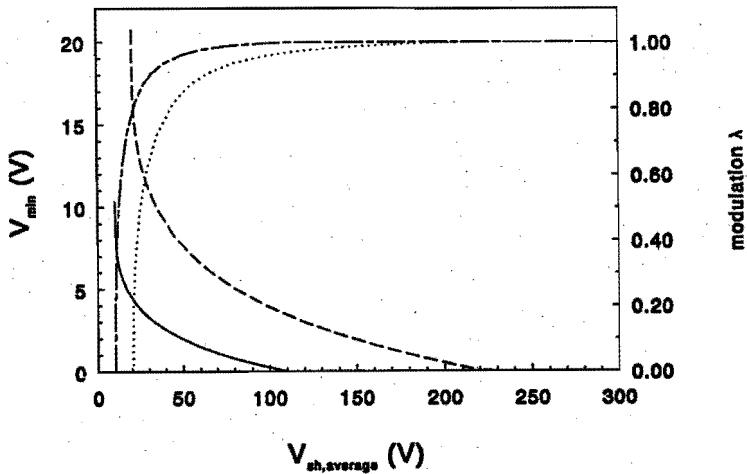
*Figure 3.15: $V_{sh,min}$ (solid line ($kT_e=2$ eV) and dashed line ($kT_e=4$ eV))
and the modulation factor λ (long-short dashed line ($kT_e=2$ eV) and dotted
line ($kT_e=4$ eV)) as function of $\overline{V}_{sh}$ in an argon high frequency plasma.*

balances the ion current. This is shown in figure 3.15 for an electron tempera-
ture of 2 and 4 eV.

From figure 3.15 we may conclude that $V_{sh,min}$ is small compared with $\overline{V}_{sh}$,
especially at high voltages where $V_{sh,min}$ has to equal zero to provide a balanced
current situation. In the model, the sheath voltage is minimized only for a very
short moment. When $\overline{V}_{sh}$ is larger than about 110 V and 220 eV in the case the
electron temperature is 2 and 4 eV respectively, $V_{sh,min}$ equals zero. To balance
the net current the moment the sheath voltage is zero has to be longer than
in the high frequency model where the sheath voltage modulation is assumed
to be sinusoidal and the electron front reaches the electrode surface only for a
very short fraction of time. In these situations an electron pulse is generated
with a width up to about 7 ns in the case $\overline{V}_{sh}$ is several hundred Volts [Wil91].

Not all the effects in the sheath which are mentioned in this section are
included in the high frequency model. These effects have only a small influence
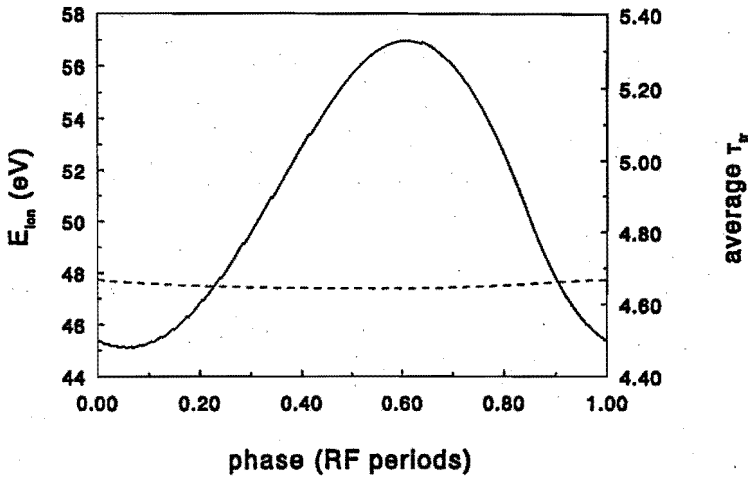on the electric field and subsequently on the IED.

Figure 3.16: The relation between the phase at which the Ar^+ ions enter the sheath and the energy they gain in the sheath (solid line) in a 13.56 MHz plasma in argon. The dashed line is the transit time of the ions through the sheath. The sheath conditions are the same as in figure 3.9.

3.3.4 The IED in the collisionless sheath

In subsection 3.3.2 an expression for the time dependent electric field in the high frequency sheath is derived. Also the sheath thickness is determined. The field is used to determine the ion dynamics in the sheath. The ions are accelerated in the time dependent electric field in the sheath towards the electrode. Because the ion transit time through the high frequency sheath is several RF periods, the ion acceleration is modulated. Consequently it is impossible to describe the ion trajectory through the sheath analytically, and numerical methods are needed.

From the numerically determined trajectories with the expressions (3.51) and (3.52) for the electric field, the relation between the energy of the ions when they reach the electrode, E_{ion}, and the phase angle at which the ions enter the sheath region at $x = 0$, φ, can be determined. This relation is shown in figure 3.16 for an Ar^+ ion in a 13.56 MHz plasma in argon for the same sheath conditions as in figure 3.10. The sheath voltage modulation is sinusoidal.

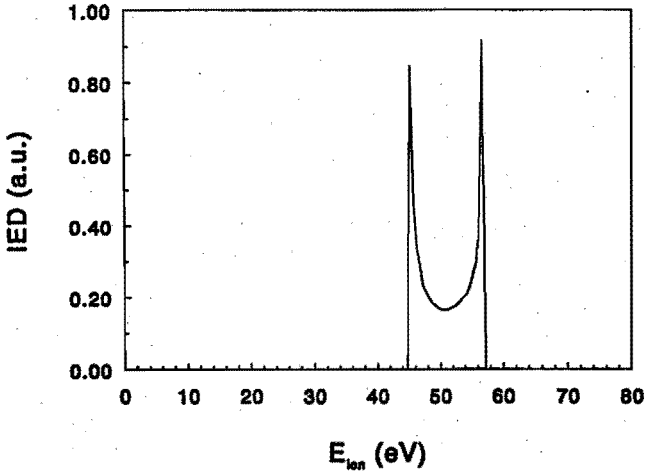The IED can be determined from the phase-angle - energy relation. When

Figure 3.17: The IED of the Ar^+ ion as determined from the phase-energy relation as shown in figure 3.13.

$\frac{d}{d\varphi}E_{ion}$ is zero, a maximum in the distribution occurs. In figure 3.17 the IED is shown as determined numerically from the relations shown in figure 3.16. The ion flux entering the sheath is assumed to be constant in time. The IED shows the typical RF saddle structure with local maxima at the lowest (E_{min}) and highest ion energies (E_{max}).

The average energy of the saddle of the IED $(\overline{E}_{sad})$ of a singly charged ion, corresponds to the average sheath potential $(\overline{V}_{sh})$. Doubly charged ions gain double as much energy in the sheath. The splitting of the IED (ΔE) depends on the average transit time $(\overline{\tau}_{tr})$ that the ions need to cross the sheath. The transit time of a certain ion (τ_{tr}) depends on the phase angle at which this ion enters the sheath, although the numerical results show that τ_{tr} is nearly constant when the ions need more than 3 RF periods to cross the sheath. $\overline{\tau}_{tr}$ for a certain sheath condition depends on $\overline{V}_{sh}$ and the mass of the ion. Ions with small masses have higher velocities and consequently $\overline{\tau}_{tr}$ will be shorter. When $\overline{V}_{sh}$ is smaller, the sheath thickness is smaller and consequently $\overline{\tau}_{tr}$ is shorter. ΔE may be scaled to $\overline{E}_{sad}$. The dependency of this ratio to $\overline{\tau}_{tr}$ is derived from the numerically determined IED's for several ions with different masses and several sheath conditions, and is shown in figure 3.18.

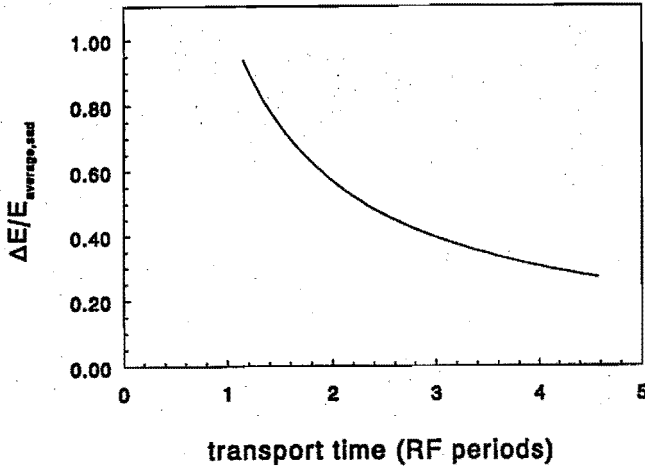Due to the fact that the ion energy at the electrode is modulated, the

transport time (RF periods)

Figure 3.18: The relation of $\Delta E/\overline{E}_{sad}$, to $\overline{\tau}_{tr}$ of the ions which cross the sheath.

ion density near the electrode is modulated too. This modulation is small in the case the transit time is longer than 3 RF periods. The density modulation for the sheath condition as discussed in figure 3.17 is 5 % with respect to the average density near the electrode. In the case of light ions or small sheath thicknesses where the transit time is shorter than 3 RF periods, the density modulation is larger than 10 %, and the assumption made in the high frequency sheath model about the constancy of the ion density is no longer valid.

3.3.5 The influence of collisions in the sheath

Collisions in the sheath become important when the mean free path of the ions is less than the sheath thickness. This will be the case for pressures higher than 5-10 mTorr. Especially ion neutral collisions have a strong influence on the ion dynamics and subsequently on the IED. Collisions mean that the average ion velocity in the sheath becomes less and the average ion energy at the electrode surface will be decreased with respect to the collisionless sheath. This means
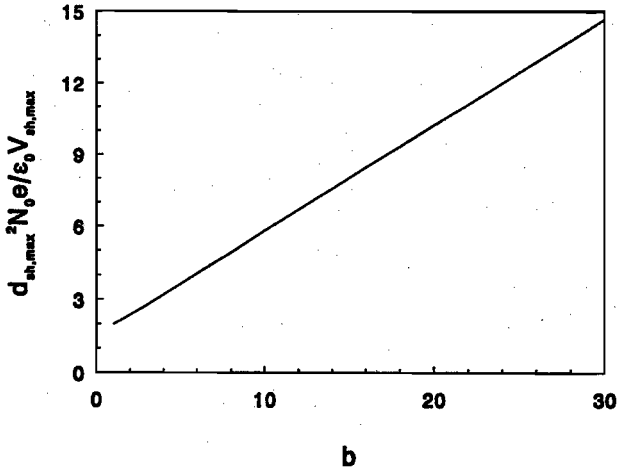
Figure 3.19: The maximum sheath thickness as function of the parameter b for the high frequency sheath model as described in subsection 3.3.2.

that equation (3.28) becomes an inequality

$$\overline{u}_{i,electrode} < \sqrt{\frac{2e\overline{V}_{sh}}{m_i} + u_{i,0}^2} \, . \tag{3.65}$$

The collisional behavior may be expressed by the model parameter b (as defined in equation 3.30), which in these cases is not anymore dependent on $\overline{V}_{sh}$. This may be assumed for the pressure region as long as the ion velocity is not determined by the ion mobility. Due to a smaller increase of the average velocity as a consequence of the collisions, the decrease of ion density towards the electrode is less and, subsequently, the sheath thickness is smaller assuming the same sheath voltages and ion density at sheath edge in comparison with the collisionless sheath. This is shown in figure 3.19.

We distinguish two types of ion-neutral collisions which have a large influence on the ion dynamics. The resonant charge exchange collisions

$$A^+ + A \rightarrow A + A^+, \tag{3.66}$$

for atomic ions have a large cross-section in the order of 10-40 10^{-16} cm^2 [McD64]. Such a collision generates a thermal ion and a fast neutral due to the exchange of an electron. The newly formed ion starts nearly at rest and is

accelerated from its position of creation towards the electrode. The direction of the ion movement is thus always perpendicular to the electrode. The ion flux does not change due to the charge exchange.

The second type of collision is momentum transfer, where the energy of the ion is distributed among the colliding particles due to the energy and momentum conservation laws. The energy and the direction of the ion thus will change. The cross-section of these collisions is in the order of 5-40 10^{-16} cm^{-2} [McD64].

To calculate the influence of the collisions on the IED's, Monte Carlo simulations are needed. Ion trajectories are determined for ions entering the sheath at several phase angles for charge exchange and elastic scattering dominated sheaths. Typically 10^5 trajectories are calculated for ions that enter the sheath at 200 different phase angles per period at equal intervals. The ions enter the sheath with the Bohm velocity directed towards the electrode. Ions formed by charge exchange start with energy 0 from the position where they are created. Whether an ion collides at a certain position is randomly chosen, related to the distance Δx an ion passes between two calculation steps with respect to the mean free path λ: when $\Delta x/\lambda$ is larger than a random value which is in between 0 and 1, a collision takes place. To provide good numerical resolution 4000 calculation steps are made in an RF period.

In figure 3.20a and 3.20b Monte Carlo simulations are shown of IED's determined by charge exchange in a high voltage sheath in a 13.56 MHz plasma in argon. V_{max} and V_{min} in both cases are 600 V and 0 V, respectively. N_0 is 5 10^{15} m^{-3} and the maximum sheath thickness is 7.75 mm. The mean free path is 5 mm in figure a and 2 mm in figure b. To show the influence of a smaller mean free path the sheath conditions are kept the same.

In figure a the saddle structure which is mainly caused by the ions that did not collide in the sheath (this is 21% of all the ions), is clearly visible. In case b, where only 2 % of the ions cross the sheath without a collision the saddle structure is visible but this is mainly caused by ions that had their last collision close to the sheath edge. The peaks and double peaks in the IED are typical for the charge exchange dominated sheath, due to the fact that the newly formed ions start with velocity 0. If the collision takes place at a moment when the local electric field is 0, the ion will not move until the field arises. All the ions generated at the same position during the period the field has vanished, will be accelerated at the same time and all will have the same trajectory and energy when reaching the electrode. This can give rise to features in the IED. In figure 3.21 the relation between the position of creation and the energy E_{y0} of these groups of ions is shown. E_{max} and E_{min} represent respectively, the
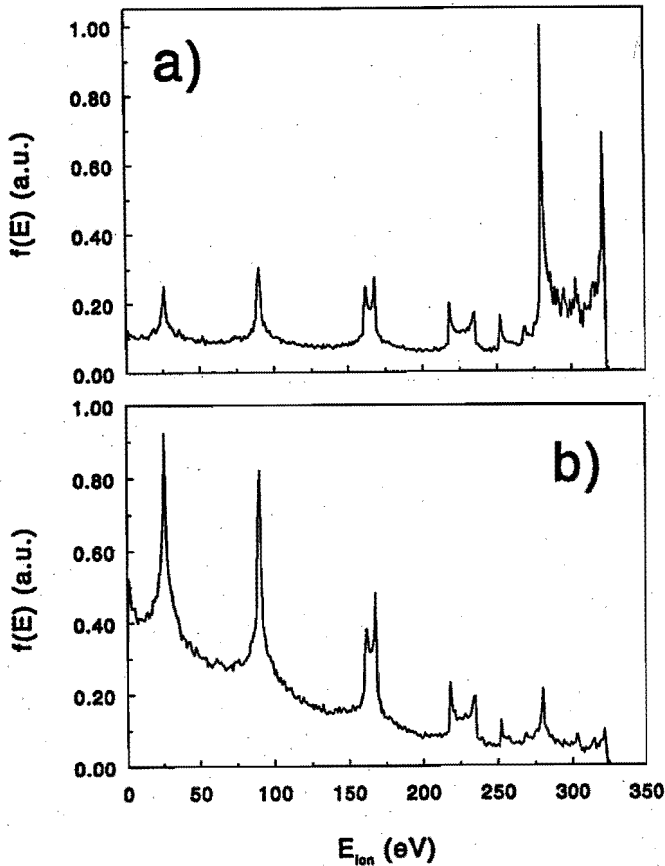
Figure 3.20: The IED's determined by Monte Carlo simulations in a 13.56 MHz plasma in argon, due to charge exchange in the sheath. V_{max} and V_{min} are 600 V and 0 V respectively. N_0 is 5 10^{15} m^{-3} and the maximum sheath thickness is 7.75 mm. The main free path is 5 mm in figure a and 2 mm in figure b.

maximum and the minimum energy an ion can have when it is generated at a certain position. The peaks in the IED occur when $\frac{d}{dy}E_{y0}$ is zero.

Elastic scattering randomizes even stronger. When we assume a hard sphere scattering model, the collision angle in the mass centered system is randomly distributed. The direction and the energy of the scattered ion are
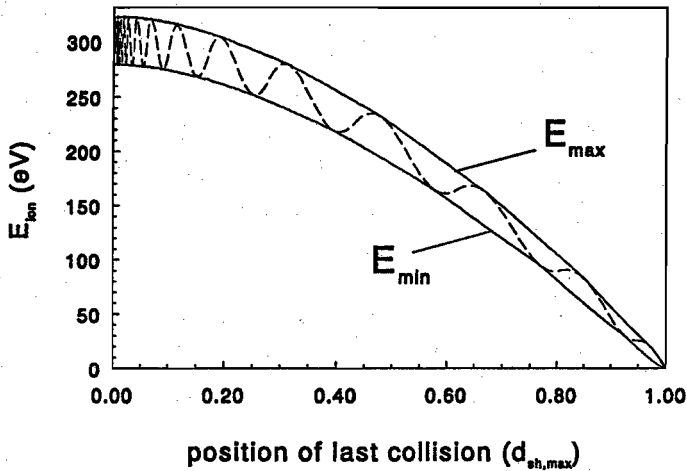
Figure 3.21: The relation between the E_{y0}, E_{max} and E_{min} and the position where the ion is created. The sheath conditions are the same as in figure 3.17.

distributed according to momentum and energy conservation. Thompson *et al.* [Tho88] compared several elastic scattering models. They concluded that there are no important differences in behavior between the hard sphere model and more realistic scattering models and hence it is justified to use the hard sphere model.

Elastic scattering means that the ions can hit the electrode at a certain angle, although the angular distribution is mainly concentrated around 90° which means that the ions mainly hit the electrode perpendicularly with a spread of 10° [Man91, Fie91]. This is due to the electric field which is directed towards the electrode. At higher pressures the angular distribution is broader. In figure 3.22 IED's are shown determined by Monte Carlo simulations for a sheath dominated by elastic scattering. The sheath parameters are the same as in figure 3.20. No collisional peaks are present. At smaller mean free paths, the saddle structure can hardly be recognized and only some small collisional peak effects are shown. These are due to head-on collisions between identical particles. In this case the ion loses all its energy and features are generated in the same way as for the charge exchange case. The features are at the same positions as the charge exchange peaks.
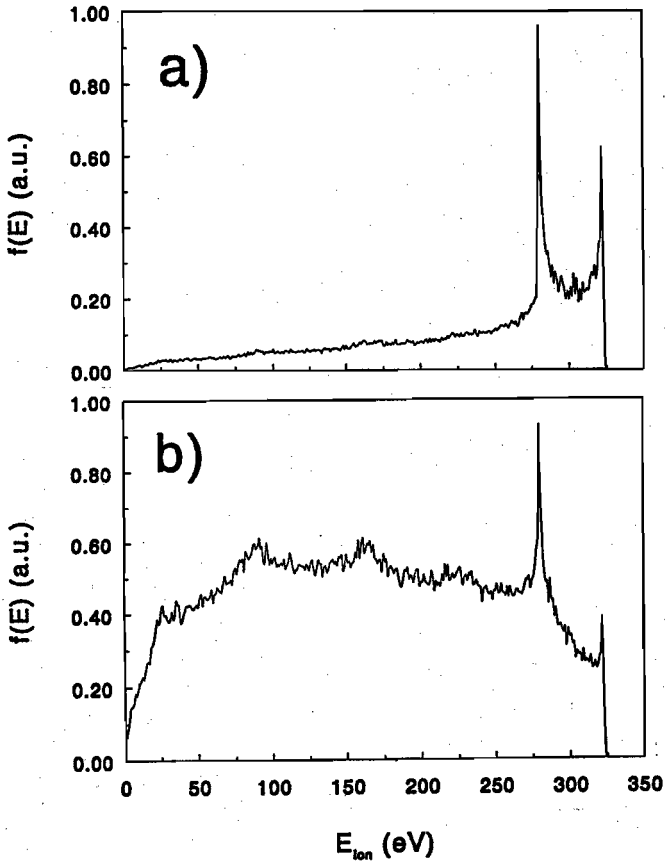
Figure 3.22: The IED's determined by Monte Carlo simulations in a 13.56 MHz plasma in argon, due to elastic scattering in the sheath. The sheath parameters are the same as in figure 3.17. The mean free path is 5 mm in figure a and 2 mm in figure b.

The production of ions in the sheath by electron impact is neglected. In the space charge region, where the electrons obey the Maxwell-Boltzmann relation, the electron density is negligible and thus also the production of ions. But during the moments the positive ion density at the positions $0 < x < x_s(t)$ is compensated by the electrons due to the high frequency voltage modulation and the movement of the electron front, the electron impact can not be neglected

anymore in this quasi neutral region. Under these conditions thermal ions are produced which, however, react identically to the ions produced by charge exchange collisions at the same position. These ions produced by electron impact can affect the relative height of the peak structure but not the position of the peaks.

3.4 Conclusions

The low frequency RF sheath may be considered as a sequence of DC discharges, where the imposed sheath voltage variation causes the modulation of the sheath conditions. The electrons which are assumed to obey the Maxwell-Boltzmann relation are repelled from the space charge region and their density may be neglected in the sheath, so the sheath may be considered purely ionic. The influence of the electrons is only felt through the Bohm velocity at which the ions have to enter the sheath. The ionic DC sheath can be described self-consistently.

The IED in the collisionless low frequency sheath is determined by the voltage modulation across the sheath. Due to the short transit time which the ions need to cross the sheath, short with respect to the RF period, the maximum and the minimum ion energies correspond to the maximum and the minimum sheath voltages, respectively.

In the high frequency case the ion density in the sheath may be asssumed constant and is determined by the time averaged potential in the sheath. The RF voltage modulation allows the electrons to penetrate in the sheath and to compensate the ion density. The remaining space charge region phase angle matches the imposed sheath voltage at that moment, according to Poisson's law. The electron front may be assumed to move in the sheath and to be step-like at the space charge edge.

The constant ion density can be described quasi-selfconsistently by an expression derived from the ionic DC sheath solution where the average voltage difference across the sheath has been taken into account. The average voltage difference determines the average ion velocity at the electrode and, subsequently, the average ion density near the electrode. The time dependent electric field in the sheath can be derived from the ion density and the movement of the electron front. It seems to be quite reasonable that this high frequency sheath model is valid when the ion transit time through the sheath is longer than about 3 RF periods. If this time is shorter, the ion density may not be considered

constant. A second model which is based on the empirical PIC result that the average ion velocity increases proportional to the position in the sheath, leads to a simpler expression for the electric field. This model is also quasi-selfconsistent but less sophisticated although the electric field is quite similar to that in the other model. The IED's determined by both models, show no significant differences.

The maximum sheath tickness is implicitly determined by the models and depends on the ion density at the sheath edge, the maximum sheath voltage, and the Bohm velocity.

The time dependent electric field in the high frequency sheath causes a modulation of the ion acceleration. This leads to a typically saddle structured IED. The average ion energy depends on the average voltage drop across the sheath and the splitting is determined by the average transit time through the sheath.

Due to the fact that newly formed ions start with thermal energy, charge exchange collisions cause typical peak and double peak structures in the IED. This is in contrast to elastic scattering where the energy and the momentum are distributed according to the conservation laws assuming a hard sphere elastic scattering model and where no clear structures are recognized. Only at rather high pressures, head-on collisions cause some distinct features.

The density of negative ions which are produced in electro-negative gases, may be neglected in the sheath. The influence of these ions is restricted to a change of the Bohm velocity. It is less compared to the Bohm velocity in a plasma without negative ions. Due to a lower Bohm velocity, the positive ion density drops more rapidly in the sheath than ion the case without negative ions. Consequently, the sheath thickness increases due to a lower space charge.

Appendix B: The high frequency sheath model B

Velocity profiles in the high frequency sheath determined by Particle-In-Cell simulations show an almost linear behavior in the phase space [Bre92, Ven90a, Ven90b] for large range of plasma and sheath conditions. In figure B.1 the phase space is shown of a 10 MHz hydrogen plasma. The figure shows the plasma glow and both sheaths. The ion velocity distribution in the plasma glow is thermal. The average sheath voltage is 200 V. The pressure is 0.5 mTorr so collisional effects in the sheath are negligible. This result is taken as an initial assumption to develop an analytical high frequency sheath model to describe the electric field in the sheath. The assumption can be written as

$$\frac{du_i(x)}{dx} = constant. \tag{B.1}$$

The time average velocity profile now becomes

$$u_i(x) = u_{i,0} + \frac{x}{d_{sh,max}} \left(\overline{u}_{i,electrode} - u_{i,0} \right). \tag{B.2}$$

The dimensionless form is

$$v_i(y) = 1 + y(b-1), \tag{B.3}$$

using the equations (3.8) and (3.30). The dimensionless density profile in the collisionless sheath now becomes

$$n_i(y) = \frac{1}{1 + y(b-1)}. \tag{B.4}$$

The velocity and density profiles are shown in figure B.2 for the sheath situation at which $V_{sh,max} = 100$ V, $V_{sh,min} = 0$ V, $kT_e = 2$ eV and $b = 7.14$, similar to the figures shown in subsection 3.3.2.

The RF modulation is treated in the same way as described in subsection 3.3.2. The electric field is described by Poisson's law as given by equations (3.37), (3.38) and (3.39). In this model the electric field is described
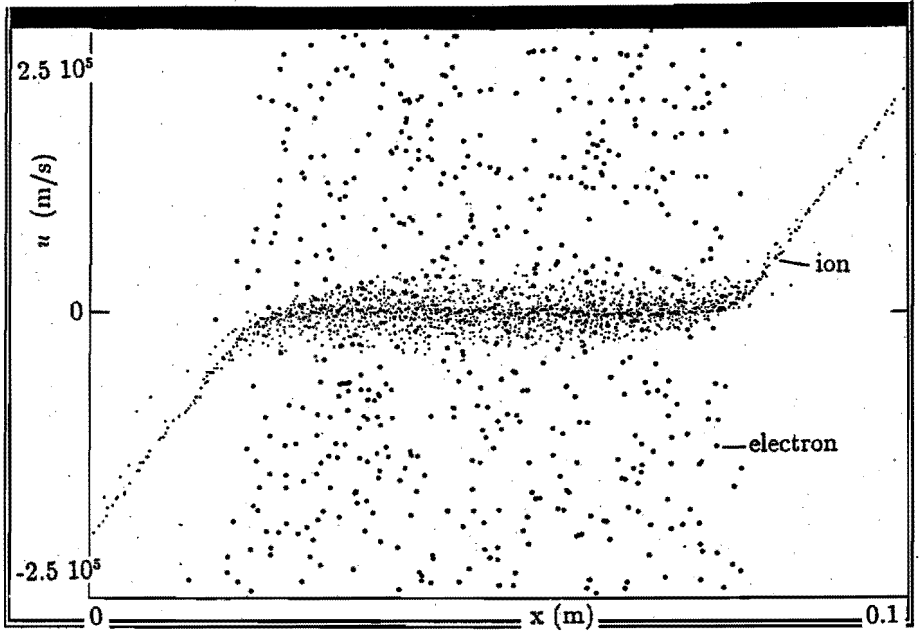
Figure B.1: The ion (small dots) and electron (large dots) velocity profile in a 10 MHz plama in hydrogen calculated with PIC method. The average sheath voltage is 200 V and the pressure is 0.5 mTorr.

by

$$\mathcal{E}(x, x_s(t)) = \frac{eN_0}{\varepsilon_0} \int_{x_s(t)}^{x} \left[1 + \frac{x'(b-1)}{d_{sh,max}} \right]^{-1} dx' \quad \text{for } x_s(t) \leq x \leq d_{sh,max}, \quad \text{(B.5)}$$

$$= 0 \qquad\qquad\qquad \text{for} \quad 0 \leq x < x_s(t). \quad \text{(B.6)}$$

In dimensionless form this becomes

$$\Psi(y, y_s(\xi)) = \Lambda^2 \int_{y_s(\xi)}^{y} \frac{dy'}{1 + y'(b-1)} \qquad \text{for} \quad y_s(t) \leq y \leq 1, \quad \text{(B.7)}$$

$$= 0 \qquad\qquad\qquad \text{for} \quad 0 \leq y < y_s(t), \quad \text{(B.8)}$$

with

$$\Lambda^2 = \frac{2}{9} (b+2)^2 (b-1). \quad \text{(B.9)}$$

Integration gives

$$\Psi(y, y_s(\xi)) = \frac{2}{9} (b+2)^2 \left[\ln(1 + y(b-1)) - \ln(1 + y_s(\xi)(b-1)) \right]$$
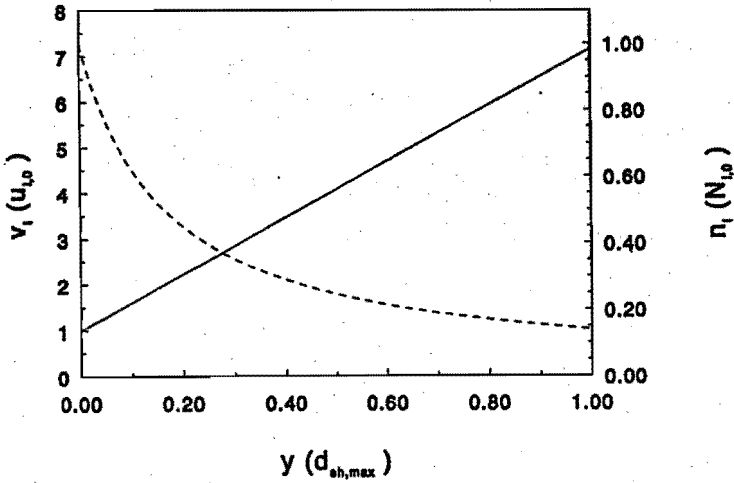
Figure B.2: The average ion velocity profile (solid line) and the ion density profile (dashed line) in a high frequency sheath. The sheath conditions are the same as in figure 3.9. The maximum sheath thickness according to this model is 2.1 mm.

$$\begin{aligned} & \text{for} \quad y_s(t) \le y \le 1, \quad \text{(B.10)} \\ = \ 0 & \text{for} \quad 0 \le y < y_s(t). \quad \text{(B.11)} \end{aligned}$$

The potential in the sheath is also determined by Poisson's law. In the dimensionless form this becomes

$$\eta(y, y_s(\xi)) = -\int_0^y \Psi(y', y_s(\xi)) \, dy' + \eta_p(\xi). \tag{B.12}$$

This leads to

$$\begin{aligned} \eta(y, y_s(\xi)) = & -\frac{2(b+2)^2}{9(b-1)} \left[(1 + y(b-1)) \ln(1 + y(b-1)) - \right. \\ & \left. - (1 + y(b-1)) \ln(1 + y_s(\xi)(b-1)) - (b-1)(y - y_s(\xi)) \right] + \\ & + \eta_p(\xi) \qquad \text{for} \quad y_s(\xi) \le y \le 1, \qquad \text{(B.13)} \\ = & \ \eta_p(\xi) \qquad\qquad\qquad\qquad \text{for} \quad 0 \le y < y_s(\xi). \quad \text{(B.14)} \end{aligned}$$

The voltage across the sheath is given by

$$\begin{aligned} \eta_{sh}(\xi) = & \ \eta_p(\xi) - \eta(1, y_s(\xi)) \\ = & \ \frac{2(b+2)^2}{9(b-1)} \left[b \ln b - b \ln(1 + y_s(\xi)(b-1)) - (b-1)(1 - y_s(\xi)) \right]. \text{(B.15)} \end{aligned}$$

For the maximum sheath voltage follows

$$
\begin{aligned}
\eta_{sh,max} &= \eta_{p,max} - \eta(1,0) \\
&= \frac{2(b+2)^2}{9(b-1)}\,[\,b\ln b - b + 1\,].
\end{aligned}
\tag{B.16}
$$

The maximum sheath thickness is given by

$$
d_{s,max}^2 = \frac{\varepsilon_0\,(b-1)^2\,V_{sh,max}}{q_i\,N_0\,(b\ln b - b + 1)}.
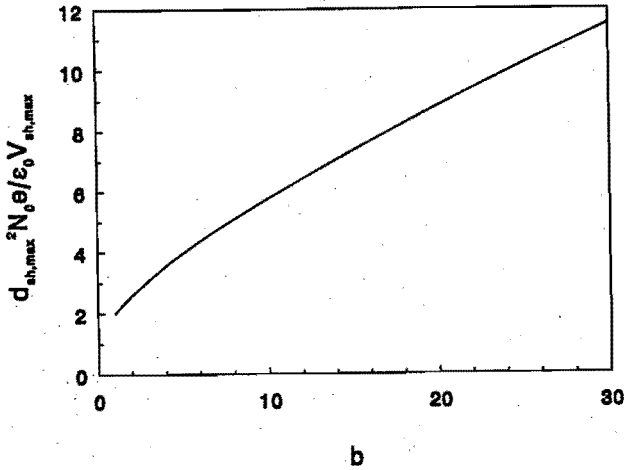\tag{B.17}
$$

This relation is depicted in figure B.3.

Figure B.3: The maximum sheath thickness as function of the parameter b for the high frequency sheath model as described in appendix B.

The position of the electron front is determined by the imposed sheath voltage $\eta_{sh}(\xi)$ and can be calculated from equation (B.15). In figure B.4 the position of the electron front is shown for the same sheath conditions as in figure 3.10.

The model is close to self-consistency, although less than the model described in subsection 3.3.2 (model A). The self-consistency is proved in the same way as in subsection 3.3.2. Figure B.5a shows the average potential in the sheath and the velocity profiles that are assumed and calculated from the average potential in the sheath, respectively. Figure B.5b shows the density
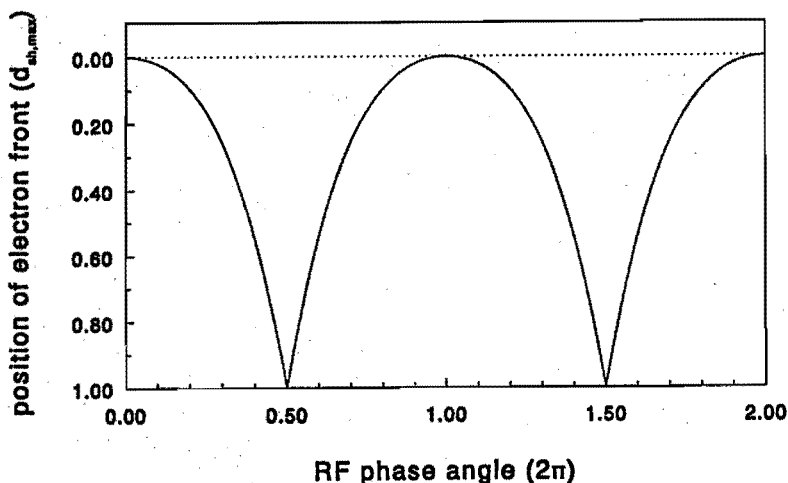
Figure B.4: The movement of the electron front in according to the high frequency sheath model as described in appendix B, due to a sinusoidal sheath voltage modulation and during two RF periods. The sheath conditions are the same as in figure 3.9.

profiles. The derivatives of the assumed profiles do not continuously connect to the presheath conditions, while the differences between the assumed profiles and the profiles derived from the average voltage profile are larger than at model A. The electric fields described by the models are rather similar for values of b up to about 15. Consequently, the sheath thicknesses in both models are the same within a margin of 5 %. In figure B.6 the time dependent electric field is shown for both models for 6 different positions of the electron front. The sheath condition corresponds to $b = 7.14$, which means a $V_{sh,max}$ and a $V_{sh,min}$ of 100 V and 0 V, respectively. The electron temperature is 2 eV. At larger b values, the thickness in model A becomes larger than in model B (up to 15 % at $b = 25$). This is in agreement with a smaller local electric field that follows from model A. The measurements have taken place under plasma conditions $b < 15$. Both models are quite similar for these conditions and are used to describe the sheath. The expressions in model B are simpler, wheras the boundary conditions in model A are more realistic.
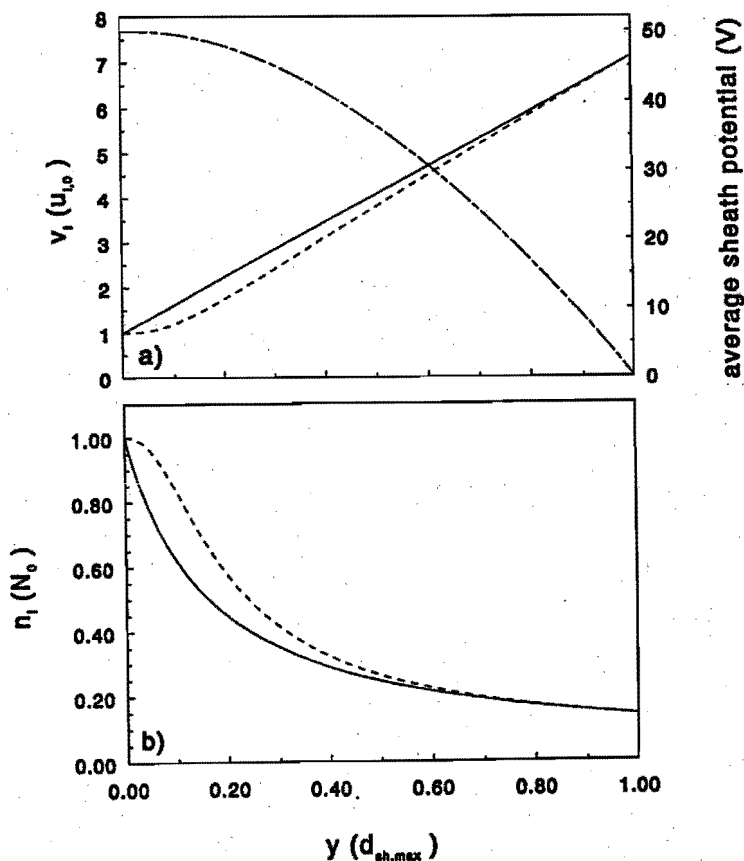
Figure B.5: The average potential in the sheath (a, dash dotted line) diverted from the sheath model as described in appendix B. The average velocity profile according to the model (a, solid line) and diverted from the average potential (a, dashed line). The density profiles are shown in figure b. The solid line represents the profile according to the model and the dashed line the profile diverted from the average potential.

References

[Boh49]   D. Bohm, *The Characteristics of Electrical Discharges in Magnetic Fields*, (McGraw-Hill, New York, 1949).

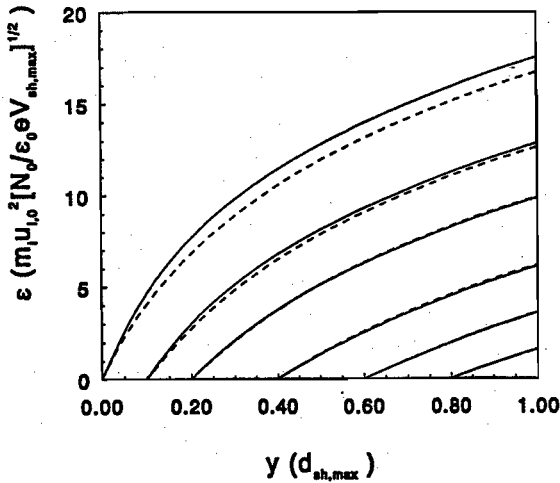[Bra88]   N.St.J. Braithwaite and J.E. Allen,

Figure B.6: The time dependent electric field in a high frequency plasma described by the model described in subsection 3.3.2 (solid lines) and the model described in appendix B (dashed lines). The field is drawn for 6 different positions of the electron front: $y_s(\xi)$=0, 0.2, 0.4, 0.6 and 0.8. The sheath conditions are the same as in figure 3.9. (b = 7.14)

J. Phys. D: Appl. Phys. **21**, 1733 (1988).

[Bre92]   J. van Breda, internal report, Eindhoven University of Technology, the Netherlands, VDF/NG 92-02, 1992.

[Car62]   A. Caruso and A. Cavaliere, *Il Nuovo Cimento*, **26**, 1389 (1962).

[Cha80]   B. Chapman, *Glow discharge processes.* (Wiley, New York, 1980).

[Fie91]   D. Field, D.F. Klemperer, P.W. May and Y.P. Song, *J. Appl. Phys.* **70**, 82 (1991).

[Har59]   E.R. Harrison and W.B. Thompson, *Proc. Phys. Soc.* **74**, 145 (1959).

[Köh85]   K.Köhler, D.E. Horne and J.W. Coburn, *J. Appl. Phys.* **58**, 3350 (1985).

[Man91]   A. Manenschijn and W.J. Goedheer, *J. Appl. Phys.* **69** 2923 (1991).

[McD64]   E.W. McDaniel, *Collision phenomena in ionized gases,* (Wiley, New York and London, 1964).

[Rie81]   K.-U. Riemann, *Phys. Fluids,* **24**, 2163 (1981).

[Rie89]   K.-U. Riemann, *Phys. Fluids,* **B1**, 961 (1989).

[Rie91]   K.-U. Riemann, it J. Phys. D: Appl. Phys. **24**, 493 (1991).

[Rie92]   K.-U. Riemann, it Phys. Fluids, **B4**, 2693 (1992).

[Tho88]   B.E. Thompson, H.H. Sawin and D.A. Fisher,
           J. Appl. Phys. **63**, 2241 (1988).
[Ton29]   L. Tonks and I Langmuir, *Phys. Rev.* **34**, 876 (1929).
[Ven90a]   D. Vender and R.W. Boswell, *IEEE Trans. Plasma Phys.* **18**, 725 (1990).
[Ven90b]   D. Vender, *Numerical studies of the low pressure RF plasma.*
           Ph.D. thesis, Canberra, Australia, 1990.
[Wil91]   C. Wild and P. Koidl, *J. Appl. Phys.* **69**, 2909 (1991).
[Yon90]   Yong-Ho Oh, Nak-Heon Choi and Duk-In choi,
           J. Appl. Phys. **67**, 3264 (1990).

4 The etch reactor and diagnostics

4.1 Introduction

During the research project concerning plasma etching at the Department of Applied Physics of the Eindhoven University of Technology, two etch reactors were built to study 13.56 MHz AC coupled etch plasmas operating at low pressures in the reactive ion etching (RIE) mode. Results obtained with the first one are described in the Ph.D. thesis of T.H.J. Bisschops [Bis87]. The second reactor had been designed to study the RF plasma with the help of spectroscopic diagnostics and the etching itself with ellipsometry. This reactor and the results of these investigations are described in the Ph.D. thesis of M. Haverlag [Hav91]. During both investigations micowave resonance techniques were used to determine the densities of electrons and negative ions. Therefore the grounded electrode was extended around the smaller driven electrode to create a microwave cavity. To use the knowledge about the RF plasma which is acquired during these investigations the electrode geometry is kept the same and the second reactor is adapted to measure the ion energy distributions mass-resolved. In this chapter the reactor, the electrode geometry and the experimental setup to determine the IED's are described.

4.2 The etch reactor

4.2.1 The electrode geometry

For the mass selection, an electrical quadrupole system is used, which is mounted behind a small sample hole in the electrode. To obtain reliable results, the quadrupole potentials have to be matched to the electrode potential. Because of the complex combination of input voltages of the quadrupole system, in which also radio frequencies are used, it is very difficult to use the plasma RF excitation voltage as an instantaneous reference potential for the quadrupole system and thus perform the experiments at the driven electrode. Therefore the diagnostic is placed behind and coupled to the grounded electrode. To measure the IED's of ions which normaly bombard the smaller driven electrode where the etching takes place, we built a new cavity with the same geometry but with a large driven electrode and a small grounded electrode. This cavity is called the inverse cavity. As shown in chapter 2, the plasma is identical, whether the driven electrode is the smallest or the largest one, provided the area ratio of the electrodes is the same. Except that the reference potential of the plasma differs, but this is of no influence on the plasma condition. In figure 4.1 the two electrode geometries are shown schematically. The cavity is cylindrically
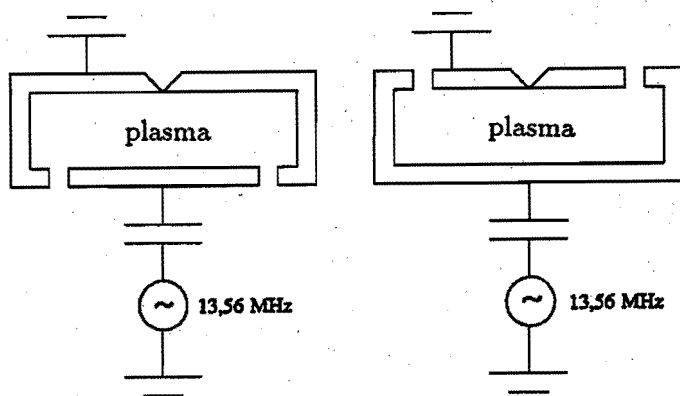

Figure 4.1: Schematical presentation of the normal and the inverse cavity

symmetric around the vertical axis. The inner diameter of the cavity is 17.5 cm and the diameter of the smallest electrode is 12.5 cm. The inner height of the cavity is 2.0 cm. In the grounded electrode a sample hole is situated through which the ions leave the plasma region and enter the detection chamber.

Normal cavity

In the normal cavity the gas is fed into the plasma region through the small opening between the driven and the grounded electrode. In the side wall of the grounded electrode, four slits are present to allow the gas to leave the cavity, to flow into the vacuum vessel and to be pumped away. Because the power deposition at the smaller electrode is much higher than at the larger electrode, the smaller electrode is water cooled. This also because the smaller electrode (the driven one) is electrically and also thermally only connected to the RF generator by a coaxial cable which does not provide a good heat contact. To avoid that a plasma is generated below the driven electrode, this part of the electrode is shielded by an insulating plate.

Inverse cavity

The inverse cavity is far more complex than the normal cavity. The driven electrode in this situation is extended around the small, grounded electrode. To avoid that a plasma is generated outside the cavity, so between the driven electrode and the reactor wall, the driven electrode has been shielded completely at the outside by an aluminum cover. The space between this shielding and the electrode is filled with ertalyte, an insulating material. Both electrodes are water cooled. The gas is fed to the plasma through a shower in the driven electrode and the gas is allowed to leave the cavity through four slits in the side wall of the electrode, the insulating and shielding mask. The gas inlet is different between the two cavities but this is not crucial. In both cases the gas is lead through the plasma before it leaves the cavity. As a matter of fact, during the former investigations, using the cavity, no influence of the gas flow was found. The RF power is coupled in at the middle of the largest electrode. A schematical picture of the inverse cavity is shown in appendix C.

4.2.2 The etch reactor

The cavity in which the plasma is produced is situated in the middle of a cylindrical vacuum vessel. The vessel is made of stainless steel and has a height of 38 cm and an inner diameter of 22 cm. In the side wall of the vessel some windows and ports are present, which among others are used for vacuum pumping and pressure measurements. The reactor can be opened by lifting the upper part of the vessel with a hoist. The vessel is pumped by a 250 m^3/h Pfeiffer WKP 250 roots blower and a 30 m^3/h Pfeiffer DUO 030A double stage primary pump. In between the roots blower and the primary pump, an oil filter is situ-

ated to avoid oil from the primary pump entering the reactor. The pressure in the vessel can be adjusted by changing the pumping speed with a Balzers IB 063 throttle valve, independently from the gas flow that in its turn is adjusted by Tylan FC 260 mass flow controllers. The absolut gas pressure in the vessel is measured with a MKS 370 HS-10 Baratron capacitance manometer. The base pressure is below 10^{-4} Torr.

4.2.3 The electrical circuit

The RF excitation voltage to sustain the plasma, is generated by a Hewlett Packard 8116A function generator in combination with a ENI 3100 LA power amplifier. The power amplifier is interlocked with the water cooling system of the electrodes: when the water flow is off, the amplifier is disabled.

The RF power is fed through 50 Ω coaxial cables and is coupled to the driven electrode by a matching network. This network matches the impedance of the plasma system to the output impedance of the amplifier. The reflected power to the RF amplifier is measured by a Bird Model 4410 power meter. During plasma experiments the reflected power level was always less than 1 %. The matching network consists of one self induction and two vacuum capacitors. One of these capacitors is the blocking capacitor and allows for AC coupling of the system.
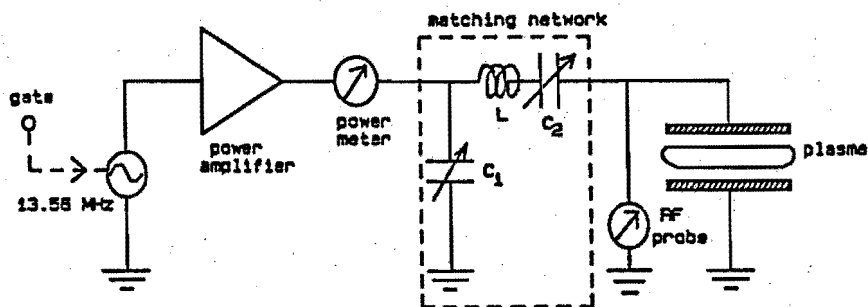

Figure 4.2: The electrical circuit used to generate the plasma

The amplitude of the excitation voltage V_{rf} and the autobias voltage V_{dc} are important parameters for the characterization of the sheath behaviour. These voltages are measured with a Tektronix P6007 RF probe. The best position to determine the V_{rf} is directly at the driven electrode itself, but because of

the reactor geometry this is virtually impossible, both with the normal and the inverse cavity. Measurements of the DC autobias voltage can be done directly at every position at a cable which is connected to the electrode.

In the normal cavity the voltages can only be measured at the powered cable because of the reactor and cavity geometry. The measurements have been done as close as possible ($\pm$ 10 cm) to the electrode. In the inverse cavity, the voltages cannot be measured at the powered cable close enough to the electrode. Therefore an extra cable is connected to the driven electrode to determine the electrode voltages.

Measurements of V_{rf} and V_{dc}, and the conclusions about the characterization of the sheath behaviour related to these voltages are presented in chapter 5.

4.3 Mass and energy spectrometer

4.3.1 Introduction

The top side of the reactor as described in the Ph.D. thesis of M. Haverlag [Hav91] is adapted to install the mass and energy analyzing system to determine mass-resolved the IED's. In figure 4.3 the set-up is depicted schematically.

In the top of the reactor vessel, a detection chamber is created which is pumped differentially by a Pfeiffer TPH 170 turbo moleculair pump and an Edwards ED 75 primary pump. The pressure in the detection chamber is measured with a Balzers TPR 010 Pirani and a Balzers IKR 020 Penning manometer. During the experiments the pressure is lower than 10^{-6} Torr, which means that there are no collisional effects in the detection chamber. The bottom of the detection chamber is formed by the central part of the grounded electrode. The height of this part is adjusted to the same height as the outer part of the electrode by millimeter screws. The sample hole through which the ions enter the detection chamber is situated in the middle of the grounded electrode. In the detection chamber, the ions have to pass successively the ion lens, the electrical quadrupole system, the energy selector and the exit slit before they are detected by the channeltron. In sections 4.3.2 to 4.3.6 these parts of the set-up are discussed.
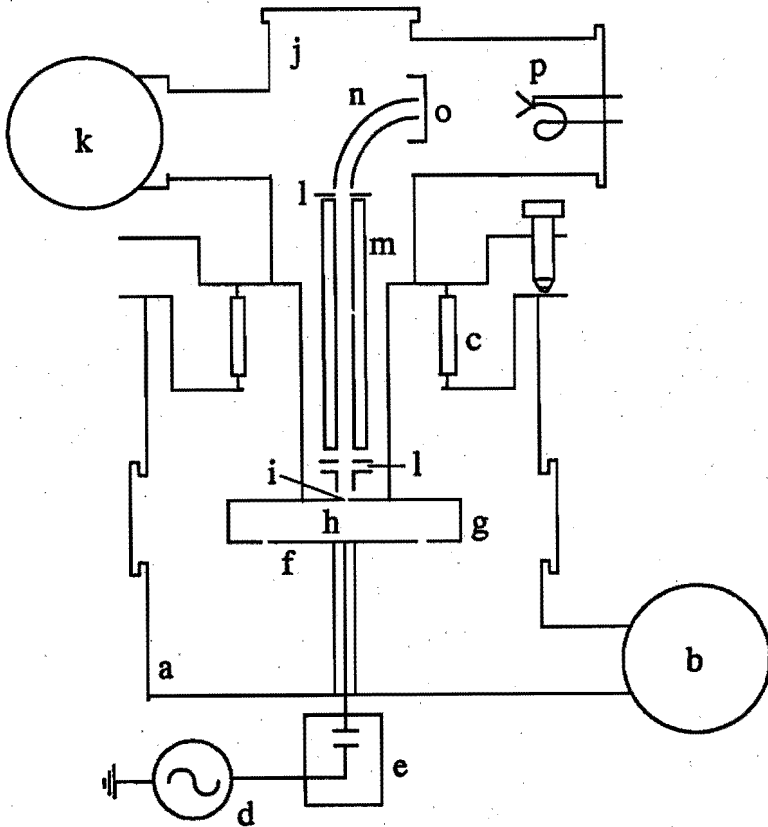
Figure 4.3: Schematical view of the diagnostic and the normal cavity. a) re-actor vessel, b) pump, c) bellows, d) RF generator, e) matching network, f) RF electrode, g) grounded electrode, h) plasma cavity, i) sample hole, j) detection chamber, k) pump, l) ion lens, m) quadrupole mass selector, n) energy selector, o) exit slit, p) channeltron.

4.3.2 The sample hole

The sample hole is drilled in a 2 mm thick molybdenum plate, which is sit-uated in the middle of the grounded electrode. The diameter of the sample hole is 40 μm. Molybdenum is used because this material does not become charged electrically and subsequently no electrical fields are generated around the sample hole which can disturb the ion passage through the sample hole [Tho86].
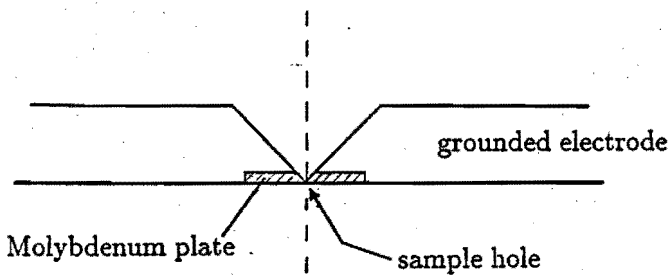
Figure 4.4: The molybdenum plate with the sample hole, as situated in the grounded electrode.

The diameter of the sample hole is small with respect to the ion mean free path which means that the collisional effects in the direct surroundings of the hole are negligible [Dra68].

4.3.3 The ion optics

We consider the IED of one ion species to be composed of separate ion fluxes, which all consist of ions with the same energy. To determine the IED successively the different ion fluxes are measured by varying the energy selection of the system. The transmission and resolution of the mass and energy selecting system depend on the kinetic energy at which the ions pass the system (E_{pas}). To avoid transmissional and resolutional effects, the ions to be measured are accelerated or decelerated to a fixed E_{pas} before they enter the quadrupole. The energy selector is adjusted to select ions with a kinetic energy E_{pas}. For this purpose the reference potential of the system is adjusted externally and the potential at the system axis (V_{axis}) is known. The initial kinetic energy of the ion (E_{ion}) can be derived from V_{axis} and E_{pas}, according to

$$E_{ion} = q_i V_{axis} + E_{pas}. \tag{4.1}$$

In figure 4.5 the measurement procedure is schematically elucidated. V_{axis} is shown for two cases: the measurement of ions with initial energies of 60 eV and 160 eV. Both ions are decelerated to a kinetic energy of E_{pas} and a potential energy of $q_i V_{axis}$. E_{pas} is 10 eV in this example. During the measurement of the ions with initial energy 60 eV, V_{axis} is 50 eV, while in the case of the 160 eV ions V_{axis} is 150 eV. The voltage of the first part of the ion lens is a little bit

higher than V_{axis}. This will be discussed in subsection 4.3.4. Ions with an initial energy less than E_{pas} are accelerated by the ion lens.
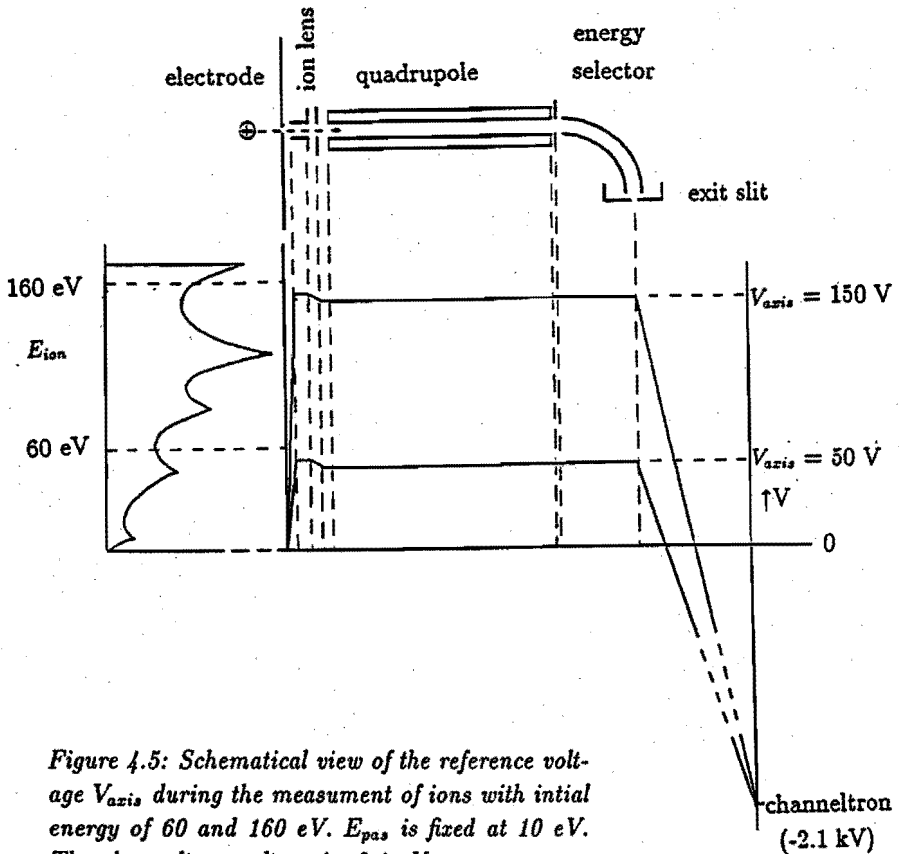

Figure 4.5: Schematical view of the reference voltage V_{axis} during the measurment of ions with intial energy of 60 and 160 eV. E_{pas} is fixed at 10 eV. The channeltron voltage is -2.1 eV.

4.3.4 The ion lens

The purpose of the ion lens is twofold: to accelerate or decelerate the ions to a kinetic energy of E_{pas} before they enter the quadrupole and to bend the ion trajectories parallel to the quadrupole axis.

The ion trajectories through the ion lens are influenced by the the electric field in the lens. This field depends on the shape and voltage of the lens in combination with the back side of the sample hole and the grounded electrode.

The shape and the voltage of the ion lens are developed by using the computer program SIMION [Dah88] so that the transmission coefficient through the lens is independent of the accelerating and decelerating rate.

During the project two lenses have been developed. One for the measurements at the normal cavity and one for the inverse cavity. This because the geometry of the backside of the sample hole is not the same in both cases. The ion lenses are made of stainless steel and are shown in figure 4.6. They consist of a cylindrical part positioned directly behind the grounded electrode, and a diaphragm in front of the quadrupole rods.

From the SIMION calculations the voltages of the ion lens are derived. The voltage of the diaphragm equals V_{axis}. The voltage of the cylindrical part of the ion lens is given by [Hop91]

$$V_{lens} = aV_{axis} + b, \tag{4.2}$$

with a and b in the normal cavity case given by

$$a = 0.971, \tag{4.3}$$

$$b = \frac{0.775 E_{pas}}{e} + 0.05V, \tag{4.4}$$

and in the inverse cavity case:

$$a = 0.969, \tag{4.5}$$

$$b = \frac{0.862 E_{pas}}{e}. \tag{4.6}$$

The ion lens bends those ions which pass the sample hole and enter the ion lens within an angle of 4° with respect to to the quadrupole axis. When the angle is larger, the ions will not pass the quadrupole. Such ions have trajectories that will cause the ions to collide with the quadrupole rods. In figure 4.7 ion trajectories in the ion lenses are shown for ions that enter the ion lens at a space angle of 4° with respect to the electrode normal. The consequence of the small acceptance angle of 4° is that only ions which bombard the electrode surface almost perpendicularly can be detected. Ions which do not collide in the sheath fulfil this condition due to the acceleration in the sheath perpendicular to the electrode. Ions which do not fulfil the condition must have collided somewhere in the sheath. This selecting operation has to be taken into account when interpreting the measured IED's. The advantage of this operation is that the influence of different collisional effects in the sheath can be distinguished.
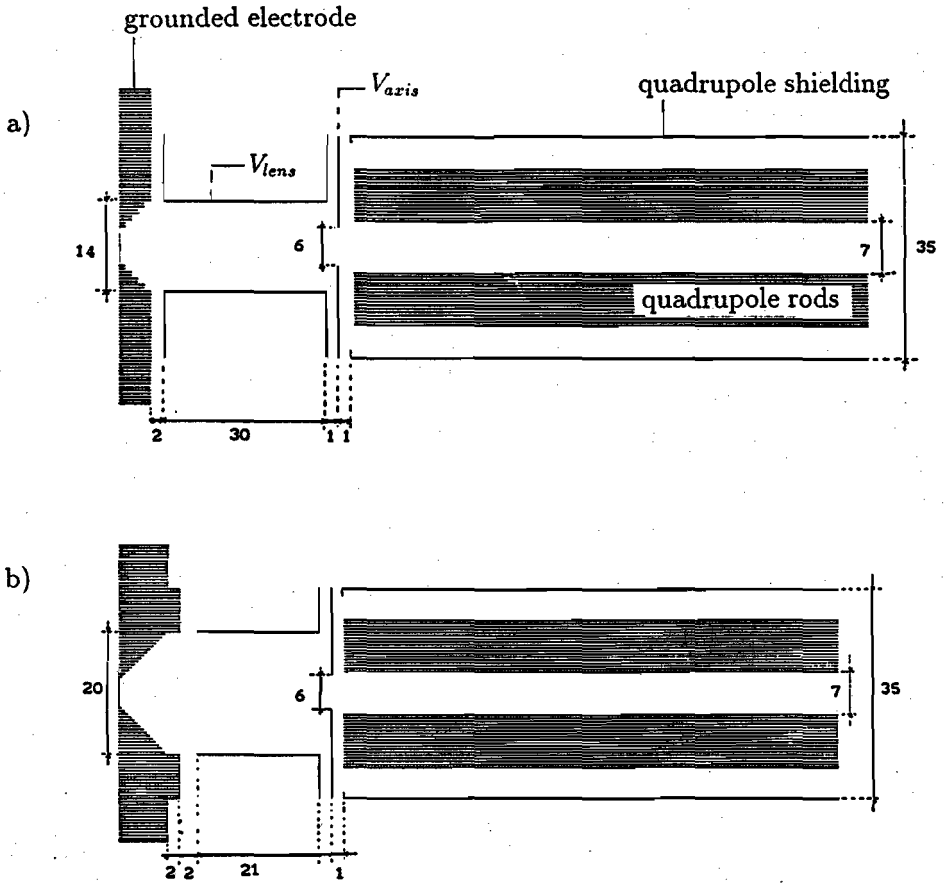
Figure 4.6: The geometry and the dimensions (in mm) of the ion lenses for the normal (a) and the inverse cavity (b).

4.3.5 The quadrupole

The ion flux is mass selected in a Balzers QMA 150 quadrupole system. This system consists of 4 parallel, round, stainless steel rods positioned as shown in figure 4.8. The distance r_0 between the field axis of the quadrupole and the rods is 3.45 mm and the length of the rods is 200 mm. The ions actually are selected as a consequence of mass dependent oscillatory ion trajectories between the rods in the x- and y-direction due to an oscillating electric field. This field is

a)

ion trajectory

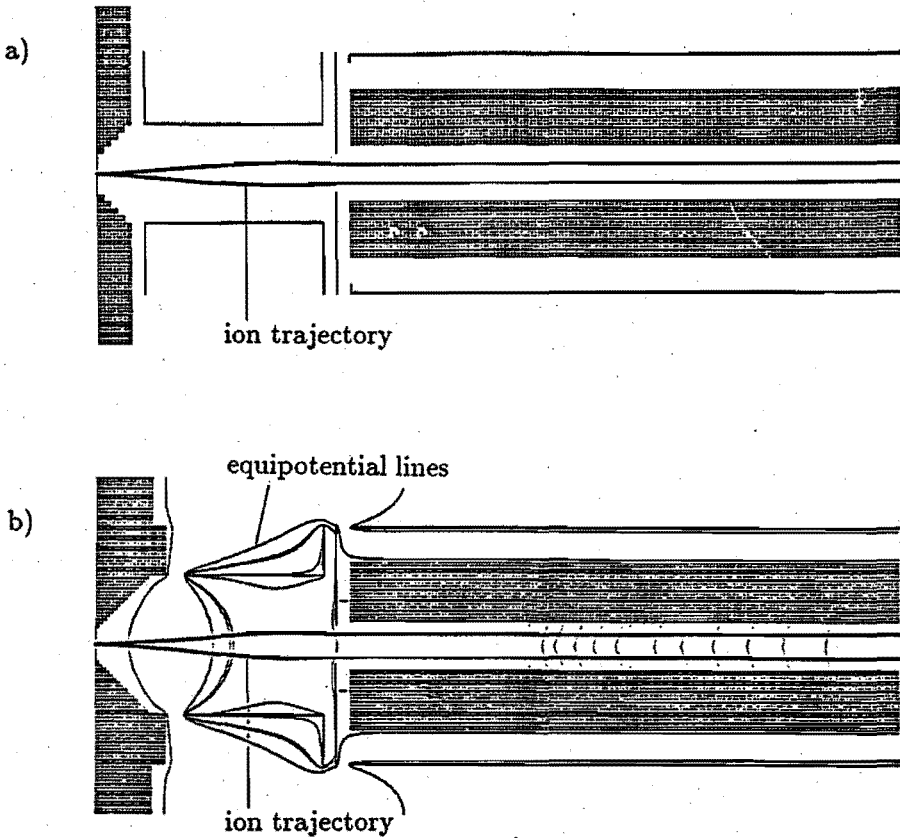equipotential lines

b)

ion trajectory

Figure 4.7: The ion trajectories in the ion lens. a) The ion trajectories in the normal cavity of an ion with an initial energy of 80 eV and $E_{pas} = 33$ eV. b) The ion trajectories in the inverse cavity of an ion with an initial energy of 200 eV and $E_{pas} = 33$ eV. Besides some equipotential lines are shown in this drawing.

caused by a combination of a DC and an RF voltage on the rods which generate a local potential distribution between the rods given by [DAW76]

$$\phi_Q(x, y, t) = (U_Q + V_Q \cos(\omega_Q t)) \frac{x^2 - y^2}{r_0^2}. \qquad (4.7)$$
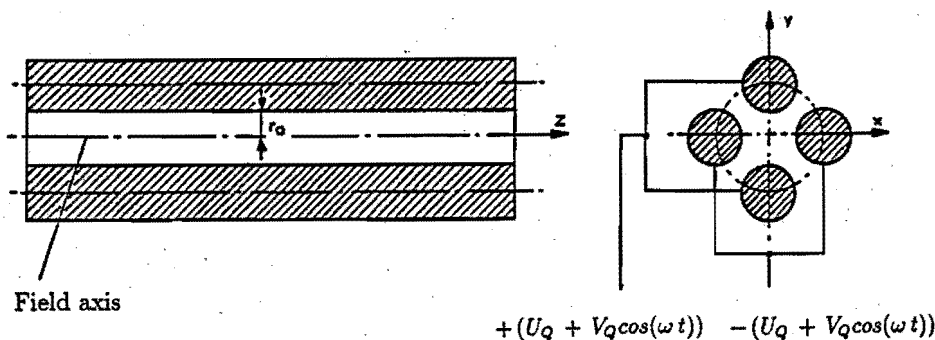
Field axis

$$+ (U_Q + V_Q cos(\omega\, t)) \quad -(U_Q + V_Q cos(\omega\, t))$$

Figure 4.8: Schematical representation of the 4 quadrupole rods. On the left a longitudinal section and on the right a cross-section.

The DC voltage U_Q and the RF voltage V_Q are generated by a Balzers QMG 311 voltage supply. These voltages are given with respect to V_{axis}. V_{axis} itself is fed externally to the voltage supply. The RF frequency ω_Q used for the mass selecting field is 1.95 or 3.0 MHz depending on the adjusted mass range. The electric field in the axial direction is zero, which means that the residence time of an ion is only determined by the passage energy. The quadrupole rods are shielded at the outside by a grounded, stainless steel cylinder. The entrance is formed by the top side of the ion lens of which the voltage is the reference voltage V_{axis}. The exit is formed by a diaphragm also biased with V_{axis}, to avoid voltage differences between the quadrupole and the energy selector. The diameter of the opening is 5 mm.

The general properties of the quadrupole system are well known and have been described extensively by Dawson [Daw76,79,80]. Only the aspects important for the understanding of the experiments are discussed here. The quadrupole transmission and resolution strongly depend on the number of oscillations which the ions perform in the quadrupole field. This number depends on the mass and the velocity of the ion in axial direction and is given by [Daw76]

$$n = \frac{\omega_Q L}{2\pi} \sqrt{\frac{m_i}{2e E_{pas}}}, \tag{4.8}$$

where L is the length of the quadrupole rods. To get a good mass selection with the quadrupole system used in these experiments, E_{pas} has to be less than 33 eV. At a fixed mass and passage energy, just as during the determination of the IED, the transmission effects of all the detected ions are the same, but

considering a mass spectrometric measurement at a fixed passage energy, transmission effects will occur. Due to the different ion masses, the number of RF cycles of the ions in the quadrupole is different. But also the quadrupole exit conditions in the phase space change as a consequence of the change of both the residence time and the local electric field [Spa88, Daw75,79]. The latter can be understood from quadrupole theory. Because the ion flux is projected at the rectangular energy selector entrance, transmission effects through the whole analyzing system are expected during a mass scan when detecting ions with a special initial energy and a fixed E_{pas}. This effect is stronger at lower mass resolution when the mass peak is broad enough to be composed of several subpeaks as shown in figure 4.9. To determine the IED of one ion species the
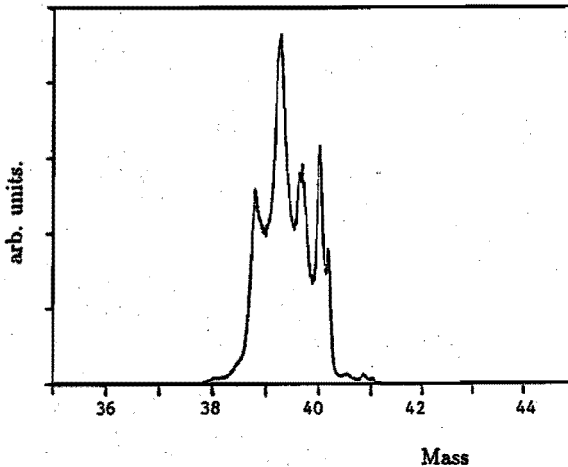

Figure 4.9: The Ar^+ mass peak, measured at a certain initial kinetic energy. Due to the transmission effects during a mass scan, the peak is composed of several subpeaks. The mass resolution is low ($\Delta m = 1.5$ a.m.u.).

mass is fixed at the local maximum preferably as close as possible to the correct mass position. The mass is adjusted externally with a voltage between 0 and 10 V which is generated by a voltage supply in combination with a PC. To avoid transmission effects the mass adjustment needs to be very stable. Experiments showed that the voltage is stable within 1.0 mV which means a mass variation of 0.01 a.m.u. The reference voltage V_{axis} is fed externally to the quadrupole system and is also generated by the voltage supply.
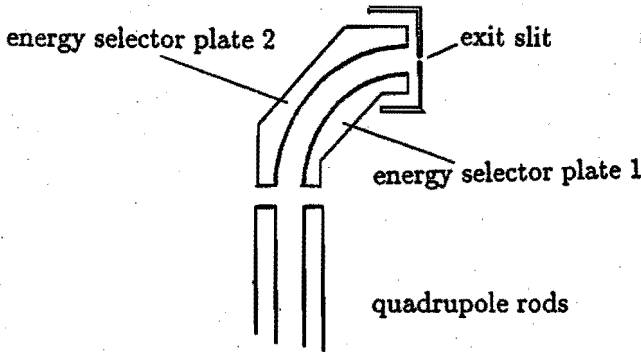
Figure 4.10: Schematical view of the energy selector.

4.3.6 The energy selector and the exit slit

After the ions have passed the quadrupole system they are energy selected in
a cylindrical mirror energy analyzer as shown in figure 4.10. The analyzer
consists of two cylindrical, aluminum plates which are bend over 90°. The
radii of the inner and outer plate are 41.0 and 47.2 mm, respectively. The
plates are covered with a gold layer to avoid charging of the surface due to
insulation effects by aluminum oxide. The ions are bent in a constant electric
field generated by the voltage difference between the two plates. The angle over
which the ions are bent, depends on the kinetic energy and the charge of the
ions. The voltage difference across the plates is chosen so that those ions of
the IED that have a kinetic energy E_{pas} when entering the energy analyzer are
selected. The absolute value of the voltage is chosen so that the voltage at the
axis of the energy selector equals V_{axis}. Laplace's equation for these conditions
in combination with the balance between the electrical and the centrifugal forces
give the voltages with which the selector plates have to be biased

$$V_{1,2} = \frac{2E_{pas}}{q_i} \ln\left(\frac{r_{1,2}}{r_{axis}}\right) + V_{axis}, \tag{4.9}$$

where r_{axis} is the radius of the axis of the energy selector. The indices 1 and 2
refer to the inner and outer selector plate, respectively. The electric field $\mathcal{E}(r)$
between the selector plates is given by

$$\mathcal{E}(r) = \frac{2E_{pas}}{q_i r}. \tag{4.10}$$

The initial ion energy can be written as

$$E_{ion} = q_i \left(V_{axis} + \frac{r_{axis} \Psi(r_{axis})}{2} \right). \tag{4.11}$$

To increase the energy resolution an exit slit of 1 mm is positioned at the end of the energy selector, centered around r_{axis}. To avoid disturbing field effects around the exit slit, the plate in which the slit is situated is biased with V_{axis}.

The energy resolution is determined by the exit slit and the stability of the voltage difference across the selector plates. The resolution ΔE as a consequence of the width of the exit slit d_{slit} is given by

$$\Delta E = \frac{4 E_{pas} d_{slit}}{\pi^2 r_{axis} - 4 d_{slit}}, \tag{4.12}$$

and is about 0.01 E_{pas} in our situation. This has also been verified with the help of computer simulations using the program SIMION.

The resolution as a consequence of the voltage instability ΔV_1 and ΔV_2 of the energy selector plates is given by

$$\Delta E = \frac{q_i(\Delta V_1 + \Delta V_2)}{2 \ln (r_2/r_1)}. \tag{4.13}$$

The voltage stability for both V_1 and V_2 is within 0.01 V, which means that these resolutional effects are smaller than 0.07 eV and are negligible with respect to the effect of the width of the exit slit.

4.3.7 The ion detection

After the mass and energy selection the ions are detected with a Philips X812AL single channel electron multiplier (channeltron) with a gain of 10^7 to 10^8. When a single ion collides with the front of the channeltron, an electron pulse is generated of 25 mV and 15 ns broad at HMFW measured at an imput impedance of 50 Ω. This pulse is amplified 200 times by a LeCroy LRS 12 channel PM amplifier, discriminated by an EG&G T105/NL Dual Discriminator and converted by a LeCroy LRS 688AL NIM-TTL convertor, before it is counted and stored by a CER PCL-720 counter card in the PC. The PC synchronizes the counts and the adjustment of the analyzing system.

The noise level of the channeltron itself is less than 10 Hz, while saturation effects become important above a count rate of 30 kHz. The detection
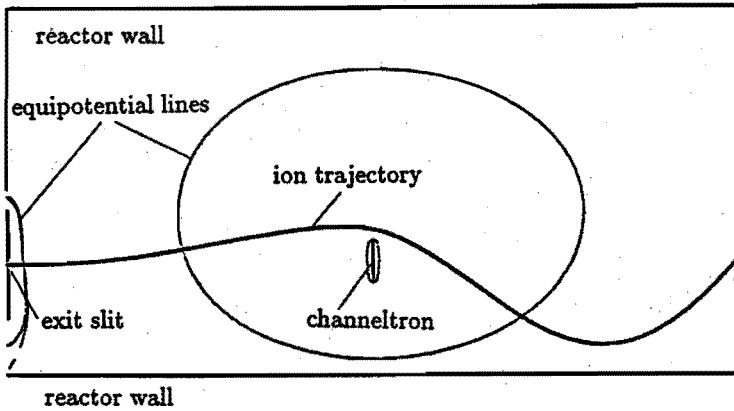
Figure 4.11: Ion trajectory in the case the exit slit the channeltron are positioned asymmetrically in the detection chamber. The initial energy of the ion is 43 eV and the channeltron is biased with -2.1 kV.

part has been extensively tested and the discrimination level is adjusted with care. The positioning of the channeltron needs special attention and has to be discussed here. The back side of the channeltron is grounded while the front which is directed to the exit slit is biased negatively with a high voltage of 2.0 - 2.5 kV. With the computer program SIMION and also experimentally, it has been demonstrated that not all the ions that leave the exit slit, hit the channeltron if both the exit slit and the channeltron are not positioned symmetrically with respect to the wall of the detection chamber. This is shown in figure 4.11 where the trajectory is shown of an ion with initial energy of 43 eV and E_{pas} of 33 eV. The potential of the exit slit is 10 V in this case. The channeltron is biased with -2.1 kV. In spite of the high negative channeltron voltage the ions do not hit the channeltron. This effect is due to the asymmetric electric field which is generated in the detection part between the exit slit and the channeltron. Also the field changes in time due to the time varying potential of the exit slit. Consequently the transmission in this part is not constant in time, if the exit slit and the channeltron are not positioned symmetrically in the detection chamber.
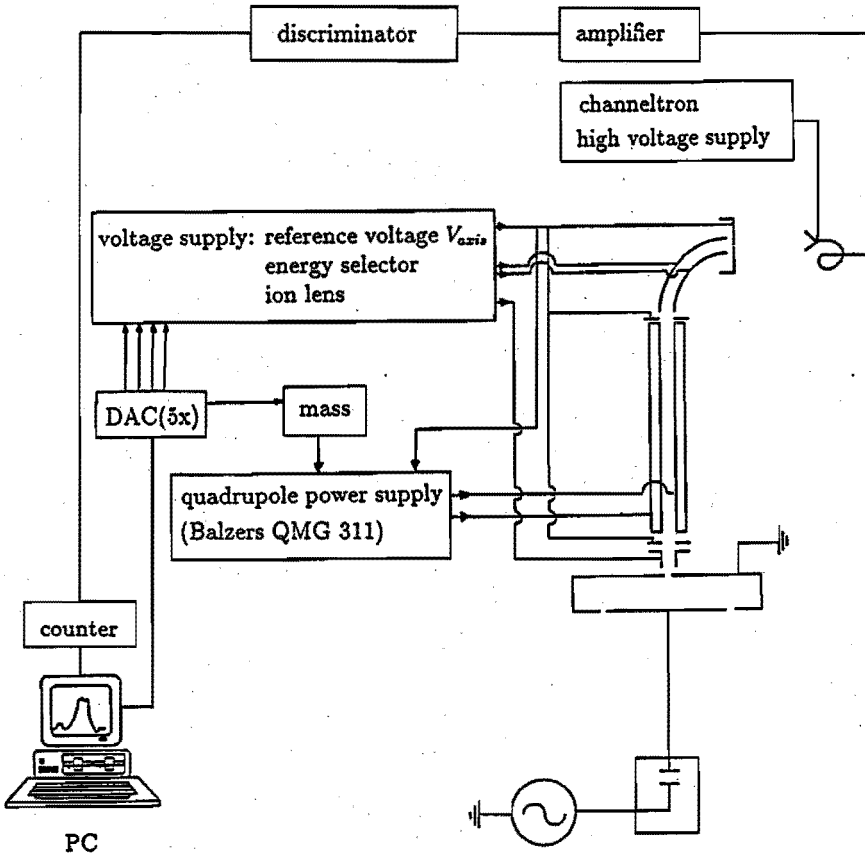
Figure 4.12: Depiction of the control and detection unit.

4.3.8 The data acquisition

The complete control and detection unit of the set-up is depicted in figure 4.12.
A home built voltage supply generates the several voltages used to manage the
experiments, like V_{axis}, V_{lens} and the energy selector voltages. Also the mass
adjustment has been set by a voltage which is generated by the voltage supply.
The voltage supply is controlled by a PC and a CER PCL-830 I/O card. The
PC also synchronizes the whole experiment.

The IED is determined by changing the reference potential V_{axis}, as explained in the former subsections. E_{pas} is fixed, just as the selecting conditions of the energy selector so that at the end only those ions are detected that we want. V_{axis} starts at $-E_{pas}/e$ and can be increased in 500 to 4000 equal steps in the range of E_{ion} of 0 to 500 eV. The ion energy at which the measurement starts and stops can be chosen freely.

Besides the determination of IED's where the mass is fixed, a mass scan can be made to survey which ions are present in the plasma. During these measurements V_{axis} and E_{pas} are fixed, and only those ions are detected which had an initial energy given by

$$E_{ion} = q_i V_{axis} + E_{pas}.\qquad(4.14)$$

So, if one wants to be certain that particular ions are present in the plasma one has to make sure that the adjusted E_{ion} is within the IED of the ion. This also means that from the mass scan experiments no conclusions can be drawn about the ratio of the ion fluxes which bombard the electrode.

When the transmission coefficient for every mass is known, the absolute ion flux can be derived by integration of the IED. To determine the mass dependent transmission coefficient, calibration plasma sources are needed of which the ion fluxes at the electrode are known. In some cases the flux can be estimated from the ion density in the glow, but in most cases and especially with molecular gasses the collisional effects in the sheath are unknown and the fluxes cannot be calibrated.
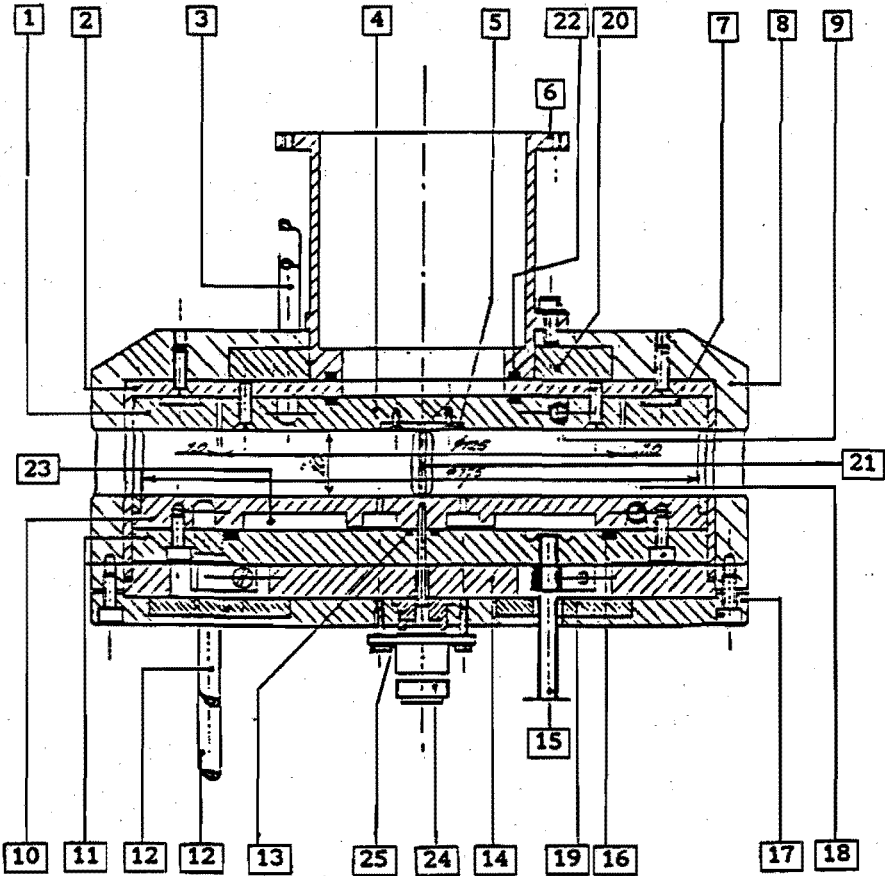
Appendix C: The inverse cavity

Figure C.1: Schematical representation of the inverse cavity.

1) upper part of driven electrode
2) insulation cylinder
3) in and outlet of cooling-water
4) grounded electrode
5) sample hole
6) wall of the detection chamber
7) insulation ring
8) shielding
9) tube of cooling-water
10) bottom part of driven electrode
    (plasma side)
11) bottom part of driven electrode
    (insulation side)
12) in and outlet of cooling-water

13) O-ring
14) insulation plate
15) gas inlet
16) O-ring
17) bottom plate of the shielding
18) tube of cooling-water
19) insulation plate
20) insulation ring
21) slit
22) O-ring
23) gas reservoir of gas inlet
24) RF power connector
25) insulation ring

The smaller electrode is grounded by three copper cables to the reactor wall, which is not shown in figure C.1.

References

[Bis87]   T.H.J. Bisschops, *Investigations on an RF plasma related to plasma etching*. Ph.D. thesis, Eindhoven University of Technology, the Netherlands, 1987.

[Dah88]   D.A. Dahl, J.E. Delmore, *The SIMION PC/PS2 user's manual version 4.0*, (Idaho National Engineering Laboratory/EG&G Idaho Inc. Idaho Falls, 1988).

[Daw75]   P.H. Dawson, *Int. J. Mass Spectr. Ion Phys.* **17**, 423 (1975).

[Daw76]   P.H. Dawson (ed.), *Quadrupole mass spectrometry and its applications*, (Elsevier Scientific Publishing Company, 1976).

[Daw79]   P.H. Dawson, *Int. J. Mass Spectr. Ion Phys.* **29**, 289 (1979).

[Daw80]   P.H. Dawson, *Int. J. Mass Spectr. Ion Phys.* **36**, 353 (1980).

[Dra68]   H.W. Drawin, *Plasma diagnostics*, (North-Holland Publishing Comp. 1968).

[Hav91]   M. Haverlag, *Plasma chemistry of fluorocarbon RF discharges used for dry etching*. Ph.D. thesis, Eindhoven University of Technology, the Netherlands, 1991.

[Hop91]   M.B. Hoppenbrouwers, internal report, Eindhoven University of Technology, the Netherlands, VDF/NG 91-06, 1991.

[Spa88]   J.C.A. Sparla, internal report, Eindhoven University of Technology, the Netherlands, VDF/NO 88-07, 1988.

[Tho86]   B.E. Thompson, K.D. Allen, A.D. Richards and H.H. Sawin, *J. Appl. Phys.* **59**, 1890 (1986).

5 The mass-resolved ion energy distribution and RF sheath analysis

5.1 Introduction

In this chapter the results are presented of the experiments described in chapter 4. The ion energy distributions have been determined in a 13.56 MHz, AC coupled plasma in argon (Ar), nitrogen (N_2) and carbontetrafluoride (CF_4) for several pressures and RF powers. Mass resolved determination of the IED offers the possibility to compare the IED's of different ion species present in the same sheath. From the IED's the collisional behaviour of the ions in the sheath can be studied and the RF sheath model as described in chapter 3 can be verified.

In section 5.2, the measurements of the RF excitation (V_{rf}) and the autobias voltage (V_{dc}) are presented. From these parameters the maximum voltage across the sheath can be derived. The sheath behaviour can be characterized by studying the average energy $(\overline{E}_{sad})$ and the splitting (ΔE) of the primary saddle structure as function of the sheath voltage.

In section 5.3, the IED's which are determined in an argon plasma, are discussed. IED's of Ar^+, Ar^{2+} and Ar_2^+ ions are measured where the densities of the latter two species are small with respect to the Ar^+ density. Charge exchange collisions have a large influence on the IED of Ar^+ and cause typical features as discussed theoretically in chapter 3. This is found to be in agreement with the experimental results. Due to small amounts of residual water vapor which always stays behind after pumping down the reactor, the IED's of hydrogen containing ions like ArH^+, H_3O^+, H_2O^+ and H_3^+ can also be

determined. Their densities are small and they hardly have any influence on the space charge in the sheath. Their IED's are influenced by elastic scattering with Ar neutrals. For the interpretation of the IED's one has to take into account that only ions which hit the electrode within an angle of 4° with the normal to the electrode can be detected. This causes that the measured IED's of the ArH^+ ions is mainly constructed by the ions which have not collided in the sheath: the measured IED's may therefore be interpreted as collisionless. Although this looks like a deficiency of the diagnostic, the benefit is that the sheath can more easily be characterized from the analysis of the "collisionless" IED's. This is illustrated in figure 5.1. In section 5.3.3 this is discussed and it will be shown that at high ion densities at the sheath edge, the sheath in front of the largest electrode can not be assumed to be purely capacitive.

In subsection 5.3.4 Monte Carlo simulations based on the time dependent electric field as calculated in chapter 3 will be presented. The simulated IED's show good agreement with experimental results. Simulations also lead to a better insight in the collisional behaviour within the sheath.

In section 5.4, IED's determined in nitrogen plasmas are presented. The space charge in the sheath is mainly formed by N_2^+, but also N^+ and N_3^+ ions are present in the plasma. The IED's of the N_2^+ show resonant charge exchange features similar to the argon case. These IED's are also simulated and good agreement with the experiments has been found.

In section 5.5, results determined in CF_4 plasmas are presented. The measured spectra show a very complex behaviour which can be attributed to ion production and loss through a large number of possible ion-neutral reactions in the sheath. Due to the very complex ion kinetics in the sheath it is hard to simulate the distributions. Simulations based on the RF sheath model described in chapter 3 are not in agreement with measured IED's because ion-neutral reactions are not included in the simulations.
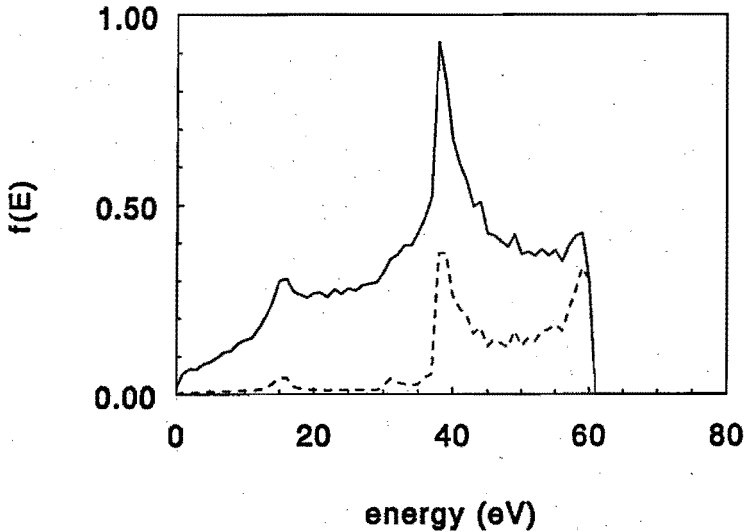
Figure 5.1: _The energy distribution of ArH$^+$ ions incident on the electrode. The solid line represents the full angular energy distribution, and the dashed line represents the central 4°, which is the only part detected by the experimental setup. The measured spectrum therefore mainly represents the ions which have not collided in the sheath, but have travelled undisturbed from the glow to the electrode. Apart from the ions that have not collided in the sheath also the ions that do have collided and that are directed towards the electrode when they hit the electrode are detected. These ions cause features in the measured IED as shown at energies at about 15 and 30 eV. The measured (= "collisionless") profile characterizes the overall sheath properties._

5.2 The RF and autobias voltage

The RF excitation voltage V_{rf} (where V_{rf} is the amplitude of the RF voltage) and the autobias voltage V_{dc} characterize the plasma conditions of plasmas generated between a certain electrode geometry and for several RF powers and pressures.

From these voltages also the maximum voltage across the sheaths $(V_{sh,max})$ can be derived. Considering the sheath in front of the smallest and the largest electrode, $V_{sh,max}$ equals $V_{rf} + V_{dc}$ and $V_{rf} - V_{dc}$, respectively. In the case of a purely capacitive sheath, the average energy of the primary saddle structure
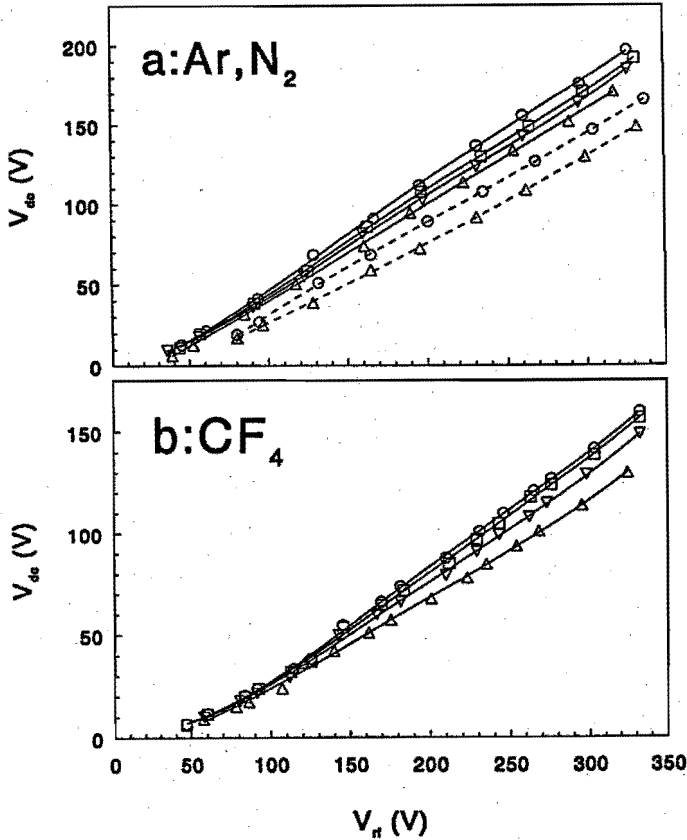
Figure 5.2: The relation between V_{rf} and V_{dc} in plasmas in a) Ar (solid lines) and N_2 (dashed lines), and b) CF_4, for several pressure conditions: 20 mTorr (o), 40 mTorr ($\square$), 80 mTorr ($\triangledown$) and 160 mTorr ($\triangle$). The plasma is generated in the inverse cavity.

$(\overline{E}_{sad})$ equals $\frac{1}{2}q_i(V_{sh,max}+V_{sh,min})$ which is confirmed by theoretically determined IED's as described in chapter 3. From analyzing $\overline{E}_{sad}$ and ΔE as functions of V_{rf} and V_{dc}, the sheath behaviour may be characterized.

In figure 5.2 the relation between V_{rf} and V_{dc} is shown for plasmas in Ar, N_2 and CF_4, for several pressure conditions and generated in the inverse cavity. In figure 5.3, the relation between V_{rf} and V_{dc} is shown as determined in an argon plasma in the normal cavity. From figure 5.2 and 5.3 which show the
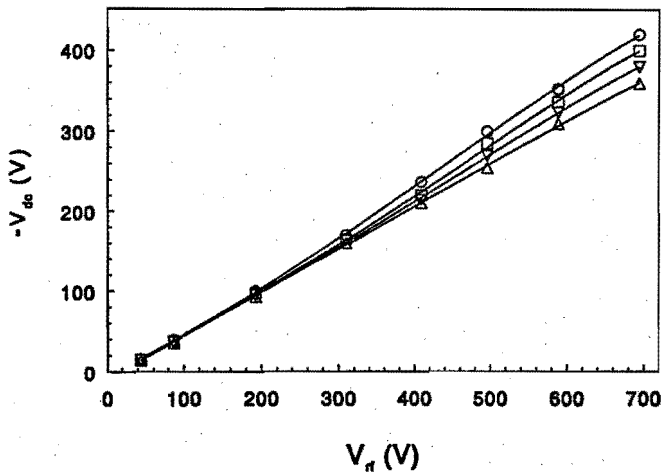
Figure 5.3: The relation between V_{rf} and V_{dc} in plasmas in Ar in the normal cavity, for the same pressure conditions as in figure 5.1: 20 mTorr (o), 40 mTorr ($\square$), 80 mTorr (∇) and 160 mTorr ($\triangle$).

same relation between V_{rf} and V_{dc}, we may conclude that the plasmas in the normal and in the inverse cavity are quite identical provided the pressure and the driving RF voltage are the same. This confirms the assumption that IED's determined at a small grounded electrode like in the inverse cavity situation, may be interpreted as the IED of the ions hitting the small driven electrode as is used for etch processes.

A difference between the normal and the inverse cavity is the stray capacitance. In the inverse cavity case the stray capacitance is in the order of 500 pF mainly due to the shielding, while this is approximately one order of magnitude less than in the normal cavity case. This means that in the case of the inverse cavity the excitation RF voltage is less than in the normal cavity case provided the generated RF power delivered by the RF source is the same. This is due to the voltage deviation in the inverse cavity where the total stray capacitance has to be taken into account. Nevertheless this does not influence the relation between V_{rf} and V_{dc} and the plasma conditions.

5.3 The IED in a 13.56 MHz plasma in argon

5.3.1 Introduction

In this section, IED's determined in an argon plasma under several conditions are shown and discussed. The IED's are measured in both the normal and the inverse cavity.

In subsection 5.3.2 the experimentally determined IED's of Ar^+, Ar^{2+} and of hydrogen containing ions like ArH^+, H_3O^+, H_2O^+ and H_3^+ are presented. These are formed by ion molecule reactions with residual water vapor. The collisionless character of the IED of ArH^+ ions is used to analyse the sheath properties. This will be discussed in section 5.3.3. Comparison with Monte Carlo simulations show a good agreement and give insight in the collisional behaviour of the different ion species in the sheath. The simulations are discussed in subsection 5.3.4.

5.3.2 Experimental results

A whole set of IED's of Ar^+ is determined in a 13.56 MHz plasma in the normal and the inverse cavity. In figure 5.4 we show IED's of Ar^+ ions incident on the grounded electrode in the normal cavity for several pressure conditions. The pressure in the plasma is 20, 40, 80 and 160 mTorr in figure a, b, c and d, respectively. The influence of charge exchange collisions is evident. Under the low pressure condition the saddle structure can be easily recognized while under high pressure conditions the saddle structure has vanished. It can be concluded that in this case hardly any ion passes the sheath without a collision. The plasma power is chosen so that the energy range of the distribution is nearly the same in the four cases.

Energy distributions of Ar^+ ions incident on the smallest, grounded electrode in the inverse cavity, show much more collisional features due to the larger sheath thickness. Even in low pressure plasmas, the ions may collide several times in the sheath and the IED shows several collisional peaks where the primary saddle structure has vanished nearly completely. This is shown in figure 5.5 for a plasma at a pressure of 40 mTorr. The RF power is 78 Watt. The height of the peaks depends on the pressure. At higher pressure more ions shift to the low energy part of the IED and the high energy part is completely depopulated, while at lower pressures relatively more ions are in the high energy part. This is shown in figure 3.20 in chapter 3, where the collisional effects are demonstrated theoretically.
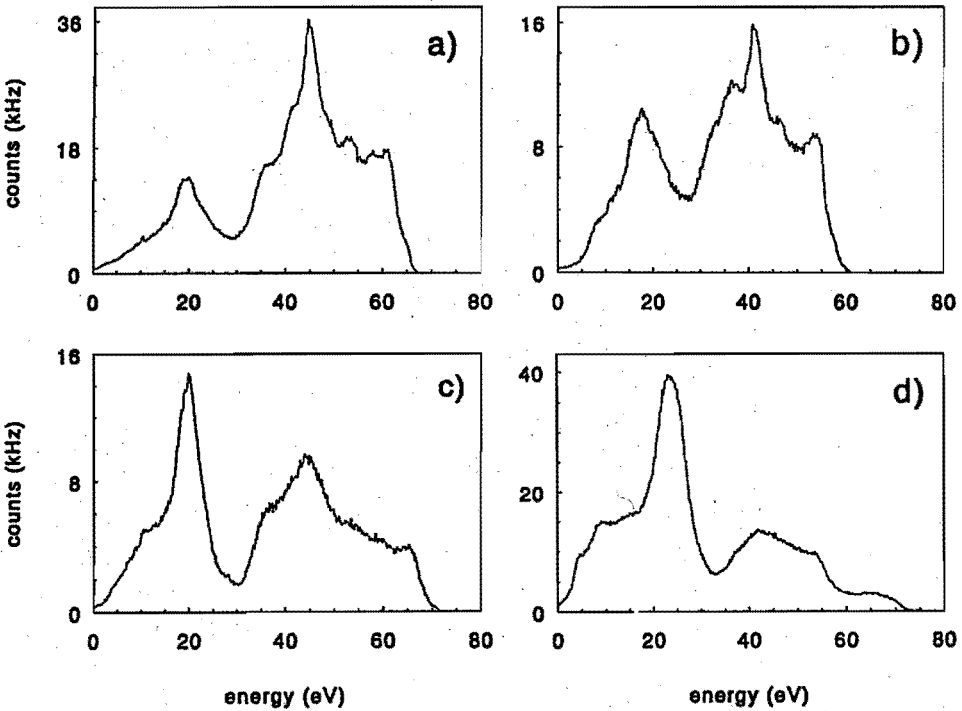
Figure 5.4: The IED's of Ar⁺ ions incident on the grounded electrode in the normal cavity for several pressure conditions: 20 mTorr (a), 40 mTorr (b), 80 mTorr (c) and 160 mTorr (d). The RF power is 48, 49,57 and 65 Watt respectively.

In figure 5.6, the measured IED of doubly charged Ar^{2+} ions incident on the grounded electrode in the normal cavity is shown. The plasma condition is the same as in figure 5.4a. The range of the ion energy is doubled with respect to the distribution of singly charged ions. The IED clearly shows the typically RF saddle structure. The feature at about 55 eV may be due to the production of Ar^{2+} ions in the sheath. Charge exchange collisions by which Ar^{2+} ions are formed, are very improbable. The Ar^{2+} density is less than the Ar^{+} density. Therefore E_{pas} during this measurement was 15 eV, which provides for a higher transmission and a better signal-to-noise ratio but also results in a lower energy resolution.
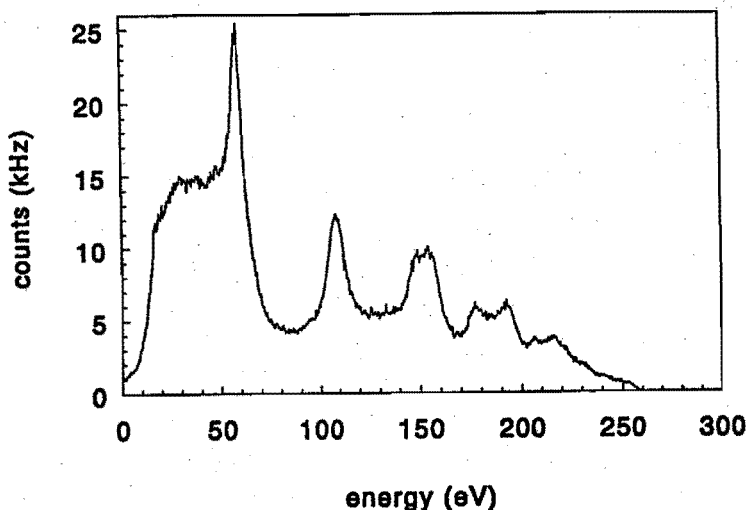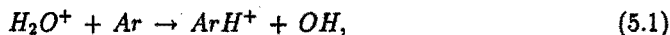
Figure 5.5: The IED of Ar^+ ions incident on the grounded electrode in the inverse cavity. The pressure is 40 mTorr and the RF power is 78 Watt.

There is always some residual water vapor in the reactor which is responsible for the formation of hydrogen containing ions like ArH^+, H_3O^+ and H_3^+ [Kne62, Cob70]. Although no absolute ratios between the ion densities can be derived from mass spectrometric measurements due to mass and energy dependent transmission, these measurements, however, show that the densities of the hydrogen containing ions are small with respect to the Ar^+ density. Because of the low density these ions hardly have any influence on the space charge in the plasma sheath. Consequently, the electric field in the sheath will be completely generated by Ar^+ ions.

The ArH^+ ions are quite stable due to the fact they have no unpaired electron, and from all the hydrogen containing ions, the density of the ArH^+ ions is the highest. ArH^+ can be formed by ion-neutral reactions like [Kne62]

$$H_2O^+ + Ar \rightarrow ArH^+ + OH, \tag{5.1}$$

or

$$Ar^+ + H_2 \rightarrow ArH^+ + H. \tag{5.2}$$

In figure 5.7 the IED of the ArH^+ ions as determined in the normal cavity, is shown. The pressure is 20, 40, 80 and 160 mTorr in figure a, b, c and d,
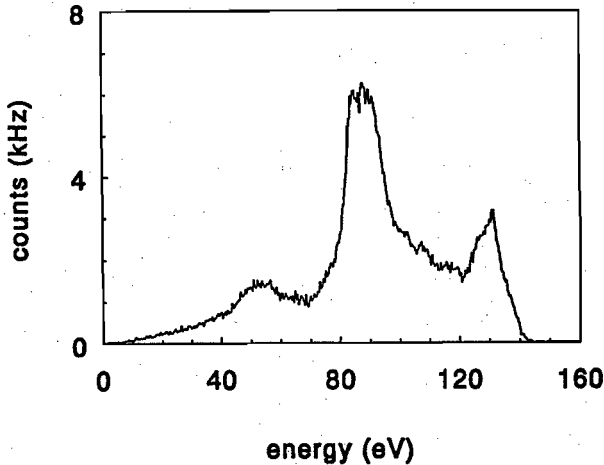
Figure 5.6: The IED of Ar^{2+} ions incident on the grounded electrode in the normal cavity. The pressure is 20 mTorr and the RF power 48 Watt.

respectively, while the plasma power is 78, 40 and 20 Watt. E_{pas} during the experiments was 15 eV.

The results are different from those of Ar^+. Even at high pressures the primary saddle structure can be recognized, while only minor collisional features are shown at energies lower than those of the primary saddle. ArH^+ ions can collide in the sheath with an argon atom and will be dissociated or scattered elastically. In the first case the ArH^+ ion is destroyed and cannot be detected anymore and thus cannot contribute to the IED. In the latter case the direction of the ions is spatially redistributed. The angular distribution at which the scattered ions hit the electrode will be much broader than 4° which is the acceptance angle of the mass and energy spectrometer. For the interpretation of the IED's one has to take into account that only those ions which strike the electrode nearly perpendicularly are detected. We distinguish three groups of ions that fulfil this condition. The first one consists of ions which do not collide in the sheath. The electric field in the sheath is perpendicular to the electrode; so they are accelerated directedly to the electrode. These ions form the primary saddle structure.

The second group consists of ions which lose nearly all their energy during their last collision before they hit the electrode. They behave identically to ions
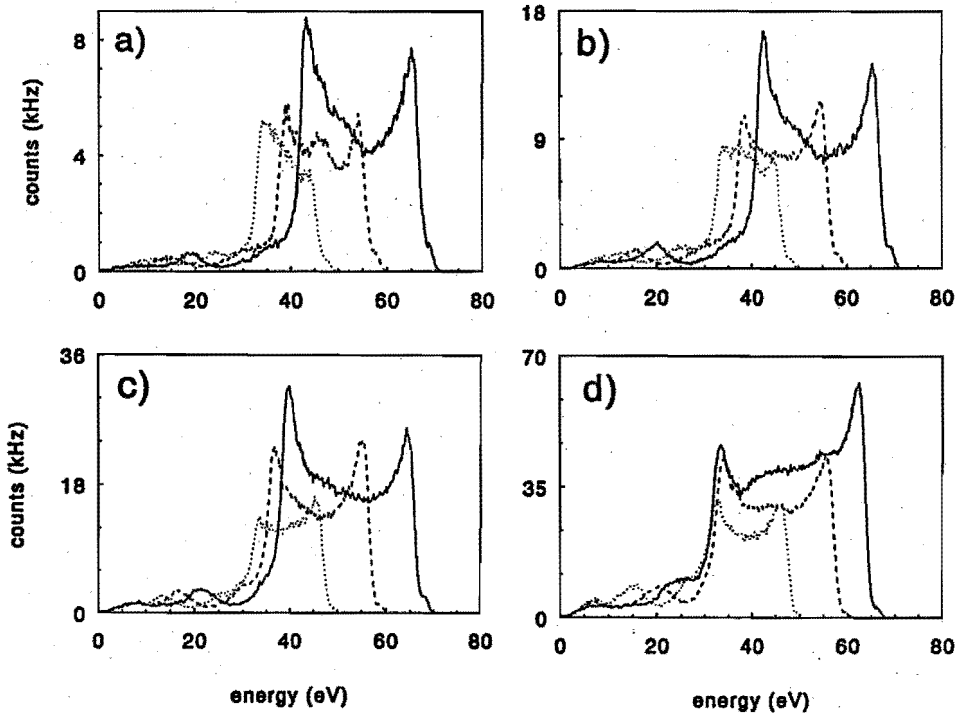
Figure 5.7: The IED's of ArH^+ ions incident on the grounded electrode in the normal cavity for several pressure conditions: 20 mTorr (a), 40 mTorr (b), 80 mTorr (c) and 160 mTorr (d). The RF power is 78 (solid line), 40 (dashed line) and 20 Watt (dotted line).

formed by charge exchange collisions and also will cause low-energy features in the IED's. In the case of ArH^+ ions scattered elastically by argon atoms, only head on collisions satisfy this condition due to the small mass difference between the two species. The energy of the ions in most of these cases is less than the energy related to the saddle structure.

The third group consists of ions that after two or more collisions are directed towards the electrode. The energy of the ions in this case is randomly distributed and no peaks will be present.

When we consider the sheath in front of the grounded electrode in the normal cavity quite a number of ions cross the sheath without any collision.

The probability that ions are in the last two groups is very small and we may conclude that the measured IED's of ArH^+ ions mainly consist of ions which have not collided in the sheath. The <u>measured</u> ArH^+ IED's may therefore be interpreted as being collisionless and therefore serve as a very illustrative "probe" of the overall sheath properties. In section 5.3.4, this conclusion is confirmed by Monte Carlo simulations.

Once again: there probably are a lot of ArH^+ ions that do collide in the sheath, but they will not be detected because of the 4° direction selection or because they are dissociated.

Other hydrogen containing ions like H_3O^+, H_2O^+ and H_3^+ are also scattered elastically in the sheath, but because these ions are much lighter than the Ar neutrals they never can lose all their energy according to the energy and the momentum conservation laws. This implies that there will be no visible collisonal features in their IED. In figure 5.8 IED's are shown of H_3O^+, H_2O^+, H_3^+ and ArH^+ all determined in the same plasma in the normal cavity. The pressure is 80 mTorr and the plasma power 20 Watt. It is shown that the average energy of the saddle structure is the same for all the ions while the splitting ΔE decreases with the ion mass.

5.3.3 Sheath characterization

The space charge in the sheath of an argon plasma mainly consists of Ar^+ ions. The behaviour of these ions characterize the sheath properties. The other ions are of minor importance for the sheath behaviour, but are interesting for sheath analysis.

Important parameters derived from the IED that characterize the sheath are the average energy of the primary saddle structure ($\overline{E}_{sad}$), the splitting of the saddle (ΔE) and the average transit time ($\overline{\tau}_{tr}$). These parameters can be analyzed as a function of the maximum sheath potential which can be derived from V_{rf} and V_{dc}. The average saddle ion energy $\overline{E}_{sad}$, devided by the ion charge, equals the time averaged voltage across the sheath as corroborated by theoretically determined IED's using the time dependent electric field as described in chapter 3 with various sheath conditions. This, however, also seems to be valid in the case the electric field in the sheath used to simulate the distributions is less realistic like, e.g., a constant or linear field. In the case of a purely capacitive sheath the average sheath voltage is half the addition of the maximum and the minumum sheath voltage so $\overline{E}_{sad}$ equals $\frac{1}{2}q_i(V_{sh,max} + V_{sh,min})$.

Collisional effects of the Ar^+ ions lead to less recognizable primary saddle
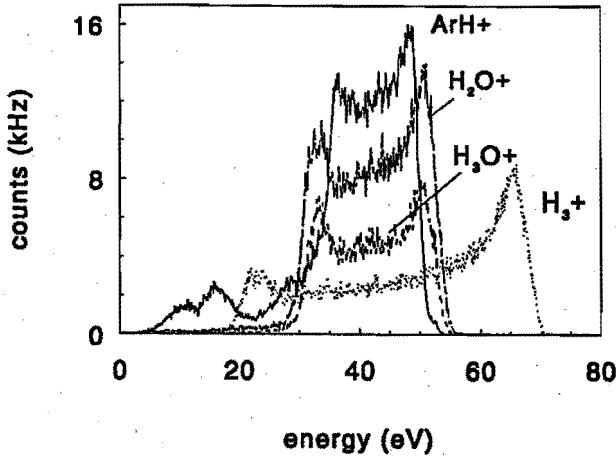
Figure 5.8: The IED's of ArH^+ (solid line), H_3O^+ (dashed line), H_2O^+ (long-short dashed line) and H_3^+ ions (dotted line) incident on the grounded electrode in the normal cavity. The pressure is 80 mTorr and the RFpower is 20 Watt.

structures. The primary saddle structure of the ArH^+ ions should be more or less the same due to the small mass difference between them. Although the small acceptance angle seems to be a deficiency of the diagnostic, the benefit is that $\overline{E}_{sad}$ and ΔE can be determined more accurately from the collisionless IED of the ArH^+ ions than from the collision dominated IED of the Ar^+ ions.

The relation between $\overline{E}_{sad}$ and ΔE determined from the IED's of the ArH^+ ions measured in argon plasmas in the normal cavity for several plasma conditions, is depicted in figure 5.9. The splitting ΔE increases with $\overline{E}_{sad}$ for all pressure conditions. The average saddle energy $\overline{E}_{sad}$ which equals the average sheath voltage, increases due to higher RF excitation voltages V_{rf}. From chapter 3 it follows that when we consider the same ion density at the plasma-sheath edge N_0, the sheath thickness increases with $\overline{E}_{sad}$ and, subsequently, ΔE has to decrease with $\overline{E}_{sad}$. Figure 5.9, however, shows an increase of ΔE for all pressure conditions. Hence N_0 increases with $\overline{E}_{sad}$. Investigations of Bisschops [Bis87] and Haverlag [Hav91] confirm this conclusion. They found that N_0 increases with the excitation voltage V_{rf}.

When we consider a certain $\overline{E}_{sad}$, we see that ΔE is larger at higher pres-
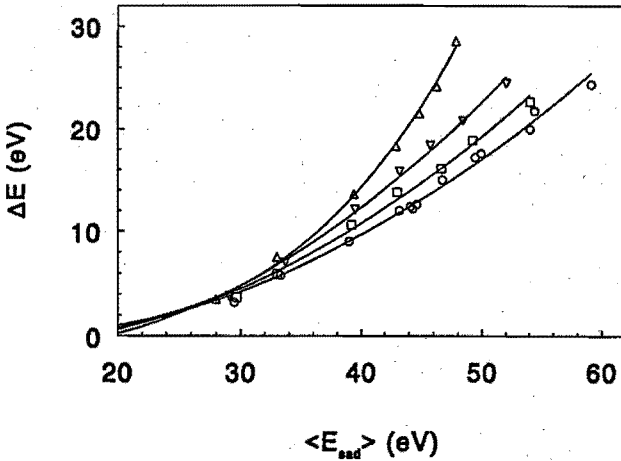
Figure 5.9: The relation between $\overline{E}_{sad}$ and ΔE in the argon plasmas in the normal cavity, determined from the IED's of the ArH^+ ions for 20 ($\circ$), 40 ($\square$), 80 ($\triangledown$) and 160 mTorr ($\triangle$).

sures. From this we may conclude that the sheath thickness for the same sheath potential in the higher pressure plasma is smaller. This must be the consequence of a larger space charge in the sheath according to a higher ion density at the sheath edge and the collisional effects in the sheath through which the ion density decreases more slowly. The higher ion density at the sheath edge for higher pressure cases is in agreement with investigations of Bisschops [Bis87].

The increase of ΔE in figure 5.9 is more than linear. This means that the ratio between ΔE and $\overline{E}_{sad}$ also increases with $\overline{E}_{sad}$ and, consequently, also with V_{rf}. This relation is shown in figure 5.10. From theoretical investigations as discussed in chapter 3 we may conclude that the transit time of the ions through the sheath (τ_{tr}), decreases with increasing plasma excitation voltage V_{rf}.

In figure 5.11 $\overline{E}_{sad}$ and the ratio between ΔE and $\overline{E}_{sad}$ is shown as function of $V_{rf} + V_{dc}$, where $V_{rf} + V_{dc}$ equals the maximum voltage across the sheath. The average sheath voltage in a purely capacitive sheath with $V_{sh,min} = 0$, equals $\frac{1}{2}(V_{rf} + V_{dc})$ which relation is represented by the dashed line. The minimum sheath voltage for the sheath conditions considered in figure 5.11 may be assumed to be negligible as shown in chapter 3. In the case $V_{sh,min}$ would be larger
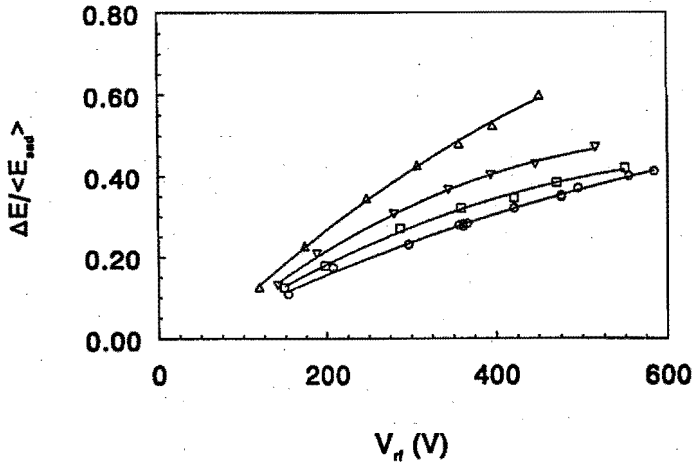
Figure 5.10: $\Delta E/\overline{E}_{sad}$ *as function of* V_{rf} *in the argon plasmas in the normal cavity as determined from the IED's of the* ArH^+ *ions for 20* (o), *40* (□), *80* (▽) *and 160 mTorr* (△).

than zero; this would mean that the average sheath voltage and also $\overline{E}_{sad}$ are larger than $\frac{1}{2}(V_{rf} + V_{dc})$ while figure 5.11a shows that $\overline{E}_{sad}$ determined from the measurements is less than $\frac{1}{2}e(V_{rf} + V_{dc})$. The difference even becomes larger at higher voltages and increases with the pressure.

From the non-linear behaviour of $\overline{E}_{sad}$ as function of the maximum sheath voltage, we may conclude that the sheath behaviour may not be assumed purely capacitive anymore. The increase of $\overline{E}_{sad}$ as function of $V_{sh,max}$ is practically linear only at smaller sheath voltages and low pressures. This linear behaviour does suggest a sheath of capacitive nature. The difference between $\overline{E}_{sad}$ and the dashed line representing the capacitive sheath behaviour considering the linear part can be explained from an error in the measurements of V_{rf}. This voltage can not be measured directly at the driven electrode, but is determined at approximately 10 cm from the electrode. Due to a mismatch which appears between the driven electrode and the coaxial cable that connects the matching network to the electrode, a part of the RF voltage is reflected. Consequently the RF voltage at a position at the powered coaxial cable at a certain distance from the electrode is different from the voltage at the driven electrode. Due to the complex geometry of the reactor and the cavity it is impossible to calculate
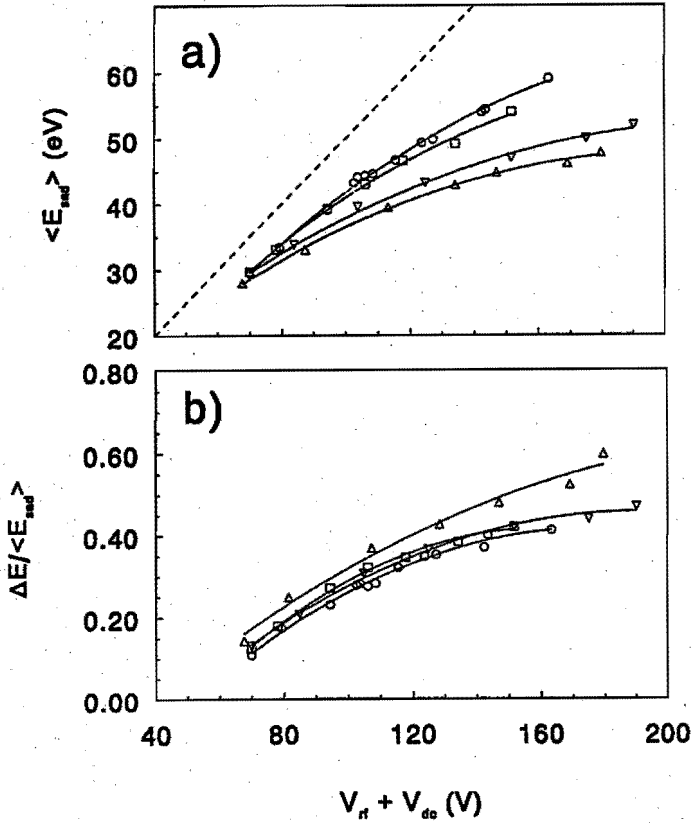
Figure 5.11: $\overline{E}_{sad}$ *(a) and* $\Delta E/\overline{E}_{sad}$ *(b) as function of half of the maximum sheath voltage* $\frac{1}{2}(V_{rf} + V_{dc})$ *in argon plasmas in the normal cavity. The results are determined from the IED's of the* ArH^+ *ions.*

exactly the reflection coefficient of the RF voltage from transmission line theory [Pau82]. But systematic errors of about 5% are realistic when we assume the plasma impedance to be capacitive and the range bewteen 0.5 and 500 Ω. The impedance of the coaxial cable is 50 Ω. This systematic error may explain the difference between the $\overline{E}_{sad}$ and the dashed line in figure 5.11a which represents the capacitive sheath behaviour.

Figure 5.11b shows the ratio between ΔE and $\overline{E}_{sad}$ as function of the maximum sheath voltage. This ratio increases with the voltage and slightly

with the pressure. From the ratio, the transit time of the ions may be obtained as shown in chapter 3. An increase of the ratio means a decrease of the transit time. A long transit time corresponds to a capacitive behaviour of the sheath. So the conclusions of figure 5.11a and b are in agreement with each other and we may expect a sheath of capacitive nature at lower sheath voltages and lower pressures.

Figure 5.12 shows the average energy of the saddle structure of IED's of ArH^+ ions determined in the inverse cavity in an argon plasma of 5 mTorr in the inverse cavity for several RF voltages. The figure shows that $\overline{E}_{sad}$ increases linearly with $\frac{1}{2}(V_{rf} + V_{dc})$ from which we may conclude that the sheath behaviour is purely capacitive for the whole voltage range considered. This also is valid for higher pressure conditions which are not shown in the figure. The capacitive nature is in agreement with the fact that the sheath thickness in front of the smallest electrode is larger than that of the sheath in front of the largest electrode as confirmed by Bisschops through optical measurements [Bis87]. This is due to higher sheath voltages across the sheath. Consequently the transit time of the ions to cross the sheath is longer ($\tau_{tr} > 8$ RF periods) and the behaviour becomes purely capacitive.

The difference between the measurements and the relation

$$\overline{E}_{sad} = \frac{1}{2}e(V_{rf} + V_{dc}),\tag{5.3}$$

represented by the dashed line in the figure, can be explained from the error in the determination of V_{rf}. In the inverse cavity V_{rf} is measured at the end of a 35 cm long coaxial cable connected to the driven electrode and not at the cable connecting the RF matching network to the driven electrode as in the normal cavity. This additional cable in the inverse cavity case is a powerless transmission line and a smaller reflection coefficient of the RF voltage is expected. A calibration experiment where V_{rf} is determined at the end of several coaxial cables with different lengths, so at several distances from the electrode, learns that a systematic error of 3 % appears when V_{rf} is determined at the end of the 35 cm long cable. This error in the RF voltage measurements may explain the difference between the measurements and the theoretical line in figure 5.12.

The average transit time of the ions to cross a certain sheath depends on their mass, and, subsequently, also the splitting of the primary saddle structure ΔE. This dependency is obtained empirically from the measurements and the simulations by determination of the primary saddle structure of several ion species which are all accelerated in the same sheath. The splitting appears to be proportional to $1/\sqrt{m_i}$. The experimentally determined relation has been
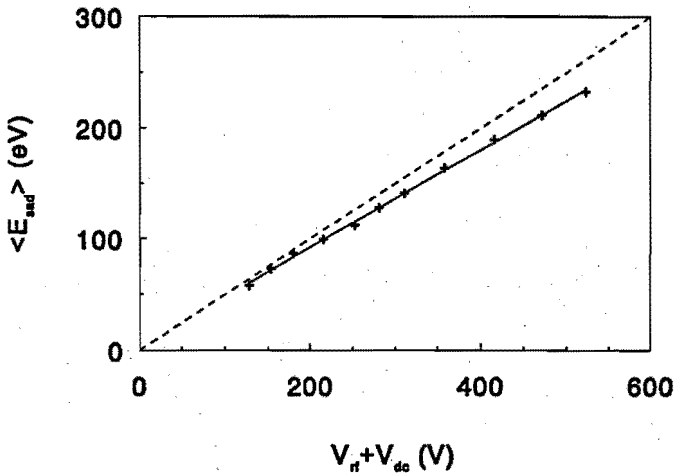
Figure 5.12: $\overline{E}_{sad}$ *as function of* $\frac{1}{2}(V_{rf}+V_{dc})$ *in argon plasmas in the inverse cavity. The pressure was 5 mTorr. The results are determined from the IED's of the ArH⁺ ions.*

acquired in an argon plasma with a small admixture of dry air. All the ions in this case have to cross the same sheath and the splittings may directly be compared with each other. This experiment has been done for both the normal and the inverse cavity. The result is shown in figure 5.13.

In the normal cavity case, the IED has been measured for the following ions: H_3^+ $(m_i(a.m.u.)/q_i(e) = 3)$, C^+ (12), N^+ (14), O^+ (16), H_2O^+ (18), H_3O^+ (19), Ar^{2+} (20), N_2^+/CO^+ (28), NO^+ (30), O_2^+ (32), HO_2^+ (33), $(H_2O)_2^+$ (36) and ArH^+ (41). The RF power is 48 Watt and the pressure 80 mTorr. $\overline{E}_{sad}$ for all the ions is 55 eV.

In the inverse cavity the IED has been measured for: H_2O^+ (18), N_2^+/CO^+ (28), NO^+ (30), O_2^+ (32), ArH^+ (41) and Ar_2^+ (80). The RF power is 48 Watt and the pressure is 5 mTorr.

The splitting of the H_3^+ ions in the normal cavity case is 71.9 eV and is not present in the figure. It is smaller than the empirical value. This is due to the short transit time of the H_3^+ ions which is in the order of 1 RF period. At this short times the ions nearly cross the sheath instantaneouly. The maximum splitting which the ions in this situation can get equals $e(V_{sh,max} - V_{sh,min})$ which means that the splitting is limited. Therefore the splitting of light ions with
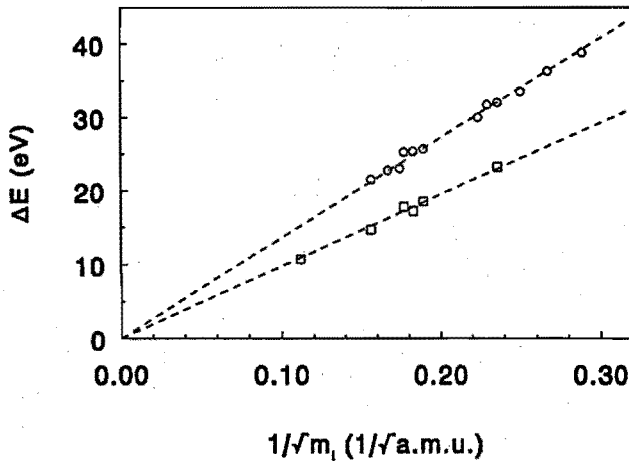
Figure 5.13: The empirically determined relation bewteen the splitting ΔE and the mass of the ion. The measurements has been done in the normal (○) and the inverse cavity (□).

short transit times deviates from the empirical result as shown in figure 5.13. This deviation is in agreement with theoretically determined distributions.

5.3.4 Simulations

Ion energy distributions of Ar^+ and ArH^+ have been simulated by Monte Carlo calculations. Therefore a number of ion trajectories have been calculated for several phase angles at which the ions enter the sheath. The ions are accelerated in the time dependent electric field as described by the model which is discussed in chapter 3.

From the sheath analysis in subsection 5.3.3 we may conclude that the sheath behaviour is not purely capacitive at higher RF sheath voltages. Consequently the sheath voltage modulation $(V_{sh}(t))$ is not sinusoidal and the average sheath potential is less than half the maximum sheath voltage $(\frac{1}{2}V_{sh,max})$ in this case, when we assume the minimum sheath voltage $(V_{sh,min})$ to be zero. For the simulations we assume the voltage modulation to be

$$V_{sh}(t) = (V_{sh,max} - V_{sh,min})\left(\frac{1}{2} + \frac{1}{2}\cos(\omega t)\right)^{\alpha} + V_{sh,min}, \tag{5.4}$$

where $\alpha > 1$ represents the non purely capacitive character of the sheath; $\alpha = 1$ means that the sheath is purely capacitive. Figure 5.14 shows the relation between α and the time averaged value of $(\frac{1}{2} + \frac{1}{2}\cos(\omega t))^\alpha$ which determines the time averaged value of $V_{sh}(t)$.
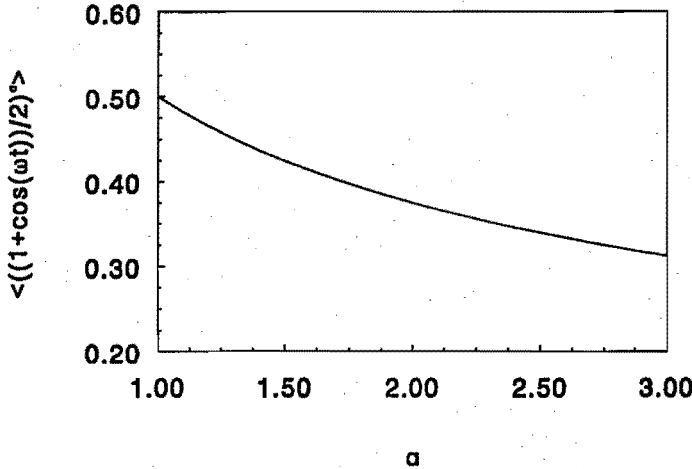

Figure 5.14: The relation between α and the time averaged value of $(\frac{1}{2} + \frac{1}{2}\cos(\omega t))^\alpha$, where α represents the non purely capacitive character of the sheath behaviour.

In figure 5.15 the simulation is depicted of the IED of Ar^+ ions in a 20 mTorr argon plasma as shown in figure 5.4a. V_{rf} and V_{dc} as measured for the considered plasma condition are 346 and -221 V, respectively, so $V_{sh,max}$ is 125 V. $V_{sh,min}$ is assumed to be zero and α is chosen to be 2.0 so that the average sheath potential equals 53 V. The other input parameters are: $N_0 = 1.15\ 10^{16}$ m^{-3} and $kT_e = 2$ eV. 140000 ion trajectories have been calculated. They are homogeneous distributed over 200 different phase angles at which the ions enter the sheath.

The mean free path for charge exchange (λ_c) and elastic scattering (λ_e) both depend on the energy of the incoming ion. This dependency is given by McDaniel [McD64]. Simulations with an energy dependent and an average mean free path average of the energies, show no significant differences. In the simulations shown in this chapter the mean free path is taken to be constant and to depend only on the pressure.
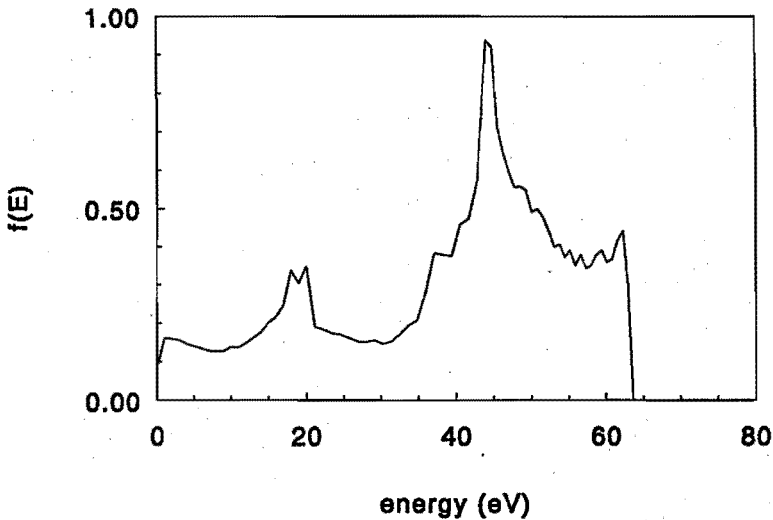
Figure 5.15: Monte Carlo simulation of the IED of Ar⁺ ions in a 13.56 MHz plasma in argon in the normal cavity. The RF excitation voltage is 346 V and the autobias is -221 V. The mean free path is 3.2 mm. The experimentally determined IED is given in figure 5.4a.

For the simulation shown in figure 5.15 only charge exchange collisions were taken into account with a mean free path of 3.2 mm. Although the mean free path for elastic scattering is of the same order as that for charge exchange collisions, elastic scattering has no significant influence on the IED.

The sheath thickness is calculated from the model and is 1.69 mm. The average transit time is 3.5 times the RF period. The simulation shows that the collisional peak at about 20 eV is originally split and formed by the mechanism discussed in chapter 3. In the experimentally determined IED, the splitting is not visible due to insufficient resolution.

In figure 5.16, the simulation is shown of the IED incident on the grounded electrode in the inverse cavity case and depicted in figure 5.5. The pressure is 5 mTorr and V_{rf} and V_{dc} are, respectively, 291 and 180 V. Due to the capacitive nature of the sheath, the sheath voltage modulation may be assumed sinusoidal. N_0 is $2.2\ 10^{15}$ m^{-3} and kT_e is 2 eV. The mean free path is 1.5 mm. Again 140000 ion trajectories have been calculated. The sheath thickness as determined from the model is 8.2 mm. From the ratio between the mean free path and the sheath thickness it follows that 0.5 % of all the ions reach the electrode without

any collision in the sheath which explains the relatively small primary saddle structure with hardly visible peaks. The positions of the secondary peaks correspond to the ones in the experimentally determined IED. From this we may conclude that the model is quite realistic. The Monte Carlo simulation shows that the secondary features are split, just like the primary saddle structure. The amount of splitting increases with energy. At low energies the amount approaches zero and no splitting is visible.

The first peak in the simulation however, is not present in the measured IED. In this part (which is in $0 < E_{ion} < E_{pas}$) the ion flux leaving the sample hole within a space angle of 4° has not completely been bent parallel to the quadrupole axis, so the transmission in this energy range is less than the transmission in the range $E_{ion} > E_{pas}$, where the transmission is constant.
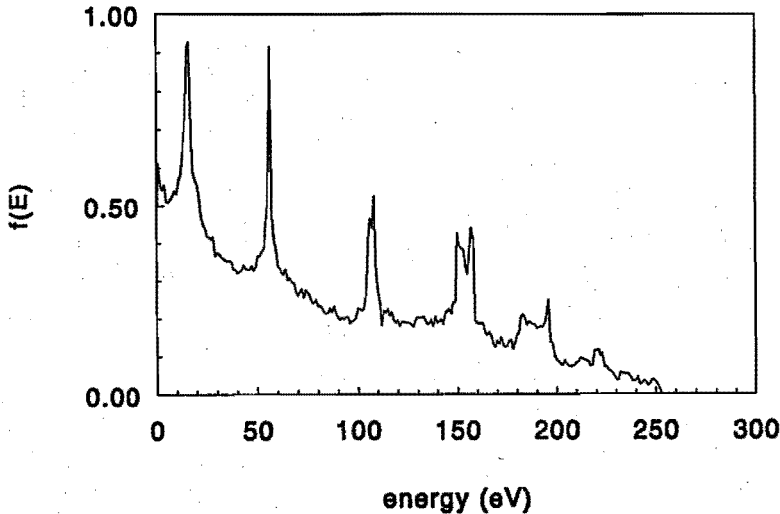

Figure 5.16: Monte Carlo simulation of the IED of Ar^+ ions in a 13.56 MHz plasma in argon in the inverse cavity. The RF excitation voltage is 291 V and the autobias is -180 V. The mean free path is 1.5 mm. The experimentally determined IED is depicted in figure 5.4.

The hydrogen containing ions are only scattered elastically. Due to this the IED is quite different from the IED of the Ar^+ ions. The minor features in the experimentally determined IED of ArH^+ ions at lower energies than the primary saddle structure (see figure 5.7), are generated by elastically scattered ions which bombard the electrode perpendicularly. All the other scattered

ArH^+ ions are not detected due to the small acceptance space angle of the mass and energy spectrometer [Sni93].

In figure 5.17 we show the measured and simulated IED's of ArH^+ ions as determined in an argon plasma of 50 Watt. The pressure is 40 mTorr. The ion density at the sheath edge used for the simulation is 1.3 10^{16} m^{-3} and the electron temperature 2 eV. $V_{sh,max}$ and $V_{sh,min}$ are, respectively, 127 and 0 V. The sheath behaviour is not purely sinusoidal and α is assumed to be 2.0. The mean free path for elastic scattering is 1 mm. The sheath thickness as calculated from the model is 1.57 mm.

The elastic collisions are treated as hard sphere elastic scattering events where the collision angle in the mass centered system is randomly distributed and the total energy and momentum are conserved. This assumption is reasonable as shown by investigations of Thompson *et al.* who compared the hard sphere model to more sophisticated models [Tho88]. The full curve in figure 5.17b represents the full angular distribution of the IED while the dashed curve corresponds to the IED of those ions which bombard the electrode within a space angle of 4°. Considering the hard sphere scattering model, the ions are only scattered perpendicularly towards the electrode, if the last collision before hitting the electrode is head-on. In this case, these ions also will lose all their energy. Consequently these ions can produce the same collisional features as ions produced by charge exchange. From the Monte Carlo simulation we know that the chance the last collision is head-on, is very small and the peaks in the corresponding IED are much lower than the peaks generated by charge exchange. As a consequence the IED as measured under these conditions appears to be nearly similar to the one of a collisionless sheath.

The measured IED's of H_3O^+, H_2O^+ and H_3^+ show no collisional features. Monte Carlo simulations confirm this. This is due to the fact that these ions can never lose all their energy when they collide elastically with an Ar atom. The probability that scattered light ions hit the electrode perpendicularly is therefore very small. Ion-molecule reactions in the sheath of these ions other than with an argon atom are negligible due to the low impurity, so hardly any production of these ions take place in the sheath and a loss mainly takes place through a collision with an argon neutral.

The electron temperature for the 13.56 MHz plasma in argon is of the order of 2-4 eV [Hav91]. Varying of kT_e in this range for several Monte Carlo simulations show no significant differences for the IED's. Therefore kT_e has been assumed to equal 2 eV for all the simulations.
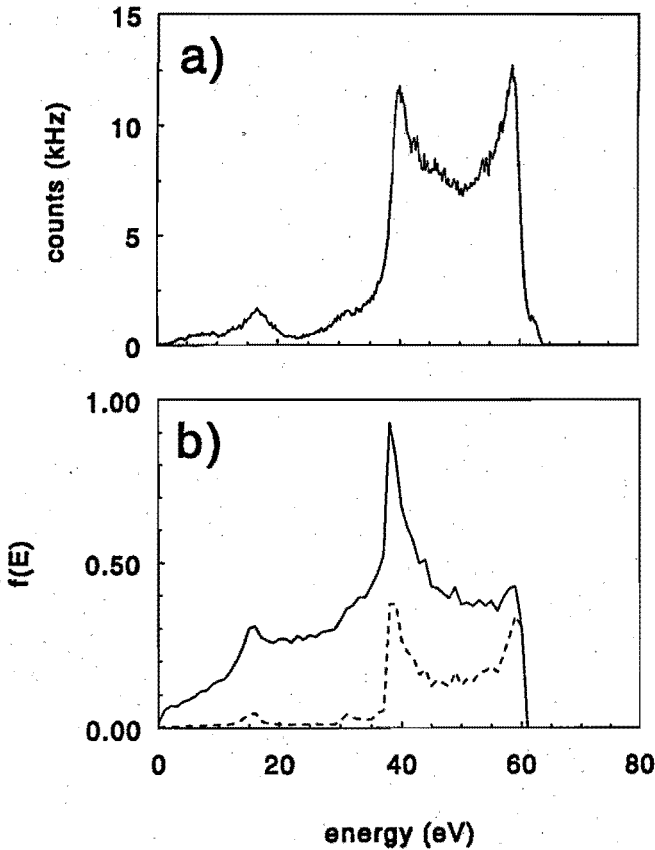
Figure 5.17: Measurement (a) and simulation (b) of the IED of ArH^+ in an agon plasma. The solid line in b, represents the full angular IED, while the dashed line represents the IED as experimentally will be determined. The RF power is 50 Watt and the pressure is 40 mTorr.

5.3.5 Conclusions

From the experimentally determined IED's of Ar^+ ions, we may conclude that charge exchange collisions generate well defined features. These features are also saddle structured although at low energy the amount of splitting approaches zero and in the measurements the splitting has vanished as a consequence of lack of resolution. The measured IED's of ArH^+, H_3O^+, H_2O^+ and H_3^+ may

be assumed collisionless: hardly any elastically scattered ions are detected due to the fact that the acceptance angle is only 4°, and ions which are destroyed in the sheath do not contribute to the IED's. The IED's of ArH^+ ions show some distinct features due to head-on elastic collisions with Ar neutrals. These scattered ions lose nearly all their energy and they generate features in the same way as ions produced by charge exchange do.

The collisionless character of the IED of the ArH^+ ions can be used to determine quite accurately ΔE and $\overline{E}_{sad}$, which parameters characterize the nature of the sheath. The sheath in front of the grounded electrode in the normal cavity case may be assumed purely capacitive at low sheath voltages. At higher voltages the behaviour is not purely capacitive anymore and the sheath modulation may not be assumed sinusoidal. This effect is more outspoken with higher pressures.

Monte Carlo simulations of the IED's, based on the time dependent electric field as described in chapter 3, show good agreement with measured IED's. This goes for $\overline{E}_{sad}$ and ΔE of the primary saddle structure, as well as the position of the collisional features.

The IED's of the ArH^+ ions show a very pronounced saddle structure with very steep slopes. From this we may conclude that the energy resolution of the diagnostic is better than 1 eV when $E_{pas} = 10$ eV. The resolution is better than 2.5 eV when $E_{pas} > 10$ eV.

5.4 The IED in a 13.56 MHz plasma in nitrogen

5.4.1 Introduction

Mass spectrometric investigations show that N^+, N_2^+ and N_3^+ ions are present in the low pressure 13.56 MHz N_2 plasma. The density of the N_2^+ molecular ions is the highest. The N_3^+ ions are only present in very small numbers and their influence on the space charge in the sheath may be neglected. Also the density of the N^+ ions is much smaller than that of N_2^+ and they will have hardly any influence on the space charge conditions in the sheath.

In this section, experimentally determined IED's of N^+, N_2^+ and N_3^+ ions are presented. The measurements took place in both the normal and the inverse cavity case. Monte Carlo simulations show good agreement with the measurements. In subsection 5.4.3 simulations of the IED's determined in the normal cavity case are discussed. The results of the N_2^+ ions show that the IED is dominated by resonant charge exchange collisions similar to the IED of Ar^+ ions.

N^+ and N_3^+ are only scattered elastically by N_2, so the measured IED's may be interpreted as collisionless. No features other than the primary saddle structure are found, which is in accordance with the unequal masses of the colliding particles. This also means that hardly any N^+ and N_3^+ ions are formed in the sheath region. The splitting of the saddle structure is inversely proportional to the square root of the ion mass.

From the investigations we may conclude that the sheath in a 13.56 MHz plasma in nitrogen behaves similarly as the one in the argon plasma. The difference between the two gases is that the ion density at the sheath edge in the nitrogen plasma is lower than the one in the argon plasma and consequently the sheath is thicker. This induces a larger number of collisonal features.

5.4.2 Experimental results

Figure 5.18 shows the IED's of N_2^+ and N^+ ions determined in the normal cavity case at pressures of 19 and 76 mTorr, respectively. In figure 5.18a also the IED of N_3^+ is shown.

The value of E_{pas} during the measurement of the IED's of the N_2^+, N^+ and N_3^+ ions was 10, 15 and 20 eV, respectively. The features of the IED's of the N_2^+ ions may be considered to be generated by resonant charge exchange between N_2^+ ions and N_2 neutral molecules according to

$$N_2^+ + N_2 \rightarrow N_2 + N_2^+. \tag{5.5}$$

The cross section of this reaction depends on the energy of the incoming ion, which has been determined experimentally by several investigators [Ste63, Utt61, Gus61] and is of the same order as the cross section of charge exchange collisons of Ar ions and neutrals. ($\sigma \approx 33 \ 10^{-20}$ m^{-2} for ion energies of 30 eV and $25 \ 10^{-20}$ m^{-2} for energies of 400 eV in nitrogen [Ste63].) The charge exchange cross section of the reaction between N_2^+ ion and N neutrals

$$N_2^+ + N \rightarrow N_2 + N^+ \tag{5.6}$$

is about 6 times less [Ste63]. Through this and because the N neutral density in the sheath is smaller than the N_2 density, the probability that a N^+ ion will be formed in the sheath may be neglected and no charge exchange features in the IED of N^+ ions are generated. The same considerations are valid for the N_3^+ ions.

The splitting of the primary saddle structure of the three ions is inversely proportional to the square root of the ion mass, similar to the IED's determined in the argon plasma.
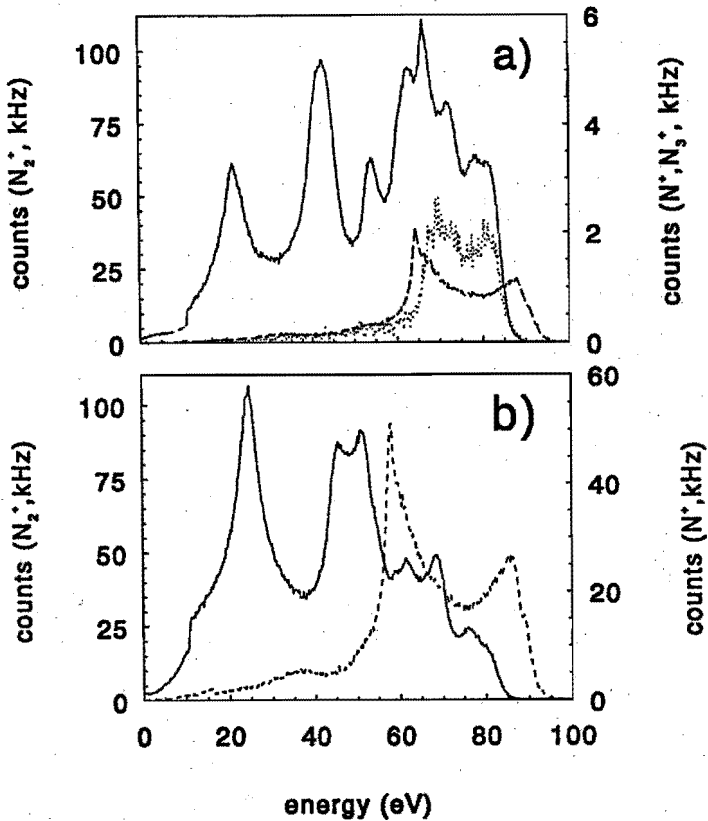
Figure 5.18: The IED's of N_2^+ (solid line), N^+ (dashed line) and N_3^+ ions (dotted line) incident on the grounded electrode in the normal cavity. The RF power is 69 Watt and the pressure is 19 mTorr (a) and 76 mTorr (b).

Figure 5.19 shows the IED of N_2^+ ions determined in the inverse cavity case at pressures of 10, 20, 40 and 85 mTorr. The RF power is 50 Watt. Due to the collisions, the primary saddle structure (with $\overline{E}_{sad}$ is 225 eV) has completely vanished. We only can distinguish the peaks generated by charge exchange, where the peaks at the low energy side become relatively higher with increasing pressure. The distance between the peaks increases with increasing pressure and we may also say, although not all the peaks are visible, that the number
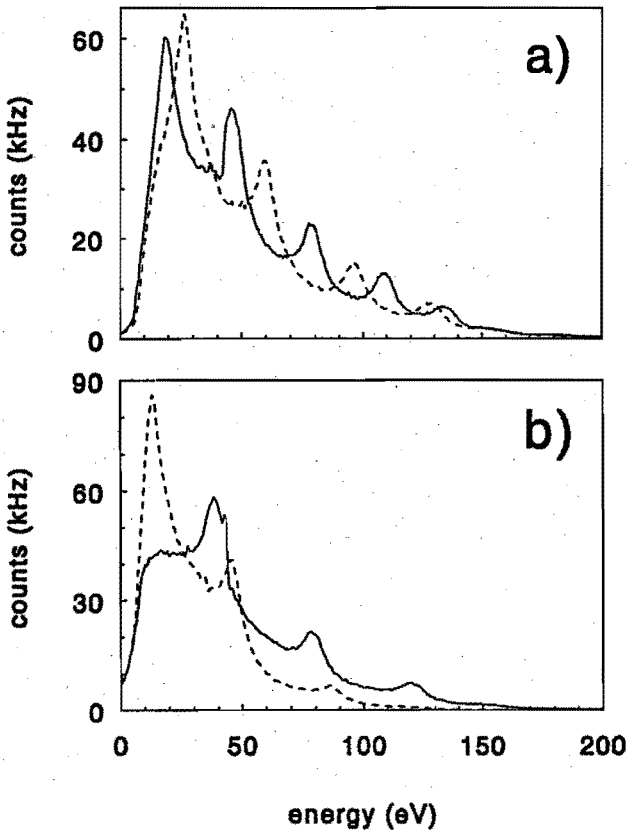
Figure 5.19: The IED of N_2^+ incident on the grounded electrode in the inverse cavity for several pressures: 10 mTorr (a: solid line), 20 mTorr (a: dashed line), 40 mTorr (b: solid line) and 85 mTorr (b: dashed line). The RF power is 50 Watt.

of peaks slowly decreases with increasing pressure. From this we may conclude that the transit time to cross the sheath becomes shorter and the sheath thickness becomes smaller at higher pressures. This may be the consequence of an increase of the ion density at the sheath edge.

5.4.3 Simulations

The high frequency model which is described in chapter 3 is also used to simulate the IED's determined in the nitrogen plasma. Several measurements have been investigated theoretically. We may conclude that the sheath in the nitrogen plasma behaves similar to the sheath in the argon plasma. A difference between the two gases is that the ion density in the nitrogen plasma is less than in the argon plasma provided we consider the same sheath voltage. Consequently, the sheath thickness is larger in the nitrogen plasma. This leads to more collisional features, which shows up in the measured IED's. The consequence for the IED's determined in the inverse cavity case is that the primary saddle structure completely vanishes.

In figure 5.20 the simulation is depicted of the IED's determined in the normal cavity case at 19 mTorr as shown in figure 5.18a where the first collisionally induced peak is missing in the experimentally determined IED. The
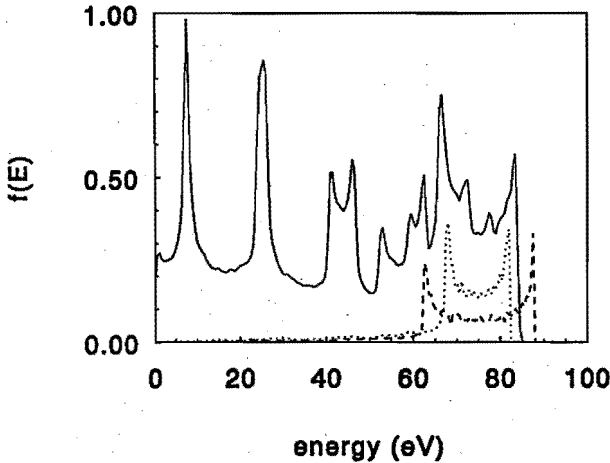

Figure 5.20: Simulation of the IED of N_2^+ (solid line), N^+ (dashed line) and N_3^+ (dotted line), incident on the grounded electrode in the normal cavity. The pressure is 19 mTorr and the RF power is 69 Watt.

sheath behaviour has been assumed to be non purely capacitive and the sheath voltage modulation parameter α has been taken to be 2.2. $V_{sh,max}$ and $V_{sh,min}$ are, respectively, 200 V and 0 V. $N_0 = 2.1 \ 10^{15} \ m^{-3}$ and $kT_e = 2$ eV. The N_2^+

ions collide elastically and experience charge exchange. The mean free path of both types of collision is 4.8 mm. The N^+ and N_3^+ are assumed to collide only elastically. The mean free path is 4.8 mm. 150000 ion trajectories are calculated, where the ions enter the sheath at 200 homogeneous distributed phase angles.

The average energy and the splitting of the primary saddle structure of all the three ions and the position of the features in the IED's of N_2^+ generated by charge exchange, are in good agreement with the experimentally determined results of figure 5.18. From the simulation we may conclude that the peaks at 22 and 44 eV are basically split and saddle structured. Because of lack of resolution this is not visible in the experimentally determined IED's.

5.4.4 Conclusions

The nature of the sheath in the nitrogen plasma is similar to that of the sheath in the argon plasma. The simulations show good agreement with the measured IED's, although the resolution of the simulation is better than that of the experiments. Consequently, the splitting of charge exchange induced peaks at low energies is not visible. The IED of N_2^+ ions is dominated by charge exchange collisions while N^+ and N_3^+ are only scattered elastically by mainly N_2 molecules.

The amount of splitting of the saddle structure is inversely proportional to the square root of the ion mass. The IED's of the N_2^+ ions in the normal cavity case show more features than similar sheath voltages in an argon plasma. This is due to lower ion densities which causes a larger sheath thickness. Hence the ion transit time increases and more features are generated. Consequently, the primary saddle structure in the IED which is determined in the inverse cavity case completely vanishes.

Experimentally no collisional features are determined in the IED's of N^+ and N_3^+. This is in accordance with the fact that N^+ and N_3^+ ions never can lose all their energy in elastic collisions with N_2 molecules. From the experimentally results we also may concluded that hardly any N^+ and N_3^+ ions are produced in the sheath region by electron impact. These ions produced by electron impact start nearly with energy zero and consequently will hit the electrode perpendicularly and thus can be detected all. In general, we may conclude that electron impact in the sheath can be neglected.

5.5 The IED in a 13.56 MHz plasma in carbontetrafluoride

5.5.1 Introduction

The ion dynamics in the sheath of a CF_4 plasma is far more complex than that of an Ar or N_2 plasma. The number of ion species is larger, just like the number of different ion-molecule reactions that can take place. This is also the consequence of the large number of radical species present in the sheath.

In a CF_4 plasma the following positive ions are present: CF_3^+, CF_2^+, CF^+, F^+, C^+ and at higher pressures also $C_2F_5^+$ ions are detected [Hav91]. Due to residual water vapor CHF_2^+ ions are formed in the plasma. These ions are probably produced by ionization of CHF_3 neutrals which can be formed by reactions between CF_n radicals and water molecules [Hav91]. The presence of CHF_3 molecules in the plasma has been shown by Haverlag [Hav91] using IR-techniques.

In the CF_4 plasma also negative ions are present. These ions, mainly F^-, are confined to the glow. In chapter 3 it is shown that the density and the temperature of these ions determine the Bohm velocity of the positive ions, but they have no further influence on the kinetics of the positive ions in the sheath. The Bohm velocity in electro-negative gases is less than in a plasma without negative ions. The consequence of this is that the sheath thickness is larger than discussed in chapter 3. Investigations of Haverlag show that the ion density in CF_4 plasmas is less than in corresponding Ar plasmas. This also leads to a larger sheath thickness.

In subsection 5.5.2 the experimentally determined IED's of CF_3^+, CF_2^+, CF^+, F^+ and CHF_2^+ ions are presented both for the normal and the inverse cavity case. These results show large differences between the IED's of the different species. From these results conclusions about the sheath behaviour and the ion kinetics in the sheath can be derived. It is shown that ions are produced in the sheath. Because of the small electron density in the sheath, these new ions must be formed by ion-molecule reactions. This will be discussed in subsection 5.5.3.

The sheath model as discussed in chapter 3 does not include ion-molecule reactions and the production and loss of ions. Therefore Monte Carlo simulations in the simple form as used before do not correspond to experimental results.
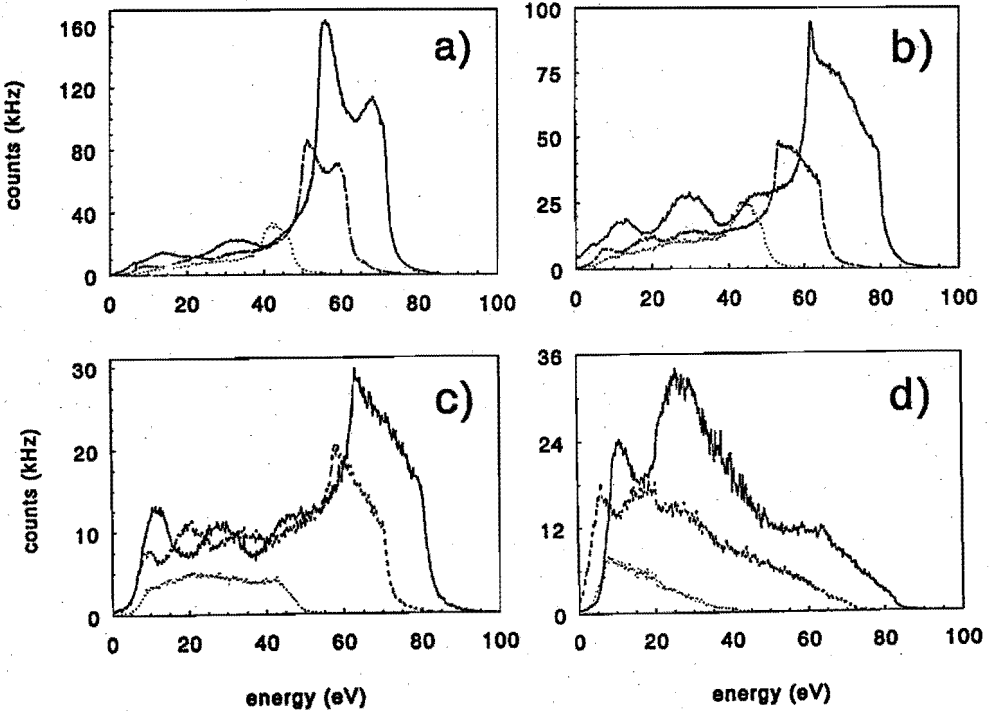
Figure 5.21: *The IED's of CF_3^+ ions incident on the grounded electrode in the normal cavity for several pressure and RF power conditions: (a) 20 mTorr: 78 (solid line), 40 (long-short dashed line) and 20 Watt (dotted line); (b) 40 mTorr: 78, 40 and 20 Watt; (c) 80 mTorr: 78, 50 (dashed line) and 20 Watt; and (d) 160 mTorr: 78, 50 and 20 Watt.*

5.5.2 Experimental results

In figure 5.21, 5.22, 5.23, 5.24 and 5.25, the measured IED's of CF_3^+, CF_2^+, CF^+, F^+ and CHF_2^+ ions, respectively, are presented for several plasma conditions in the normal cavity case. The density of these ions is lower than the ion densities of the species in the argon and nitrogen plasmas. To increase the transmission, E_{pas} was 20 eV during these measurements. This means that the energy resolution is less than the one in the argon and nitrogen measurements.
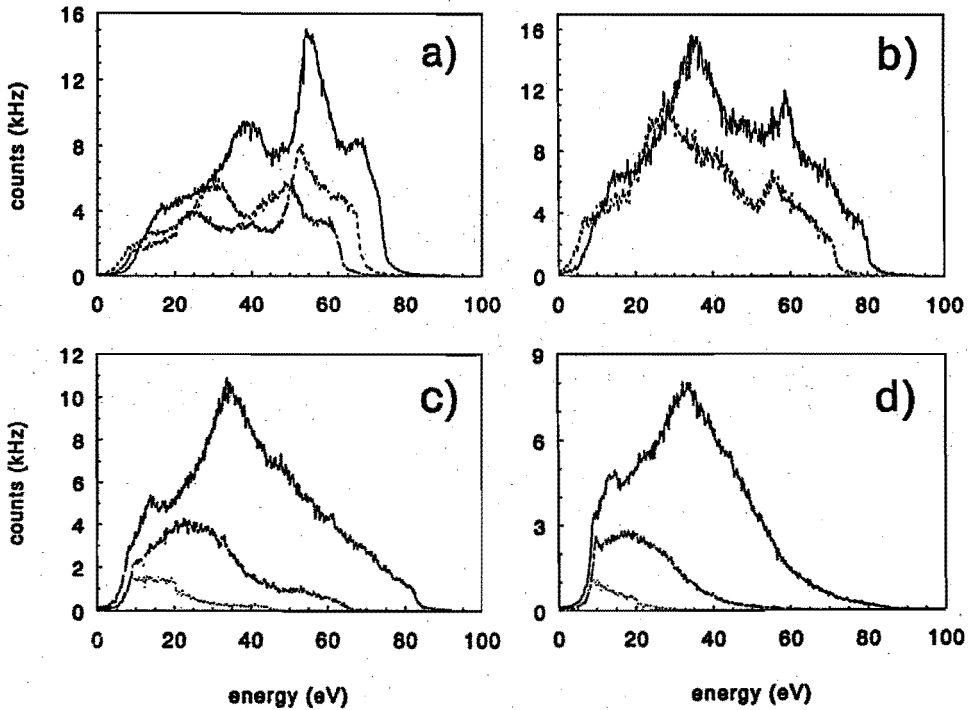
Figure 5.22: The IED's of CF_2^+ ions incident on the grounded electrode in the normal cavity for several pressure and RF power conditions: (a) 20 mTorr: 78 (solid line), 50 (dashed line) and 40 Watt (long-short dashed line); (b) 40 mTorr: 78 and 50 Watt; (c) 80 mTorr: 78, 40 and 20 Watt; and (d) 160 mTorr: 78, 40 and 20 Watt.

The behaviour of CHF_2^+ ions is identical to ArH^+ ions in an argon plasma. The most probable reactions of CHF_2^+ ions are elastic scattering with CF_4 neutrals or an ion-molecule reaction. In the latter case the ion will be destroyed and can not contribute any more to the IED. Because of the mass difference between the CHF_2^+ ion and the CF_4 neutral, the ion will never lose all its energy when it collides elastically. This means that the measured IED's of CHF_2^+ ions contain mainly the ions which do not collide in the sheath and no elastic scattering features as in the IED's of the ArH^+ ions are to be expected.

The density of the CF_3^+ ions is the highest of all the considered ions. When
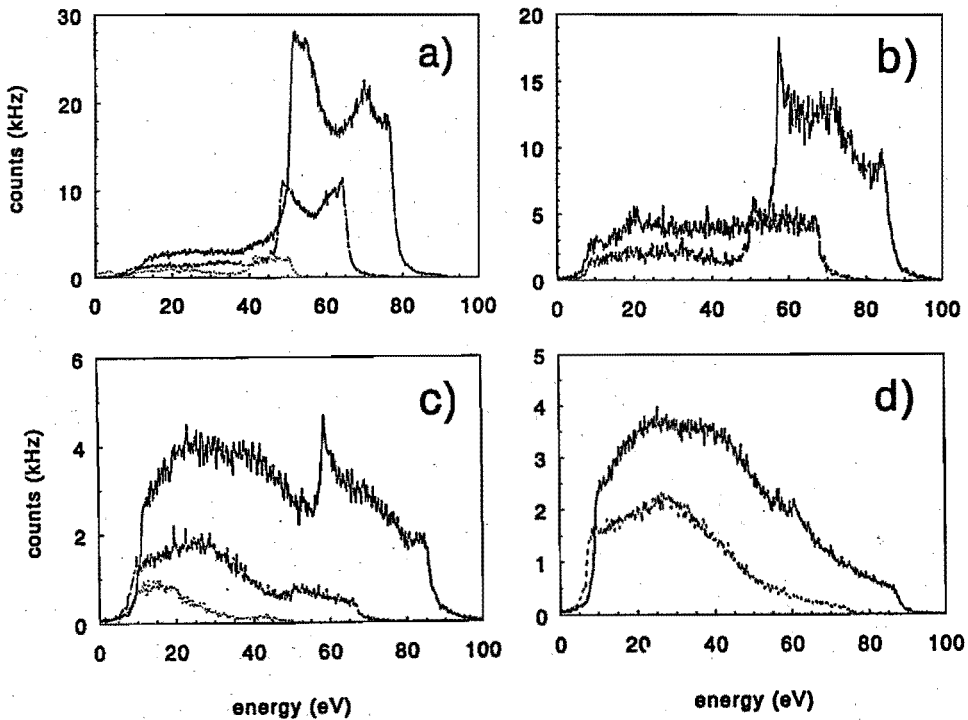
Figure 5.23: The IED's of CF^+ ions incident on the grounded electrode in the normal cavity for several pressure and RF power conditions: (a) 20 mTorr: 78 (solid line), 40 (long-short dashed line) and 20 (dotted line); (b) 40 mTorr: 78 and 40 Watt; (c) 80 mTorr: 78, 40 and 20 Watt; and (d) 160 mTorr: 78 and 50 Watt (dashed line).

we consider the IED's of the CF_3^+ ions, we can recognize the primary saddle structure in the low pressure case (20 and 40 mTorr), while this structure vanishes at higher pressures (160 mTorr). In the low pressure case, the IED's show some small features at energies lower than the saddle structure. These features can not be generated by elastic scattering because the elastically scattered CF_3^+ ions do not contribute to the IED's. Therefore the features must be generated by newly formed CF_3^+ ions generated in the sheath by ion-molecule reactions and which ions start with small energy, or by charge exchange reactions where by CF_3^+ ions are generated. In the IED's in figure 5.21 we distinguish 3 peaks
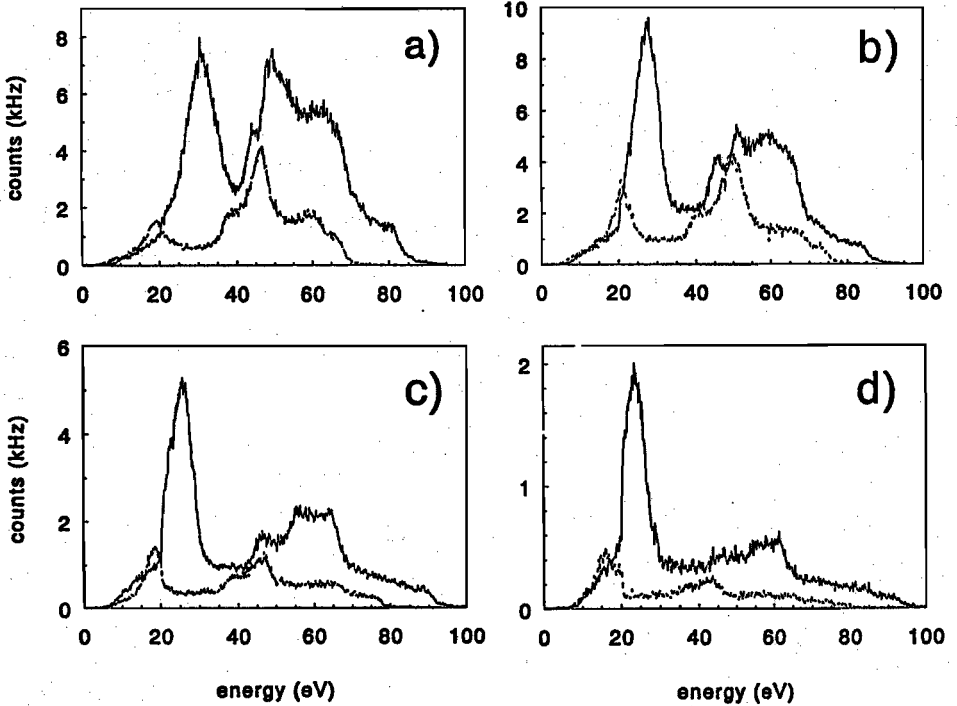
Figure 5.24: The IED's of F^+ ions incident on the grounded electrode in the normal cavity for several pressure and RF power conditions: (a) 20 mTorr: 78 (solid line) and 40 Watt (long-short dashed line); (b) 40 mTorr: 78 and 50 Watt (dashed line); (c) 80 mTorr: 78 and 40 Watt; and (d) 160 mTorr: 78 and 50 Watt.

that have a lower energy than the saddle. This number is higher than in IED's determined in the normal cavity case with argon plasmas. One must conclude that the sheath thickness is larger in the CF_4 plasma.

When we consider the IED's of the CF_2^+ ions in figure 5.22, we can only recognize the primary saddle structure at 20 mTorr. At higher pressures this structure vanishes. From the measurements of the IED's of CF_3^+ ions at 40 mTorr it follows that the primary saddle structure is visible. This means that CF_3^+ ions from the glow can reach the electrode without colliding in the sheath. The primary saddle structure in the IED's of the CF_2^+ ions at 40 mTorr is hardly
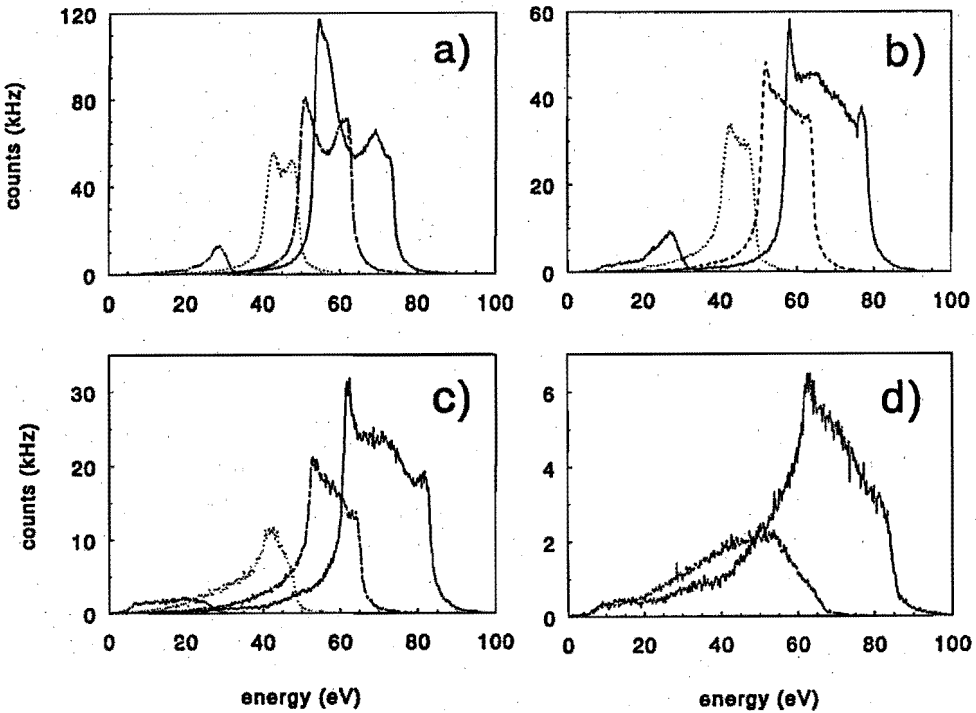
Figure 5.25: The IED's of CHF_2^+ ions incident on the grounded electrode in the normal cavity for several pressure and RF power conditions: (a) 20 mTorr: 78 (solid line), 40 (long-short dashed line), 20 (dotted line) and 5 Watt (long-short-short dashed line); (b) 40 mTorr: 78, 40, 20 and 5 Watt; (c) 80 mTorr: 78, 40, 20 and 5 Watt; and (d) 160 mTorr: 78 and 40 Watt.

visible. This means that the CF_2^+ ions from the glow are mainly scattered elastically or destroyed by reactions, so the probability that CF_2^+ ions cross the sheath without any collision is very small. The relatively large chance the CF_2^+ ions will be destroyed in the sheath is in accordance with the fact that they have one unpaired electron, while ions like CF_3^+, CF^+ and CHF_2^+ have only paired electrons. Therefore the CF_2^+ ions are more reactive. The feature in the IED's of the CF_2^+ ions at energies smaller than the primary saddle must be generated through production of CF_2^+ ions in the sheath. The production rate

is relatively large which compensates the rather high loss responsible for the vanishing of the primary saddle.

The IED's of CF^+ ions can be compared with those of the CF_3^+ ions: the primary saddle structure can be recognized up to about 80 mTorr. The strong increase of low energy ions can again only be explained by production in the sheath. The smaller number of features can be understood by the low mass of the CF^+ ions resulting in a short transit time and by possible excess energy after the formation reaction.

The primary saddle structure in the IED's of F^+ ions is recognizable at low pressures (20 and 40 mTorr), while also one very sharp peak can be distinguished up to 160 mTorr. This may be produced by newly formed ions from ion-molecule reactions, also by resonant charge exchange reactions. From investigations of Haverlag it is known that the density of F neutrals is about five times as high as the CF_3 neutral density [Hav91]. One should take into account that the F^+ ions can not disappear by dissociation reactions as CF_n^+ ions do.

In subsection 5.5.3 several ion-molecule reactions will be discussed that can appear in the CF_4 sheath. From the measured IED's we may conclude what reactions are dominant.

In figure 5.26, 5.27 and 5.28, the IED's of CF_3^+, CF_2^+ and CF^+ ions are presented as measured in the inverse cavity case in a CF_4 plasma of 5, 14.5 and 72 mTorr, respectively. E_{pas} was 33 eV because of the low ion fluxes.

The position of the saddle structure of the IED's of the CF_3^+ ions is only recognizable at low pressures up to about 15 mTorr. At higher pressures the saddle vanishes due to the small chance of the ion to cross the sheath without any collision. The IED's of the CF_2^+ ions looks nearly similar for the whole pressure range. The average energy of the whole IED decreases with increasing pressure and the saddle structure vanishes, which corresponds to the results determined in the normal cavity. The same may be concluded for the IED's of the CF_3^+ ions. This conclusion is also in agreement with the results of the normal cavity case extrapolated to a sheath with a larger thickness.

5.5.3 Sheath analysis

From the IED's in which the primary saddle structure can be recognized, the amount of splitting can be derived. This is the case in the low pressure range for IED's determined in the normal cavity case. The amount of splitting appears to be inversely proportional to $\sqrt{m_i}$. This empirical relation is also valid in the
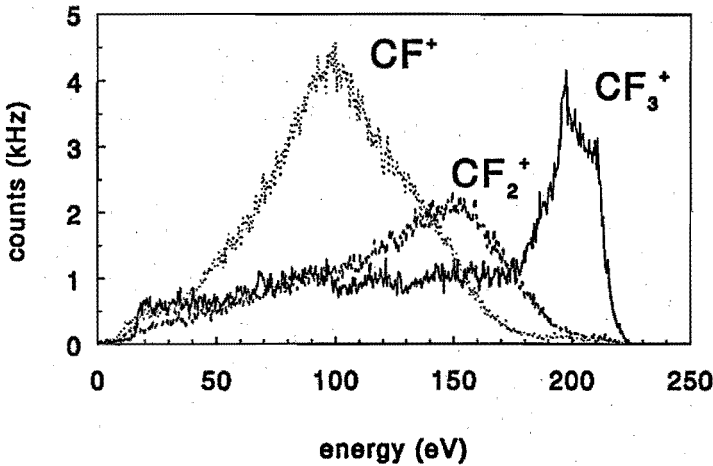
Figure 5.26: The IED's of CF_3^+ (solid line), CF_2^+ (dashed line) and CF^+ ions (dotted line) incident on the grounded electrode in the inverse cavity. The pressure is 5 mTorr and the RF power is 85 Watt.

argon and nitrogen plasmas.

In figure 5.29 the splitting ΔE of the saddle structure of the IED's of the CF_2^+ ions, is given as function of $\overline{E}_{sad}$. ΔE increases with $\overline{E}_{sad}$ which means that the ion density increases with $\overline{E}_{sad}$ which, at its turn, increases with the average sheath voltage. Due to the increase of the ion density the sheath thickness decreases.

When we consider the splitting for different pressure conditions at a certain $\overline{E}_{sad}$, we see that the amount of splitting is the largest at the lowest pressure. From this we may conclude that the sheath thickness is the smallest at the lowest pressure, which may be the consequence of a higher ion density at lower pressure in comparison with the higher pressure conditions. Investigations of Bisschops confirm the decrease of the ion density with increasing pressure [Bis87]. This is in contrast with the argon plasma where the ion density increases with pressure and the amount of splitting is the largest for IED's determined in high pressure plasmas.

From the measurements, the relation between the maximum sheath voltage $(V_{rf} + V_{dc})$ and $\overline{E}_{sad}$ can be determined. In figure 5.30 this relation is shown for the IED's of the CF_3^+ ions, determined in a CF_4 plasma at pressures of
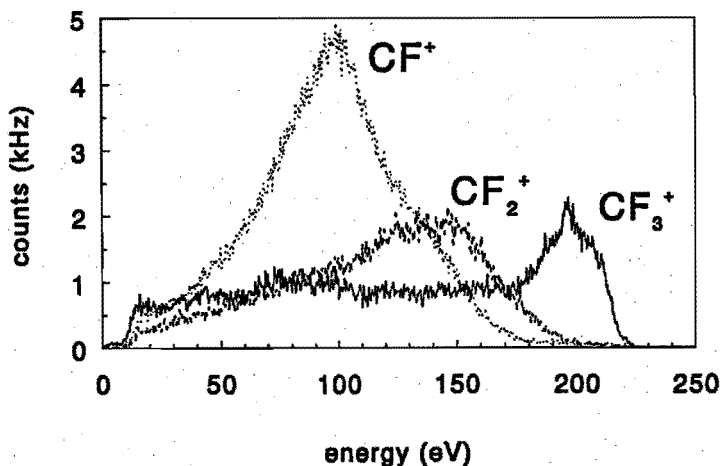
Figure 5.27: The IED's of CF_3^+ (solid line), CF_2^+ (dashed line) and CF^+ ions (dotted line) incident on the grounded electrode in the inverse cavity. The pressure is 14.5 mTorr and the RF power is 85 Watt.

5 and 20 mTorr. From this figure we may conclude that the sheath voltage modulation is not sinusoidal at high RF voltages and that this effect is larger for low pressures where the ion density is higher and the sheath thickness smaller. This conclusion is in agreement with the sheaths in argon plasmas where the ion density for high pressure plasma is the largest and, consequently, the deviation from a sinusoidal voltage modulation the largest.

To explain the IED's of the ion species which are present in the sheath of a CF_4 plasma ion-molecule reactions have to be taken into account. The most important reactions are discussed in this section. *Exact data about cross-sections of reactions in which CF_n^+ ion species are involved are not known yet. Therefore we will adapt the reaction enthalpy as a "measure" for the reaction rate. This is only partly justified, but as a first estimation in terms of tendencies towards equilibrium a consideration of the enthalpies can be very useful. Furthermore, electron impact reactions have not been considered. This is backed by the results in N_2 plasmas as discussed in section 5.4.*

The ions which are present in the plasma, can collide with a CF_4 molecule
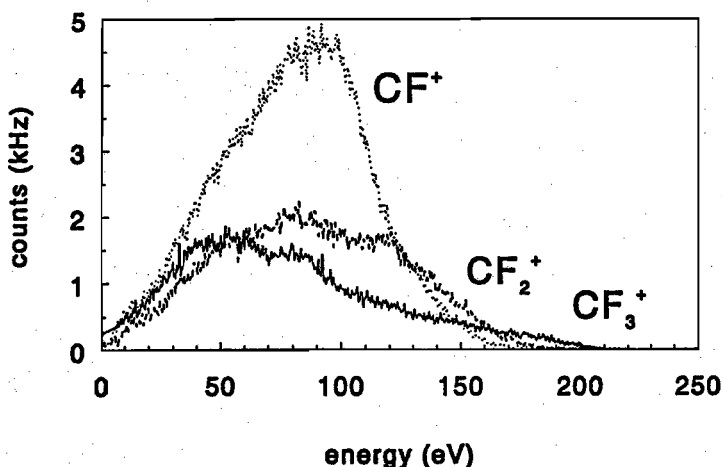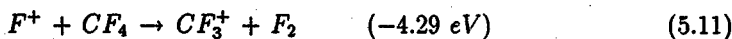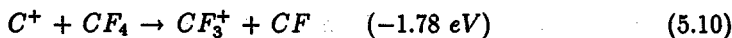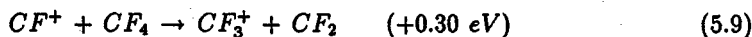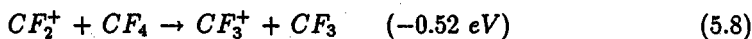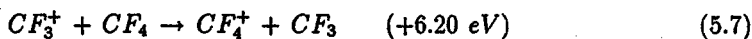
Figure 5.28: The IED's of CF_3^+ (solid line), CF_2^+ (dashed line) and CF^+ ions (dotted line) incident on the grounded electrode in the inverse cavity. The pressure is 72 mTorr and the RF power is 85 Watt.

and a fluorine atom transfer reaction may take place. The following reactions may be distinguished with the energy difference of the products after and before the reaction given between brackets [Pab76, Cem91] ('+' means an endothermic reaction and '−' means an exothermic reaction):

$$CF_3^+ + CF_4 \rightarrow CF_4^+ + CF_3 \quad (+6.20 \; eV) \tag{5.7}$$
$$CF_2^+ + CF_4 \rightarrow CF_3^+ + CF_3 \quad (-0.52 \; eV) \tag{5.8}$$
$$CF^+ + CF_4 \rightarrow CF_3^+ + CF_2 \quad (+0.30 \; eV) \tag{5.9}$$
$$C^+ + CF_4 \rightarrow CF_3^+ + CF \quad (-1.78 \; eV) \tag{5.10}$$
$$F^+ + CF_4 \rightarrow CF_3^+ + F_2 \quad (-4.29 \; eV) \tag{5.11}$$

At reaction 5.7 a CF_4^+ ion is formed. This ion however decomposes directly to CF_3^+ and F which reaction is slightly exothermic [Pab76]. The exothermic reactions may occur spontaneously. The endothermic reactions may occur when the energy difference is supplied by the accelerated ion in the sheath.

Also charge exchange reactions may occur in the sheath. The cross-sections of charge exchange reactions between two identical species (symmetric charge exchange) are quite large and in the order of 10^{-18} m^{-2}. The cross-
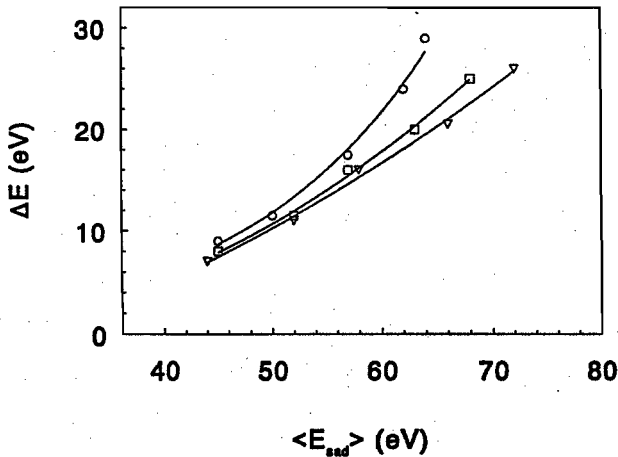
Figure 5.29: The relation between $\overline{E}_{sad}$ and ΔE in the CF_4 plasmas in the normal cavity, determined from the IED's of the CF_2^+ ions for 20 ($\circ$), 40 ($\square$) and 80 ($\triangledown$).

sections of charge exchange reactions between unlike ions and atoms (asymmetric charge exchange) is in general smaller than in the case of symmetric charge exchange [Has64, McD64]. Asymmetric charge exchange cross-sections are in the order of 10^{-21} m^{-2}. The smaller cross-sections are mainly the consequence of an energy difference between the ionization levels of the involved ions. In the cases of resonant asymmetric charge exchange, in which resonance means that the energy difference between the two involved ionization levels is zero, the cross-section can be in the same order of magnitude as comparable symmetric charge exchange reactions.

We consider the following symmetric (resonant) charge exchange reactions:

$$CF_3^+ + CF_3 \rightarrow CF_3 + CF_3^+ \tag{5.12}$$
$$CF_2^+ + CF_2 \rightarrow CF_2 + CF_2^+ \tag{5.13}$$
$$CF^+ + CF \rightarrow CF + CF^+ \tag{5.14}$$
$$F^+ + F \rightarrow F + F^+ \tag{5.15}$$

Apart from the cross sections, the probability that these reactions occur depends on the densities of the neutrals. These densities are much lower than the
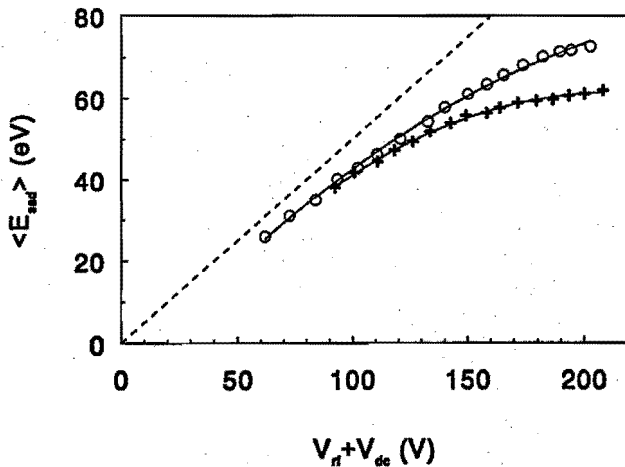
Figure 5.30: $\overline{E}_{sad}$ as function of the maximum sheath voltage $V_{rf} + V_{dc}$ in CF_4 plasmas in the normal cavity. The results are determined from the IED's of the CF_3^+. The pressure is 5 mTorr (+) and 20 mTorr (○).

CF_4 density, but due to the large cross sections these reaction may occur in the sheath.
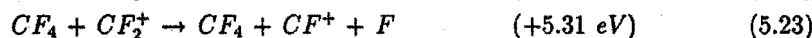
In the case asymmetric charge exchange reactions will occur, this will mainly take place between an ion and a CF_4 neutral. This because the CF_4 density is the highest neutral density. We distinguigh the following asymmetric charge exchange densities:

$$CF_3^+ + CF_4 \rightarrow CF_3 + CF_4^+ \tag{5.16}$$
$$CF_2^+ + CF_4 \rightarrow CF_2 + CF_4^+ \tag{5.17}$$
$$CF^+ + CF_4 \rightarrow CF + CF_4^+ \tag{5.18}$$
$$F^+ + CF_4 \rightarrow F + CF_4^+ \tag{5.19}$$

where the newly formed CF_4^+ ions decompose directly to a CF_3^+ ion and a F atom. The reactions 5.16 to 5.19 are endothermic and the energy differences between the species after and before the reactions are 6.2 eV for reaction 5.16, 6.3 eV for reaction 5.18 and 2.7 eV for reaction 5.19 due to the non-resonance [Nak92, Pab76]. The energy difference for reaction 5.18 is unknown. Because of the energy difference between the ionization levels of the two involved ions, the cross-sections of these reactions will be quite small.

The CF_3 and CF_2 neutral densities is about 2 to 3 orders of magnitude lower than the CF_4 density [Hav91]. Therefore asymmetric charge exchange reactions may occur in the sheath even in the same order as the symmetric charge exchange reactions.

The next ion-molecule reactions which we discuss and which may occur in the sheath, are dissociation reactions of CF_n^+ ions by a collision with a neutral, most of the times a CF_4 atom. We distinguish the following reactions where the energy which is needed, is derived from the binding energy:

$$CF_4 + CF_3^+ \rightarrow CF_4 + CF_2^+ + F \qquad (+3.77 \ eV) \qquad (5.20)$$
$$CF_4 + CF_3^+ \rightarrow CF_4 + CF^+ + 2F \qquad (+8.08 \ eV) \qquad (5.21)$$
$$CF_4 + CF_3^+ \rightarrow CF_4 + C^+ + 3F \qquad (+13.7 \ eV) \qquad (5.22)$$
$$CF_4 + CF_2^+ \rightarrow CF_4 + CF^+ + F \qquad (+5.31 \ eV) \qquad (5.23)$$
$$CF_4 + CF_2^+ \rightarrow CF_4 + C^+ + 2F \qquad (+10.9 \ eV) \qquad (5.24)$$
$$CF_4 + CF^+ \rightarrow CF_4 + C^+ + F \qquad (+5.59 \ eV) \qquad (5.25)$$
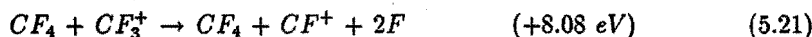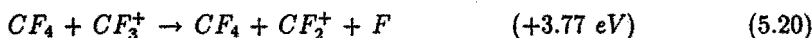
The last reaction we will discuss is the dissociation and ionization reaction of a CF_4 molecule by an incoming energetic ion. The CF_4 neutral may be dissociated in a CF_3^+ positive and a F^- negative ion:

$$ion + CF_4 \rightarrow ion + CF_3^+ + F^- \qquad (5.26)$$
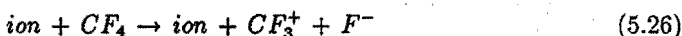
The energy needed for the dissociation is delivered by the incoming ion. Apart from the dissociation energy, the incoming ion may also transfer momentum to the newly formed ions, according to the momentum conservation law. No data about this reaction is available. Therefore it is hard to estimate whether this reaction will occur in the sheath.

From a classical point of view, a neutral atom or molecule can be ionized by a highly energetic ion, with energies higher than some keV's [Has64]. These energies can not be obtained in the sheath of an RF plasma as discussed in this thesis; so ionization reactions of neutrals by highly energetic ions may not be expected in the sheaths.

From the measured IED's we may conclude which reactions take place in the sheath. We have to keep in mind that the density of the CF_4 neutrals is 2 to 3 orders of magnitude higher than the density of the CF_n and F radicals [Hav91]. The density of F radicals is higher than that of CF_2, while the CF_2 density is higher than the CF_3 density [Hav91]. Accurate data about the cross sections of the different reactions are not known. From mass spectrometric measurements we can not derive the absolute ratios between the ion species,

but from a rough estimation we may conclude that the density of the CF_3^+ ions is higher than that of the other ion species. The IED's of the CHF_2^+ ions show that elastic scattering does not influence the IED's.

When we consider the IED's of the CF_2^+ ions, we may conclude that the absence of the primary saddle shows that only very few ions cross the sheath without any collision. Comparison of these IED's with the IED's of CF_3^+ and CF^+ ions learn that there must be a reaction with a large reaction rate through which CF_2^+ ions are lost. This may be reaction 5.8, an exothermic reaction. Due to the high density of the CF_4 molecules, the probability that this reaction takes place will be large. (Reactions 5.7 and 5.9 are endothermic and can explain why the primary saddle in the IED's of CF_3^+ and CF^+ ions does not vanish.) The charge exchange reactions 5.13 and 5.17 also lead to a loss of CF_2^+ ions from the glow but their contribution to the total loss will be much less than that of reaction 5.8.

From the IED's of the CF_2^+ ions, we may also conclude that there must be a reaction through which CF_2^+ ions are produced. The reaction rates of the charge exchange reaction 5.13 is small due to the small density of the CF_2 radicals. That this reaction is no dominant production line of CF_2^+ ions is confirmed by the fact that no charge exchange peaks in the IED's of the CF_2^+ ions can be observed. Therefore the dissociation reaction 5.20 of CF_3^+ ions is the most probable production line of CF_2^+ ions in the sheath.

The CF_3^+ ions are involved in several reactions. Among these there are producing as well as destroying reactions. Through reactions 5.7, 5.12 and 5.16 CF_3^+ ions are destroyed but at the same time also produced. By reactions 5.17 to 5.19 CF_3^+ ions are produced. Although the cross section of resonant charge exchange is quite large, the probability that reaction 5.12 occurs is small due to the low CF_3 radical density. Also the contribution of the asymmetric charge exchange reactions 5.16 to 5.18 to the production of CF_3^+ ions will not be very large due to the small cross-sections. This suggests the conclusion that CF_3^+ ions are mainly produced in the sheath by the fluorine atom transfer reaction 5.7 where the CF_4^+ ion decomposes into a CF_3^+ ion and a F radical. Because the newly formed CF_4^+ ions immediatly decompose, the newly formed CF_3^+ ions generate features in the IED's similar to those generated by charge exchange reactions. The main mechanism through which CF_3^+ ions are destroyed is by the dissociation reaction 5.20.

The CF_3^+ ions may also be produced by the dissociation and ionization reaction of CF_4 (reaction 5.26). Ions produced by this reaction however do not generate special features in the IED's: the incoming ion may transfer kinetic

energy to the newly formed ions so they do not need to start with zero energy as ions produced by charge exchange do. Their direction even does not need to be pointed towards the electrode, which means that a part of the newly formed ions will not be detected. Therefore, it is hard to conclude from the IED's whether this reaction may occur in the sheath.

In the CF^+ case the same kind of reactions are responsible for the production and loss mechanisms as in the CF_2^+ situation. The difference is that reaction 5.9 is slightly endothermic. The consequence is that the ratio between loss and production reactions is different from the CF_2^+ case and that in the IED's of the CF^+ ions the primary saddle structures can be recognized up to higher pressures than in the CF_2^+ case.

F^+ ions are destroyed by the ion transfer reaction 5.11. This reaction is exothermic and due to the large CF_4 density the chance for this reaction to occur in the sheath will be quite large.

The IED's of F^+ ions show large peaks, which suggest that the charge exchange reaction 5.15 occurs in the sheath. This seems to be quite likely because the F radical density is quite high (is about 5 times higher than the CF_3 and CF_2 radical densities) and the cross section for resonant charge exchange is large.

5.5.4 Conclusions

The sheath in a CF_4 plasma is far more complex than in an argon or nitrogen plasma. This is due to the number of ion species present and ion-molecule reactions which may occur in the sheath. This leads to significant loss and production rates of the ion species. The CF_3^+ ion density is the highest density of all ion species.

From the IED's of the ion species one may conclude which reactions are dominant for the production and loss of every ion species. Newly formed CF_3^+ ions in the sheath which are responsible for the features in the IED's are mainly generated by the fluorine atom transfer reaction (5.7)

$$CF_3^+ + CF_4 \rightarrow CF_4^+ + CF_3 \quad (+6.20 \ eV),$$
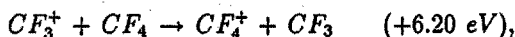
where the CF_4^+ ion directly decomposes to a CF_3^+ ion. This reaction, however, also leads to the loss of CF_3^+ from the glow. CF_3^+ ions are also lost by the dissociation reaction 5.20

$$CF_3^+ \rightarrow CF_2^+ + F \quad (+3.77 \ eV).$$

This reaction is also responsible for the formation of CF_2^+ ions in the sheath. The most important reaction which leads to the loss of CF_2^+ ions in the sheath is the fluoride transfer reaction 5.8

$$CF_2^+ + CF_4 \rightarrow CF_3^+ + CF_3 \quad (-0.52 \ eV).$$
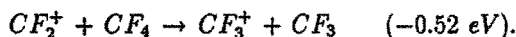
Most CF^+ ions that are formed in the sheath are produced by the dissociation reaction 5.21 of CF_3^+ ions

$$CF_3^+ \rightarrow CF^+ + 2F \quad (+8.08 \ eV).$$

The fluoride ion transfer reaction 5.9 is mainly responsible for the loss of CF^+ ions in the sheath

$$CF^+ + CF_4 \rightarrow CF_3^+ + CF_2 \quad (+0.30 \ eV).$$
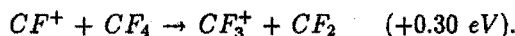
The collisional induced features in the IED's of the F^+ ions are mainly generated by F^+ ions that are generated in the sheath by resonant charge exchange collisions according to reaction 5.15

$$F^+ + F \rightarrow F + F^+ \qquad .$$
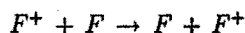
The most F^+ ions are lost in the sheath by fluoride ion transfer reactions such as reaction 5.11

$$F^+ + CF_4 \rightarrow CF_3^+ + F_2 \quad (-4.29 \ eV).$$
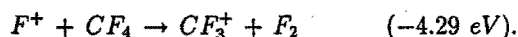
Although this analysis gives insight in the ion kinetics in the sheath of a CF_4 plasma, more detailed knowledge about the ion molecule reactions is needed for a quantitative treatment of the ion kinetics. Therefore simulations in the simple form as used for the argon and nitrogen plasma, cannot be expected to be in agreement with the measurements.

The IED's of the CHF_2^+ ions contain mainly the ions which do not collide in the sheath. This is so because the elastically scattered ions are not detected and there are no reactions by which CHF_2^+ ions are produced in the sheath. Therefore the IED's of CHF_2^+ ions may be interpreted as collisionless and can be used to analyse the sheath behaviour due to the $\overline{E}_{sad}$ and ΔE of the primary saddle structure.

From the IED's it may be concluded that the behaviour of the sheath in front of the largest electrode is capacitive at low sheath voltages and becomes non-purely capacitive at higher voltages. The sheath in front of the smallest

electrode may be assumed purely capacitive for the whole voltage range. From the average energy of the primary saddle structure it may be derived that the non-purely capacitive behaviour is stronger at low pressures. This is due to higher ion densities at low pressures through which the sheath thickness is smaller and the transit time of the ions through the sheath shorter. This conclusion is into agreement with the amount of splitting of the primary saddle structure as function of the pressure.

The variation of the splitting is also associated with the fact that the transit time decreases with increasing sheath voltage. This is mainly due to the increase of the ion density with increasing sheath voltage. This causes the sheath thickness to become smaller at a higher sheath voltage. The amount of splitting of the primary saddle structure determined from the measured IED's is inversely proportional to $\sqrt{m_i}$ which is in accordance with saddle structures in the argon and nitrogen RF plasmas.

References

[Bis87]   T.H.J. Bisschops, *Investigations on an RF plasma related to plasma etching.* Ph.D. thesis, Eindhoven University of Technology, the Netherlands, 1987.

[Cem91]   Ce Ma, M.R. Bruce and R.A. Bonham, *Phys. Rev. A*, **44**, 2921 (1991).

[Cob70]   J.W. Coburn, *Rev. Sci. Instruments*, **41**, 1219 (1970).

[Gus61]   E. Gustafsson and E. Lindholm, *Arkiv. Fysik*, **18**, 219 (1961).

[Has64]   J.B. Hasted, *Physics of atomic collisions*, (Butterworths, London, 1964).

[Hav91]   M. Haverlag, *Plasma chemistry of fluorocarbon RF discharges used for dry etching.* Ph.D. thesis, Eindhoven University of Technology, the Netherlands, 1991.

[Kne62]   P.F. Knewstubb and R. Tickner, *J. Chem. Phys.* **36**, 674 (1962).

[McD64]   E.W. McDaniel, *Collisional phenomena in ionized gases*, (Wiley, New York, 1964).

[Nak92]   T. Nakano and H. Sugai, *Jap. J. Appl. Phys*, **31**, 2919 (1992).

[Pab76]   M.J.K.Pabst, H.S. Tan and J.L. Franklin, *Int. J. Mass Spec. Ion Phys.* **20**, 191 (1976).

[Pau82]   C.R. Paul and S.A. Nasar, *Introduction to electromagnetic fields*, (McGraw-Hill, New york, 1982).

[Sam93]   M.J.M. van Sambeek, internal report, Eindhoven University of Technology, the Netherlands, VDF/NG 93-05, 1993.

[Sni93]   R.J.M.M. Snijkers, M.J.M. van Sambeek, G.M.W. Kroesen and F.J. de Hoog, *Appl. Phys. Lett.* **63**, 308 (1993).

[Ste63]   R.F. Stebbings, B.R. Turner and A.C.H. Smiths, *J. Chem. Phys.* **38**, 2277 (1963).

[Tho88]   B.E. Thompson, H.H. Sawin and D.A Fisher, *J. Appl. Phys.* **63**, 2241 (1988).

[Utt61]   N.G. Utterback and G.H. Miller, *Rev. Sci. Instr.* **32**, 1101 (1961).

Summary

Radio frequency (RF) plasmas are commonly used in industry for surface modification processes, e.g. for etching and deposition of semiconductor surfaces in the manufacturing of integrated circuits. The RF plasma is usually generated between two electrodes. The RF voltage is applied to one of the electrodes while the other electrode is connected to ground. The quasi-neutral plasma glow is situated between the electrodes and is separated from the electrode by a sheath, across which a voltage drop arises. In the plasma glow ions, electrons and radicals are created by inelastic collisions between the electrons and the background gas. Due to the voltage drop, the electrons are repelled from the sheath region while the ions are accelerated towards the electrode at which a substrate may be placed. Energetic ions bombard the substrate surface and play an important role in the surface modification processes. To achieve better modification results, knowledge of the ion energy distribution (IED) when the ions hit the surface is indispensable.

This thesis concerns the ion dynamics in the sheath of an RF plasma. Therefore the electric field in the sheath in which the ions are accelerated is modelled. The electric field in the sheath is generated by the positive ionic space charge which occurs in the sheath, and the boundary potentials. In the case of an RF plasma, the voltage across the sheath is RF modulated and consequently, the electric field is spatially and temporally varying. In the case of a low frequency RF plasma (*ion plasma frequency* > *radio frequency*), the ions respond instantaneously to the field oscillations in the sheath while in the high frequency RF plasma (*ion plasma frequency* < *radio frequency* < *electron plasma frequency*) the ions respond to an averaged electric field. Separate models for the electric field have been devised for the two cases. The models are proved to be close to self-consistency and are used to simulate the (typically saddle-structured) IED's. Monte Carlo techniques are used to simulate collisions in the sheath and their influence on the IED. For that purpose we distinguished charge exchange collisions and elastic scattering. The first type of collisions gives rise to typical peak structures in the IED's where the number of peaks depends on the sheath thickness, the mass of the ion and the sheath voltage.

Negative ions are repelled from the sheath, just like the electrons, and are confined to the glow. Due to the quasi-neutrality in the plasma glow, the electron density in the glow is smaller than the positive ion density. The influence of the negative ions is expressed in the Bohm velocity at which the positive ions have to enter the sheath region so that a stable positive space

charge region occurs.

To determine the IED's experimentally, a setup has been built to measure the mass-resolved distributions of the ions hitting the electrode. IED's have been determined in an argon (Ar), nitrogen (N_2) and carbontetrafluoride (CF_4), 13.56 MHz, AC coupled RF plasma at both the largest and the smallest electrode. The mass and energy spectrometer only detects ions that hit the electrode within an angle of 4°. Consequently, a small number of the elastically scattered ions will be detected. Ions produced by charge exchange start with zero energy and consequently, their trajectories are perpendicular to the electrode. Therefore these ions are all detected.

The IED's of Ar^+ ions determined in an argon plasma show typical charge exchange peaks. Due to residual water in the reactor, also hydrogen containing ions like ArH^+, H_3O^+, H_2O^+ and H_3^+ are detected. These ions are scattered elastically and the measured IED's contain mostly ions that have not collided in the sheath as a consequence of the small detection angle of the diagnostic. Therefore the measured IED's of the ArH^+ may be interpreted as collisionless. Simulations show good agreement with the experimentally determined IED's when the small detection angle of the diagnostic is taken into account.

From the collisionless character of the IED's of the ArH^+ ions it is easy to determine the average energy and the splitting of the primary RF saddle structure. These parameters, related to the sheath voltage, characterize the behaviour of the sheath. In low power plasmas, the sheath behaviour is purely capacitive. The sheath voltage modulation may be considered purely sinusoidal and the ions need more than 3 RF periods to cross the sheath from the glow to the electrode. Higher powers cause a higher ion density in the plasma. Consequently, the space charge and the electric field in the sheath increases and the sheath thickness decreases, even though the sheath voltage is higher. The sheath behaviour is no longer purely capacitive.

In a nitrogen plasma N^+, N_2^+ and N_3^+ ions are detected. The IED's of the N_2^+ ions show typically charge exchange effects, while the IED's of the N^+ and the N_3^+ ions may be interpreted as collisionless. Simulations show good agreement with the measurements.

CF_4 plasmas are much more complex than Ar and N_2 plasmas. This is due to the large number of radical and ion species, and the possible ion-molecule reactions which may also occur in the sheath. This means that ions are produced and destroyed in the sheath. From the measured IED's of the CF_3^+, CF_2^+, CF^+ and F^+ ions and with the help of a consideration of the enthalpy of the possible ion-molecule reactions, we may conclude which loss and production reactions

are dominant in the sheath of a CF_4 plasma. CHF_2^+ ions, which are formed in the plasma due to residual water, are scattered elastically or are destroyed when they collide in the sheath. Consequently, the measured IED's show a collisionless, saddle structured distribution which is useful for the interpretation of the other ionic distributions measured in the CF_4 plasmas.

The theoretically and experimentally determined IED's in the argon and the nitrogen plasmas contribute to the understanding of the ion dynamics in the sheath of an RF plasma. Important for CF_4 RF plasma processes are the energies of the ions when hitting the substrate. The measured IED's in the CF_4 plasma give insight in the complex reaction kinetics in the sheath of an RF plasma.

Samenvatting

Radiofrequente (RF) plasma's worden in de industrie veel gebruikt voor oppervlakte-modifictie-processen, b.v. voor het etsen en deponeren van halfgelei-der oppervlakken bij de produktie van geïntegreerde schakelingen. Het RF plasma wordt gewoonlijk gegenereerd tussen twee elektroden. De RF span-ning wordt toegevoerd aan een van de elektroden, terwijl de andere geaard is. Het quasi-neutrale plasma-glimgebied bevindt zich tussen de elektroden en wordt van de elektrode gescheiden door een grenslaag, waarover een span-ningsverschil staat. In het glimgebied worden ionen, elektronen en radicalen gecreëerd door inelastische botsingen tussen de elektronen en het achtergrond gas. Als gevolg van de spanningsval worden de elektronen teruggedreven uit de grenslaag, terwijl de ionen versneld worden naar de elektrode waarop een substraat geplaatst kan worden. Energetische ionen bombarderen het substraat-oppervlak en spelen een belangrijke rol in het oppervlakte-modificatie-proces. Om betere modificatie-resultaten te bereiken, is kennis van de ionen-energie-verdelingsfunktie (IEV) wanneer de ionen het oppervlak bereiken, onontbeer-lijk.

In dit proefschrift wordt de ionen-dynamica in de grenslaag van een RF plasma beschreven. Daartoe zijn modellen ontwikkeld om het elektrisch veld in de grenslaag, waarin de ionen versneld worden, te beschrijven. Het elektrisch veld in de grenslaag wordt gegenereerd door de positieve ruimtelading van ionen die ontstaat in de grenslaag, en de potentialen aan de randen. Bij een RF plasma wordt ook de spanning over de grenslaag gemoduleerd met als gevolg dat het elektrisch veld varieert als funktie van de plaats en tijd. In het geval van een laag frequent RF plasma $(ionen-plasma-frequentie > radio-frequentie)$, reageren de ionen direct op de oscillaties van het elektrisch veld in de grenslaag, terwijl in een hoog frequent RF plasma $(ionen-plasma-frequentie < radio-frequentie < elektronen-plasma-frequentie)$ de ionen kinetiek overeenkomt met de reactie op een gemiddeld elektrisch veld. Aparte modellen zijn ontwikkeld voor beide frequentiegebieden. Bewezen is dat de modellen redelijk zelf-consistent zijn. De modellen zijn gebruikt om de IEV-en te simuleren, welke gekenmerkt wor-den door een typische zadelstructuur. Monte Carlo technieken zijn gebruikt om botsingen in de grenslaag en hun invloed op de IEV te simuleren. Daartoe maakten we ondersheid tussen ladingsruil en elastische botsingen. De eerst ge-noemde soort botsingen veroorzaken typische piekstructuren in de IEV, waarbij het aantal pieken afhangt van de grenslaagdikte, de massa van het ion en de grenslaagspanning.

Negatieve ionen worden ook teruggedreven uit de grenslaag, net als de

elektronen, en worden opgesloten in het glimgebied. Als gevolg van de quasi-neutraliteit van het glimgebied is de elektronendichtheid in het glimgebied lager dan de dichtheid van de positieve ionen. De invloed van de negatieve ionen komt tot uitdrukking in de Bohm snelheid, waarmee de positieve ionen het grenslaag gebied binnen moeten gaan opdat een stabiel, positief ruimteladings-gebied ontstaat.

Om de IEV-en experimenteel te bepalen is een opstelling gebouwd, waarmee de massa-opgeloste, energieverdeling van de ionen aan de elektrode, gemeten kan worden. IEV-en zijn gemeten in een argon (Ar), stikstof (N_2) en koolstofte-trafluoride (CF_4), 13,56 MHz, AC gekoppeld RF plasma aan zowel de grootste als de kleinste elektrode. De massa- en energiespectrometer detecteert alleen ionen, welke de elektrode treffen binnen een hoek van 4° met de normaal. Dit heeft als gevolg dat slechts een klein deel van de elastisch verstrooide ionen gedecteerd wordt. Ionen welke door ladingsruil-botsingen geproduceerd wor-den, starten met energie nul, met als gevolg dat hun banen loodrecht op de elektrode gericht zijn. Deze ionen worden daarom allemaal gedetecteerd.

De IEV-en van Ar^+ ionen, bepaald in een argon plasma, vertonen typische ladingsruil pieken. Als gevolg van enkele achtergebleven water moleculen in de reactor, worden ook waterstof bevattende ionen zoals ArH^+, H_3O^+, H_2O^+ en H_3^+ waargenomen. Deze ionen worden alleen elastisch verstrooid en de gemeten IEV-en bevatten vooral ionen welke niet in de grenslaag gebotst hebben als gevolg van de kleine detectiehoek van de meetopstelling. De gemeten verdelin-gen van de ArH^+ ionen mogen daarom als botsingsloos geïnterpreteerd worden. Simulaties vertonen goede overeenstemming met de experimenteel bepaalde IEV-en, als rekening wordt gehouden met de kleine detectiehoek van de meet-opstellling.

Uit het botsingsloze karakter van de IEV-en van de ArH^+ ionen, kan gemakkelijk de gemiddelde energie en de opsplitsing van de oorspronkelijke zadel structuur bepaald worden. Deze parameters, gerelateerd aan de grenslaag-spanning, karakteriseren het gedrag van de grenslaag. In laag vermogens-plasma's is het gedrag van de grenslaag puur capacitief. De modulatie van de spanning over de grenslaag mag puur sinusoïdaal beschouwd worden en de ionen hebben meer dan 3 RF perioden nodig om de grenslaag, van het glim-licht naar de elektrode, over te steken. Hogere vermogens hebben een hogere ionendichtheid in het plasma tot gevolg. Hierdoor neemt ook de ruimtelading en de elektrische veldsterkte in de grenslaag toe en de grenslaagdikte neemt af, ondanks de hogere spanning over de grenslaag. Het gedrag van de grenslaag is niet meer puur capacitief.

In een stikstof plasma worden N^+, N_2^+ en N_3^+ ionen waargenomen. De IEV-

en van de N_2^+ ionen vertonen typische ladingsruil pieken, terwijl de IEV-en van de N^+ en N_3^+ ionen geïnterpreteerd mag worden als botsingsloos. Simulaties vertonen een goede overeenstemming met de metingen.

CF_4 plasmas zijn veel complexer dan Ar en N_2 plasma's. Dit is het gevolg van de grote verscheidenheid aan radicalen en ionen en de mogelijke reacties tussen ionen en moleculen welke kunnen optreden in de grenslaag. Dit betekent dat ionen geproduceerd en vernietigd kunnen worden in de grenslaag. Uit de gemeten IEV-en van de CF_3^+, CF_2^+, CF^+ en F^+ ionen en met behulp van een beschouwing op grond van the enthalpie van de mogelijke reacties tussen de ionen en de moleculen, kunnen we concluderen wat de dominante productie en verlies reacties in de grenslaag van een CF_4 plasma zijn. CHF_2^+ ions, die in het plasma gevormd worden doordat enkele water moleculen achter gebleven zijn, worden elastisch verstrooid of vernietigd als ze botsen in de grenslaag. Het gevolg hiervan is dat de gemeten IEV-en een botsingsloze verdeling met een karakteristiek zadel vertonen. De verdelingen kunnen gebruikt worden voor de interpretatie van de verdelingen van de andere ionen in een CF_4 plasma.

De theoretisch en experimenteel bepaalde IEV-en in de argon en de stikstof plasma's dragen bij aan het begrip van de ionen-dynamica in de grenslaag van een RF plasma. Van belang voor de RF plasma processen in een CF_4 plasma, zijn de energieën van de ionen wanneer ze het substraat-oppervlak bereiken. De gemeten IEV-en in het CF_4 plasma geeft inzicht in de complexiteit van de reactiekinetic in de grenslaag van een RF plasma.

Tot slot

Een proefschrift is zelden het werk van een promovendus alleen. Graag wil ik tot slot enkele mensen bedanken voor hun bijdrage aan het tot stand komen van dit proefschrift.

Frits de Hoog, mijn eerste promotor, wil ik in het bijzonder bedanken. Na mijn afstuderen, bood hij mij de mogelijkheid om te gaan promoveren. Het vertrouwen wat hij de afgelopen 4 jaar in mij heeft gehad, heb ik zeer op prijs gesteld, evenals de vrijheid om een persoonlijke draai aan het onderzoek te geven. Zijn begeleiding heb ik altijd als goed en zeer prettig ervaren. Mede door deze inbreng van mijn leermeester, kijk ik dan ook met genoegen terug op mijn promotie-periode.

Frans Sluijter, mijn tweede promotor, wil ik bedanken voor de mogelijkheid welke hij geschapen heeft om een gedeelte van mijn promotiewerk binnen zijn groep te laten plaats vinden en uiteraard voor zijn persoonlijke bijdrage aan het tot stand komen van dit proefschrift.

Gerrit Kroesen, mijn copromotor, wil ik met name bedanken voor zijn bijdrage op het experimentele vlak en voor de kennis welke ik op dit gebied van hem heb mogen over nemen. Zijn immer optimistische houding was een extra stimulans op de weg naar de uiteindelijke resultaten. Tevens wil ik hem langs deze weg nogmaals bedanken voor zijn gids-aktiviteiten in New York en Boston, welke steden we samen bezochten op weg naar de Gordon Conferentie.

Leon Kamp, mijn adviseur, wil ik met name bedanken voor zijn adviezen welke bijgedragen hebben aan het vervolmaken van het theoretische model.

Daan Schram en Piet Schram, beiden leesleden van de promotie-commissie, wil ik bedanken voor het ontdoen van laatste onvolkomenheden van het proefschrift.

I want to thank professor Turban for the pleasant and instructive stay in Nantes (France) in April 1990.

Voor de onontbeerlijke technische ondersteuning wil ik Lambert Bisschops en Hans Freriks bedanken. Zij zochten altijd naar snelle wegen om op vakkundige wijze mijn technische wensen in vervulling te laten gaan. Hierbij wil ik ook Ries van de Sande betrekken, wie in het begin mijn promotie-onderzoek nog bij het ets-project betrokken was en Bertus Husken waar ik altijd een beroep op kon doen bij soft- en hardware problemen. De mensen van de faculteitswerkplaats wil ik bedanken voor het snel en bekwaam vervaardigen van de inverse cavity en alle "losse onderdeeltjes". Piet Magendans wil ik bedanken voor het uittekenen van de inverse cavity en de technische tips.

Veel experimenten zijn behaald met de hulp van studenten. Speciaal de

Curriculum vitae

28 oktober 1964	Geboren te Schaesberg
mei 1983	Diploma ongedeeld VWO (met lof), Eijkhagen College, Landgraaf.
december 1988	Doctoraal examen Technische Natuurkunde, Faculteit Tecnische Natuurkunde, Technische Universiteit Eindhoven.
januari 1989 -	Assistent in Opleiding, vakgroepen Deeltjesfysica en Theoretische Natuurkunde van de faculteit Technische Natuurkunde, Technische Universiteit Eindhoven.

STELLINGEN

behorende bij het proefschrift

"The sheath of an RF plasma:
measurements and simulations of the ion energy distribution"

door

Rob Snijkers

12 oktober 1993

Reacties tussen ionen en moleculen in de grenslaag van een radiofrequent (RF) plasma in CF_4 hebben grote invloed op de ionen-energieverdeling van de ionen aan het elektrode-oppervlak.

Dit proefschrift

Ten onrechte veronderstellen Olthoff *et al.* dat een tweemaal geïoniseerd argonatoom bij het doorlopen van de grenslaag in een radiofrequent plasma evenveel kinetische energie verkrijgt als een enkelvoudig geïoniseerd argonatoom.

J.K. Olthoff, R.J. van Brunt en S.B. Radovanov,
*J. Appl. Phys, **72**, 4566 (1992).*

Modellen van de grenslaag van een radiofrequent (RF) plasma die typische zadelstructuren en botsingspieken genereren in de ionen-energieverdeling, hoeven op grond daarvan nog niet als realistisch beschouwd te worden.

Als de transmissiecoëfficiënt van een massa- en energiespectrometer bekend is, is de integratie van de ionen-energieverdeling de beste methode om de ionenflux en de ionendichtheid aan de elektrode te bepalen.

Wanneer de polariserende eigenschappen van een enkele polarisator vergeleken worden met die van twee van dergelijke polarisatoren achter elkaar met evenwijdige transmissie-assen, verbeteren de prestaties kwadratisch.

De toenemende druk op wetenschappers om te publiceren leidt tot meer publicaties, welke op zeer korte termijn achterhaald worden. Het moeten lezen van deze publicaties leidt op zijn beurt weer tot een grotere belasting van de wetenschappers. Dit leidt op zijn beurt weer tot meer onjuiste publicaties.

De oorlog in het voormalige Joegoslavië toont de machteloosheid aan van de VN om een einde te maken aan oorlogssituaties. Zij kunnen hun invloed op het oorlogsgeweld slechts laten blijken door zelf oorlogshandelingen te plegen.

Een verdergaande ontwikkeling van het individualisme in de samenleving, waarbij de nadruk ligt op het vergroten van de eigen kansen, leidt tot egocentrisme en vaak ook tot egoïsme.

Vrijwilligerswerk vormt een belangrijk en niet meer weg te denken element bij het in stand houden van de verzorgingsstaat.

Door de complexiteit van de eisen en de verwachtingen in onze samenleving t.a.v. opgroeiende kinderen is een ouderschapscursus voor opvoeders wenselijk.

De term "milieuvriendelijk", welke vaak gebruikt wordt om bepaalde produkten aan te prijzen, is misleidend. Een betere uitdrukking zou zijn "minder schadelijk voor het milieu".